Instituto Politécnico de Lisboa

Instituto Superior de Engenharia de Lisboa

Escola Superior de Tecnologia de Saúde de Lisboa

Effect of Mesenchymal Stem Cell Source on the Molecular Profile of Extracellular Vesicles for Cell Therapy

Filipa Adriana Rego Pires

Thesis to obtain the Master Degree in

Biomedical Engineering

Definitive version

Supervisors:

Dr. Ana Margarida Pires Fernandes Platzgummer (Instituto Superior Técnico, Universidade Lisboa)

Dr. Cecília Ribeiro da Cruz Calado (ISEL, IPL)

December 2019

Instituto Politécnico de Lisboa

Instituto Superior de Engenharia de Lisboa

Escola Superior de Tecnologia de Saúde de Lisboa

Effect of Mesenchymal Stem Cell Source on the Molecular Profile of Extracellular Vesicles for Cell Therapy

Filipa Adriana Rego Pires

Thesis to obtain the Master Degree in

Biomedical Engineering

Definitive version

Supervisors:

Dr. Ana Margarida Pires Fernandes Platzgummer (Instituto Superior Técnico, Universidade Lisboa)

Dr. Cecília Ribeiro da Cruz Calado (ISEL, IPL)

Examination Committee

Chairperson:

Dr. Miguel Minhalma (ISEL, IPL)

Members of the Committee:

Dr. Pedro Sampaio (Universidade Lusófona)

Dr. Cecília Ribeiro da Cruz Calado (ISEL, IPL)

[This page is intentionally left blank]

One day, in retrospect, the years of struggle will strike you as the most beautiful

Sigmund Freud

[This page is intentionally left blank]

Effect of Mesenchymal Stem Cell Source on the Molecular Profile of Extracellular Vesicles for Cell Therapy

Filipa Adriana Rego Pires

This work was partially conducted at *Institute for Bioengineering and Biosciences (iBB), Instituto Superior Técnico* and *Engineering & Health Laboratory*, *Instituto Politécnico de Lisboa*, that resulted from a collaboration protocol established between Universidade Católica Portuguesa and Instituto Politécnico de Lisboa. This work was partially supported by iBB and the grant IDI&CA/IPL/2018/RenalProg/ISEL from *Instituto Politécnico de Lisboa*.

[This page is intentionally left blank]

Acknowledgments

Firstly, I would like to thank to Professor Cecilia Calado, my supervisor, who introduced me to FTIR spectroscopy and multivariate data analysis and trusted me enough to suggest me to develop the work at iBB and at Engineering & Health Laboratory.

I would like to thank to Professor Ana Fernandes Platzgummer also for accepting being my supervisor during this thesis on a so interesting matter and for allowing me to attend the laboratories of the iBB, TagusPark.

Most important, I would like to thank to both supervisors for the continuous support and enormous knowledge throughout this thesis.

Also, I would like to leave my gratefulness to all colleagues at iBB, who enriched my personal experience and who helped me with patience, especially Raquel Cunha and Elga Vargas-Carreño. A tremendous thank you to both you for always doing your best at making me feel comfortable in TagusPark.

At Engineering & Health Laboratory, my gratitude goes to Rúben Araújo and to Luís Ramalhete as well, for their patience to listen to my concerns, being always available to talk and discuss, being there to answer to my endless questions and doubts or solving problems at any hour of the day.

Finally, I want to thank to my family and friends for being there for me, being able to calm me down and making me always smile in the most stressful moments.

Without all of you, this work would not be possible.

[This page is intentionally left blank]

Abstract

Mesenchymal stem cells (MSCs) obtained from different sources have been considered for cell therapeutics against several diseases, were its derived extracellular vesicles (EVs) are the primary mediators of the cells paracrine effect.

The present work aimed to evaluate the influence of different MSC sources, as adipose tissue, bone marrow and umbilical cord matrix on the molecular profile of EVs acquired by Fourier-Transform Infrared (FTIR) Spectroscopy after spectra pre-processing and its principal component and hierarchical cluster analysis. It was evaluated the EVs, MSCs and conditioned media molecular profiles in function of MSC source, MSC donor (i.e. 3 donors per source) and media composition (xenogeneic-free (XF) vs serum-containing medium (DMEM-FBS)). Two replicates cultures per donor were considered.

EVs were obtained from the MSC conditioned media based on a kit assay using a polymer that, however, absorbs on the EVs surface leading to an interference on the EVs spectra signal. The EVs high dilution factor leads to the polymer partial desorption, as observed by other authors. Due to variability of the desorption process, a lower reproductible spectra from EVs were obtained. Despite that, it was possible to observe that EVs molecular profile depended on the media type and, for each MSC source, on the MSC donor. It was also observed that EVs molecular profile obtained from DMEM cultures apparently presented a more homogenous chemical profile than EVs obtained with XF medium. Diverse ratios between infrared spectral bands were identified, that discriminate at a 5% significance, in mean terms, the EVs molecular profile in function of the culture medium composition.

The MSC spectra were also highly variable due to different growth patterns. Even so, it was possible to observe that MSC molecular profile depended on the culture media type, being observed a more homogeneous molecular profile when cells were cultured in XF than in DMEM medium. When grown on DMEM medium, it was possible to observe that MSC molecular profile depended on the MSC source. MSC molecular profile also apparently depended on the MSC donor.

A very similar conditioned media spectra were obtained from the different cultures and, consequently, higher reproducible molecular profiles were obtained in relation to MSC and EVs analyses. It was observed that conditioned media molecular profile depended on MSC source, MSC donor and culture media composition. A lower variable molecular profile was observed when using XF medium, as observed with MSC molecular profile.

From the EVs, MSC and conditioned media molecular profiles, the best reproductive results were obtained from the conditioned media, that pointed that it was affected by the MSC donor and source. The impact of the culture media type, MSC source and donor was also partially observed on the EVs and MSC molecular profile. All these results point to the impact of the culture media, MSC source and donor on the EVs molecular profile. Therefore, in therapies-cell based and based EVs-based, the impact of culture media, MSC source and donor should be considered.

Keywords: Mesenchymal Stem Cells, Extracellular Vesicles, FTIR Spectroscopy

Resumo

As células estaminais mesenquimais (CEM's) obtidas de diferentes fontes têm sido em diversas terapias celulares contra inúmeras doenças, sendo consideradas como mediadores dessas atividades as vesículas extracelulares (VEs) derivadas das CEM's. O presente trabalho teve como objetivo avaliar o efeito de diferentes fontes de CEM's, tais como de tecido adiposo, medula óssea e da matriz do cordão umbilical. O perfil molecular foi analisado por espectroscopia de infravermelho de Transformada de Fourier (IVTF) após o pré-processamento dos espetros e da sua análise de componentes principais e de agrupamento hierárquico. Foi avaliado o perfil molecular das VEs, CEM's e meios condicionados em função da fonte e dadores de CEM's (i.e., 3 dadores por fonte) e composição do meio (StemPro XenoFree (XF) vs DMEM). Efetuaram-se duplicados de culturas por dador.

As VEs foram isoladas de meios condicionados de CEM's a partir de um kit baseado num polímero. No entanto, o polímero absorve à superfície das VEs, interferindo no sinal espectral das VEs. Fatores de diluição elevados das VEs levam à desorção parcial do polímero, como observado por outros autores. Devido à variabilidade do processo de desorção, os espectros de VEs apresentaram uma baixa reprodutibilidade. Apesar disto, foi possível observar que o perfil molecular das VEs dependeu do tipo de meio e, para cada fonte, do dador de CEM's. Observou-se também que o perfil molecular de VEs de culturas de DMEM apresentaram aparentemente maior homogeneidade, em relaçao às VEs obtidas em XF. Foram identificadas diferentes razões entre bandas espectrais que discriminam a 5% de significância e em termos de média, os perfis moleculares de VEs em função da composição do meio de cultura.

Os espetros de CEM's também apresentam uma elevada variabilidade devido a padrões de crescimento diferentes. Mesmo assim, observou-se que o perfil molecular das CEM's dependeu do tipo de meio de cultura, havendo uma maior homogeneidade nos perfis moleculares das células cultivadas em XF do que em DMEM. O perfil molecular das células crescidas em meio DMEM dependeu da fonte de CEM's. O perfil molecular das células também dependeu aparentemente do dador. Foram obtidos espetros de meios condicionados muito similares e consequentemente, os respetivos perfis moleculares apresentaram elevada reprodutibilidade. Foi observado que os perfis moleculares dos meios condicionados dependem da fonte e do dador de CEM's e da composição do meio de cultura. Foi observado que os meios condicionados apresentaram perfis moleculares mais homogéneos quando as células mantidas em meio XF, tal como observado com o perfil molecular de CEM's.

Dos perfis moleculares de VEs, CEM's e meios condicionados analisados, os resultados mais reprodutíveis foram obtidos com os meios condicionados, que apontaram que o perfil molecular depende do dador e da fonte de CEM's. O impacto do tipo de meio de cultura, fonte de CEM's e dador foi observado parcialmente no perfil molecular de VEs e CEM's. Assim, nas terapias celulares e acelulares baseadas em VEs, deve ser considerado o impacto do meio de cultura, do dador e da fonte de CEM's.

Palavras-chave Células Estaminais Mesenquimais, Vesículas Extracelulares, Perfil Molecular, Espectroscopia de IVT.

Relevant publication in the master field

Proceeding

F.A.R. Pires, L.M. Ramalhete, E. Ribeiro, C.R.C. Calado. Impact of the solvent extraction method on the plasma metabolome profile. ENBENG-2019, 6th IEEE-EMB Bioengineering Portuguese Meeting, 22-23 February 2019, ISEL-Instituto Superior Engenharia de Lisboa, Lisbon, Portugal. **DOI:** 10.1109/ENBENG.2019.8692496. http://embs.ieee-pt.org/6th-enbeng-2019/program-overview/

Conference Communication

R.M.S. Cunha, E.J. Vargas, F.A. Pires, C.R.C. Calado, J.M.S. Cabral, C.L. da Silva, A. Fernandes-Platzgummer. Towards the development of standardized and robust platforms for the production and characterization of mesenchymal stromal cell-derived extracellular vesicles. ISEV Workshop: open, reproducible and standardized EV research. ISEV-International Society for Extracellular Vesicles. 2 December, Ghent University, Belgium.

[This page is intentionally left blank]

Índice

List of Figures

List of Tables

List of Abbreviations

ApoBDs	Apoptotic bodies
AT	Adipose tissue
ATR	Attenuation total reflection
BM	Bone marrow
BMT	Bone marrow transplantation
CFU-f	Colony-forming unit-fibroblast
DF	Dilution Factor
DLS	Dynamic light scattering
DMEM	Dulbecco's modified eagle medium
DMSO	Dimethyl Sulfoxide
ECM	Extracellular matrix
ECSs	Embryonic stem cells
EVs	Extracellular vesicles
FBS	Fetal bovine serum
FDA	Food and Drug Administration
FGF	Fibroblast growth factors
FIR	Far-infrared
FTIR	Fourier-transform infrared
GVHD	Graft versus host disease
HCA	Hierarchical cluster analysis
HGF	Hepatocyte growth factor
HSCs	Hematopoietic stem cells
IL	Interleukin
iPSCs	Induced pluripotent stem cells
IR	Infrared
ISCT	International Society of Cellular Therapy
ISEV	International Society of Extracellular Vesicles
MHC	Major histocompatibility complex
MIR	Mid-infrared
miRNA	MicroRNA
MSC	multiplicative scatter correction
MSCs	Mesenchymal stem cells
MVB	Multivesicular bodies
MVs	Microvesicles
NIR	Near-infrared
NSCs	Neural stem cells

NTA	Nanoparticle tracking analysis
OSCs	Oligopotent stem cells
PCs	Principal components
PEG	Polyethylene glycol
SEM	Scanning electron microscopy
SG	Savitzky-Golay
SNR	Signal-to-noise ratio
SNV	Standard normal variate
TEM	Transmission electron microscopy
tRPS	Tunable resistive pulse sensing
UC	Ultracentrifugation
UCM	Umbilical cord matrix
XF	Xenofree

[This page is intentionally left blank]

Chapter 1: Introduction

1.1. Stem Cells

The concept of stem cells is not new, dating from 1975, and it was an accidental discovery, as many others in science, of James Till at the Toronto's University.[1] Stem Cells are unspecialized cells that have specific and fundamental proprieties for categorize a cell as a stem cell.[2] These proprieties are the ability to proliferate and to self-renew during cellular division, that enables to preserve the stem cells' unspecialized status; the ability to differentiate themselves into a diverse range of specialized cell type, depending on the developmental potency of stem cells.[2,3] Consequently, stem cells are classified according to their potency as a totipotent, pluripotent, multipotent, unipotent and oligopotent.[4]

Totipotent stem cells, such as zygote until it achieves the first eight cellular conformations, have the highest potential to give rise to all types of cells and extra-embryonic structures. Pluripotent stem cells have the capacity to differentiate into all derivates of the germ layers (endoderm, mesoderm and ectoderm). Completely pluripotent stem cells are, for example, embryonic stem cells (ESCs) and induced pluripotent stem cells (iPSCs). iPSCs are reprogrammed to assume an embryonic stem cell-like state by inducing factors for maintain the similar properties of ESCs. The biggest advantage of iPSCs is that do not apply the ethical issues associated with ESCs, which means that problems as immune rejection or infection after transplantation are suppressed potentially.[5–7] Multipotent cells can only give rise to cells of the tissue from which they are isolated. Examples include mesenchymal stem cells (MSCs), hematopoietic stem cells (HSCs) and neural stem cells (NSCs). Oligopotent stem cells (OSCs) can differentiate into a few cell types, such as lymphoid or myeloid stem cells. Unipotent stem cells can produce only one cell type, their own, maintaining the ability of self-renewal. [4,8,9]

Furthermore, stem cells can be classified into four broad types based on their source: embryonic stem cells, fetal stem cells, infant stem cells and adult stem cells. Adult stem cells have been recognized for their regenerative potential due to being essential cells to provide the tissue maintenance and to repair damaged cells, restocking them [4,10]

1.1.1. Mesenchymal Stem Cells

1.1.1.1. Background

Mesenchymal Stem Cells (MCSs) are adult multipotent stem cells and originate in the human embryo. Due to their characteristics and to their multipotentiality, these cells have become an activity of growing importance over the years in science research as well as in clinical field. The **figure 1.1** shows the increasing publications of scientific articles until today in mesenchymal stem cells fields. There are more than one-hundred thousand papers published about MSCs, as well as more than 900 MSC clinical trials in the world. The most of them still in early-stages but nevertheless they have

demonstrated safety and efficacy.[11] In addition, this great interest with MSCs is due to these cells show superior properties for cell therapy and regenerative medicine use compared to using other cells such as ESCs and iPSCs in these situations, namely, the low risk associated of teratoma formation[12] and the free involvement of ethical issues.[13]

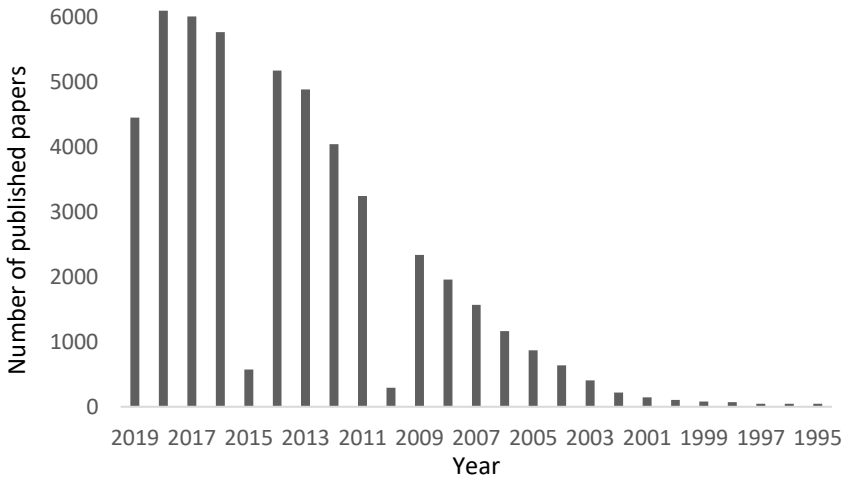

Figure 1.1 Number of published papers per year that were obtained with keyword Mesenchymal stem cells. Data obtained from Pubmed

The discovery of MSCs dates back to the early 1900's when the German pathologist Julius Cohnheim suggested the presence of non-hematopoietic progenitors in bone marrow and that these progenitors had a fibroblast-like morphology, with the bone marrow as a source of fibroblasts in wound healing.[14,15] Based on the Russian scientist Alexander Maximow's proposal of the existence of a type of precursor cell within the mesenchyme that could differentiate into a variety blood cell type[16], Friedenstein and colleagues, in the 1960s and 1970s, isolated, from bone marrow cultures, plastic-adherent, fibroblast-like appearance, clonogenic cells, designed by colony forming unit-fibroblast (CFU-f) with a high proliferative capacity *in vitro*, which were multipotential and could differentiate into osteoblasts, chondrocytes, adipocytes and hematopoietic supporting stroma when a single CFU-f was re-transplanted *in vivo.* [15–18] Only two decades later, after studies following the findings of Friedenstein and in light of the capacity of differentiation and of emerging link to the embryonic development of various mesenchymal tissues, Arnold Caplan coined the term of the "mesenchymal stem cell". [19,20]

1.1.1.2. MSC Characterization

Since the discovery of MSCs, a consensus about the definition of them was never thoroughly uniformed among investigators, thus to standardize designations and methods of isolate and expand MSCs, in 2006, the International Society of Cellular Therapy (ISCT) proposed criteria for the minimal identification of MSCs: adherence to plastic under standard culture conditions, expression of surface markers CD105, CD73, and CD90, lack of expression of surface markers CD45, CD34, CD14 or CD11b, CD79α or CD19, and HLR-DR, and *in vitro* differentiation into osteogenic, chondrogenic, and adipogenic cell lineages.[17,20,21]

1.1.1.3. MSC Culture Conditions

The need to cultivate MSCs in a defined medium is important for homogeneity between cell production processes. Traditionally, the media for MCSs expansion in clinical protocols is Dulbecco's modified Eagle's medium (DMEM) supplemented with animal serum, typically 10% fetal bovine serum (FBS). Although these media are simples, inexpensive and convenient for *in vitro* MSC culture, they contain an animal derived (xeno) source of growth factors and immunogenic proteins (from FBS) that might be transmitted to the recipient of MSC therapy. Moreover, the composition of FBS remains unclear and often there are significant variations between lots which consequently might cause unexpected cell growth characteristics, cytotoxicity. [22,23] Nevertheless, clinical trials with FBS have been approved by the US Food and Drug Administration (FDA) due to this risk of transmission being considered small and there have been no reports of adverse effects. Alternatively, available pre-defined xeno-free (XF) culture medium preserve the functional properties of MSCs and therefore they should be encouraged and a better option.[24–26]

1.1.1.4. MSC Sources

MSCs, originally identified from bone marrow (BM), can be isolated from almost every tissue of the organism, including adult sources such as adipose tissue (AT) and Peripheral blood, as well as perinatal sources such as umbilical cord matrix (UCM), placenta and many other tissues. Although BM was the main MSC source during several years, the quantify of MSCs found in it is very low and ranges from 1/10000 to 1/100000 of cells in the BM tissue, depending to the donor´s health, age and exposure to environmental stresses. Therefore, potential alternative and main sources for clinical use are AT, BM and UCM. The **figure 1.2** represents the different sources of MSC.

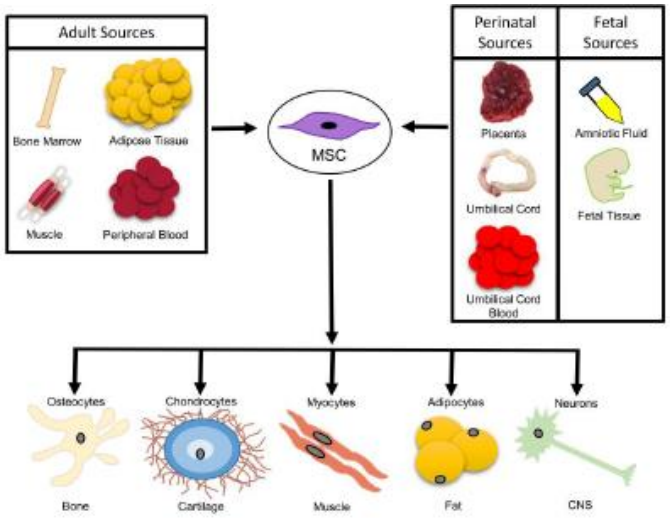

Figure 1.2 MSC Sources and their differentiation's potential [29]

Yet MSCs that are derived from adult sources result in invasive and difficult procedures that cause discomfort and eventual adverse effects to the patient/donor. On the other hand, UCM is considered most suitable because it is free from ethical issues and easy to isolate via non-invasive

methods.[27–30] The **table 1.1** describes a brief comparison between three sources along their characteristics and dis/advantages.

Table 1.1 Comparison of MSC sources: BM, AT and UCM. Adapted from[28–31]

Source	Differentiation Potential	Method of procurement	Advantages	Disadvantages
BM	Adipocytes, Astrocytes, Cardiomyocytes, Chondrocytes, Hepatocytes, Osteoblasts, Muscle cells, etc.	BM aspirate.	Potential to differentiate much like AT-MSC.	Procurement is painful. Risk of infection. Differentiation Potential depends on donor characteristics.
AT	Adipocytes, Chondrocytes, Osteocytes, Muscle cells.	Lipid aspirate.	Less Invasive. Large quantities. High isolation efficiency. Proliferative.	Inferior differentiation Potential.
UCM	Adipocytes, Chondrocytes, Osteocytes, neurons, hepatocytes.	Umbilical Cord (from childbirth).	Noninvasive. Proliferative. More desirable source: routinely discarded after delivery as biological waste. Ready availability.	Some differentiation abilities are partial.

1.1.1.5. Therapeutic Characteristics of MSC

The clinical therapeutic potential of MSCs focuses in their biological properties and functions. In fact, these cells have immunomodulatory proprieties based on the secretion of cytokines and soluble active and growth factors, acting as multidrug delivery vehicles. Other properties include ability to differentiate into various cell linages. migration to sites of inflammation and tumor microenvironments and, moreover, protect from injury and directly promote tissue repair/regeneration. [32–34] The promotion of tissue repair/regeneration and the modulation the immune system will subsequently be applied.

- **Promotion of Tissue Repair/Regeneration**

MSCs have dual functions in tissue regeneration and repair. First, they regenerate and repair tissues such as musculoskeletal tissues (bone, cartilage, ligament, tendon, muscle, etc.) and second, they provide a microenvironment for hematopoietic stem cells trough the secretion of trophic factors that have both autocrine and paracrine functions.[35] Furthermore, growth factors produced stimulate endothelial cells, fibroblasts and tissue progenitor cells *in situ*. Therefore the tissue repair is facilitated through angiogenesis, remodeling of the extracellular matrix (ECM) and the differentiation of tissue progenitor cells.[36] The **figure 1.3** describes both functions of MSCs.

An example of the idea that paracrine signals could play a key role in tissue repair is in cardio-protection, especially in myocardial infarction, where the increase in neo-angiogenesis and vascularization is crucial.[37] BM-MSCs have been participate in osteogenic and chondrogenic regeneration; AT-MSCs contribute to vessel formation and act as pericytes and *in vitro* differentiate

into hepatocyte-like cells in the presence of certain growth factors such as hepatocyte growth factor (HGF) and fibroblast growth factors 1 and 4 (FGF1, FGF4).[38] Other conditions where MSCs are being explored include orthopedic injuries, graft versus host disease (GVHD) following bone marrow transplantation (BMT), cardiovascular diseases, autoimmune diseases, and liver diseases.[37]

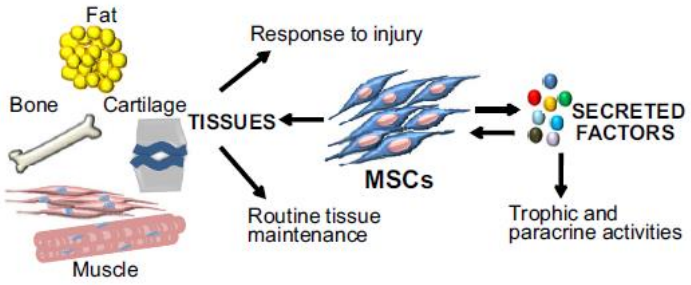

Figure 1.3: Dual functions os MSCs in tissue regeneration and repair. [35]

- **Modulation the Immune System**

The mechanisms underlying immunoregulation by MCSs are not fully understood due, not only, to that MCSs from different sources may differ in their capacities for immunomodulation, which induce to complexity of mechanisms. Although it is known that involve interactions between lymphocytes associated with both the innate and adaptative immune systems, as well as secretory mechanisms. MCSs suppress T cell proliferation, B cell functions, natural killer cell proliferation and cytokine production, and prevent the differentiation, maturation, and activation of dendritic cells. Also, MSCs recruit regulatory T cells (T_{reg}) and plasmacytoid dendritic cells to produce interleukin (IL)-10, which indirectly active suppress effector T cell.[33,35]

Considering the paracrine action of MSCs and the injection of condition media from MCSs was overexpressing the gene *Akt1* and, consequently, it would reduce acute myocardial infarction in rat models, therapeutically-active components were studied.[39] To highlight the fractioning of MSCs from condition media by ultracentrifugation, recovering the MSC's activity. Upon characterizing the pellet, vesicular structures with sizes between 80 nm and 1 µm were discovered, which were deciphered as microvesicles, a subtype of extracellular vesicles.[40]

1.2. Extracellular Vesicles

1.2.1. Background

Extracellular Vesicles (EVs) were first discovered during maturation of sheep reticulocytes in the 1980s.[41] Under various physiological and pathological conditions, namely during cellular activation, many cell types secrete EVs including B cells, dendritic cells, mast cells, T cells, platelets, Schwann cells, tumor cells, sperm, neuronal cells, endothelial cells, MSCs, and others. They are also

found in physiological fluids such as normal urine, plasma and bronchial lavage fluid.[42–44]

Similar with stem cells, there are than one-hundred thousand papers published about EVs and the tendency is to go on increasing the numbers of publications in therapeutic field (search term "extracellular vesicle" at *https://www.ncbi.nlm.nih.gov*). Due to increasing interest of EV-based therapies, there are 32 clinical trials associated with its application, of which 4 are at stages 3 and 4. [11]

To further increase the number of EV therapeutic applications, it is critical to optimize the EV production in function of cell culture, MSC type and donor. For that it is relevant to study the influence of these parameters on EV molecular characterization.[45]

1.2.2. **EVs types**

EVs are nano-sized and heterogenous lipid membrane-bound involved in important processes such as immune responses, homeostasis maintenance, coagulation, inflammation, cancer progression, angiogenesis, and antigen presentation, participating in both normal physiological and pathological conditions.[46] The EVs are diverse and their quantity and quality depend on the type and origin of the cells that release them, thus, they can be classified based on their cellular origin/biogenesis and physicochemical properties.[47]

Based on the vesicles' biogenesis, there are three main classes of EVs: apoptotic bodies (ApoBDs), microvesicles (MVs) and exosomes. The last two EVs are formed by viable cells and they are smaller EVs. Exosomes are formed by inward budding of early endosomes and secreted by fusion of these multivesicular bodies (MVB) with the plasma membrane. MVs are created by direct outward budding of the plasma membrane. ApoBDs are the largest vesicle and they are generated upon programmed cell death-induced membrane budding.[48–50]

The **figure1.4** schematics the major paths for biogenesis and secretion of EVs and the **table 1.2** describes the protein/genetic material content, size characteristics as well as the cellular origin and surface markers that distinguish the three EV's subtypes. In general, the content, or cargo, of EVs consists of lipids, nucleic acids, and protein, specifically proteins associated with the plasma membrane, cytosol and those involved in lipid metabolism. The more specific EV's contents may reflect cellular origin and function of EV's subtype.[51]

As can be seen in **table 1.4**, there is no strict border separating different EV subtypes since their size distribution and their cargo molecules are very similar. Consequently, for example, highly purified exosomes completely devoid of other EV subtypes are difficult to obtain after isolation, then until a reproducible method for their isolation which clearly specifies and distinguishes all the subtypes, there are no absolute certainly in determined case that this is an only one subtype.

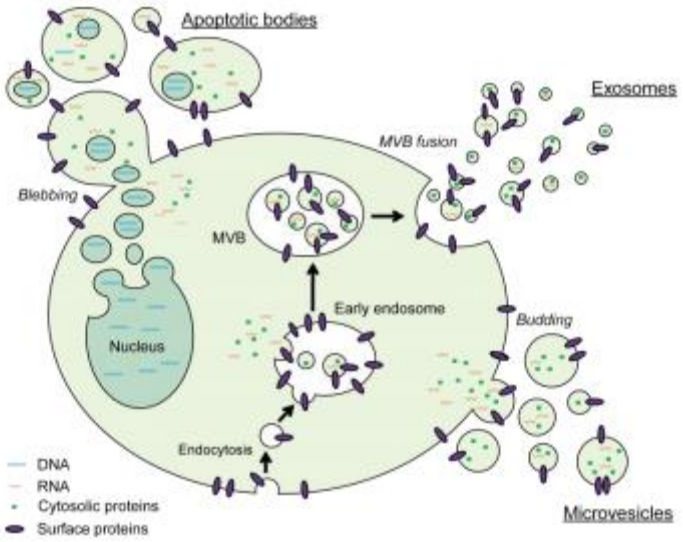

Figure 1.4 The family of EVs can be separated into three major classes based on their biogenesis: exosomes, microvesicles and apoptotic bodies. [50]

In fact, when EV's are isolated not only the desired structures are attained, some contaminants of intracellular matrix and extracellular environment, such as proteins, lipoproteins and nucleic acids are co-isolated with EVs. Furthermore, the problem associated with supplements (such as FBS) from cell culture continues, leading to a potential over-estimation of, for example, the protein cargo of EVs or/and contributing to their function and to significant inconsistencies of results.[47]

Table 1.2 Key features of exosomes, microvezicles and apoptotic bodies, including their origin, size, markers and contents. [42,47,52,53]

Vesicle Type	Origin	Size (nm)	Markers	Contents
Exosomes	Endolysosomal pathway; Intraluminal budding of MVBs; Fusion of MVB with cell membrane	40 -120	Tetraspanins (TSPAN29 and TSPAN30) ESCRT components; PDCD6IP, TSG101, flotillin, MFGE8	mRNA, microRNA (miRNA) and other non-coding RNAs; cytoplasmic and membrane proteins including receptors and major histocompatibility complex (MHC) molecules
Microvesicles	Cell surface; outward budding of cell membrane	50-1000	Integrins, selectins, CD40 ligand	mRNA, miRNA, non-coding RNAs, cytoplasmic proteins and membrane proteins, including receptors
Apoptotic bodies	Cell surface; Outward blebbing of apoptotic cell membrane	500-2000	Extensive amounts of phosphatidylserine	Nuclear fractions, cell organelles

1.2.3. **Characterization**

Due to the heterogeneity of EVs and to the difficulty to describe many their properties and mechanisms [44], it is important to standardize the isolation and characterization methods to be possible not only to generate comparable data but also to transform EV-based diagnostics into clinical use. Thus, the International Society of Extracellular Vesicles (ISEV) established some minimal parameters for the study of EVs [54] and to interpret and reproduce the experiments. These parameters are based on the sample collection and storage, isolation/separation and characterization methods.

- **Sample collection and storage**

Blood fluids (serum and plasma) are the most commonly used biofluids in EVs studies, but it is also possible to isolate EVs from cell culture supernatant.[55] Once isolated, aliquots of EVs are stored at -70 to -80ºC until use for up to a year and they should undergo only one freezing/thawing cycle. In spite of that, in diverse studies, it was observed that multiple freezing cycles do not affect the size and composition of EVs.[56] However, storage at -20ºC result in a major loss of EVs, while storage at -80ºC don't have no effect on the EV recovery. Some authors, have observed, however, that the size/diameter of EVs decrease with the duration of the storage period (for 2 days) and at 4 ◦C and 37 ◦C, indicating a structural change or degradation.[57,58]

- **Separation/isolation methods**

There are six main methods for isolating EVs from biologic fluids or cell culture medium: differential ultracentrifugation, density gradient centrifugation, size exclusion chromatography, polymer-based precipitation, filtration and immunoaffinity capture. Each of these methods can be applied in combination to obtain a higher enriched suspension of purified EVs.[47]

As can be seen in **table 1.3,** where the characteristics of these methods are summarized including the respective principle as well as advantages and challenges of each one, all of them have limitations such as co-isolation of contaminating materials, loss of EV components due to damaged membrane integrity during isolation. Also, there is the failure to completely isolate EV fractions due to the problem of removal of serum proteins and lipoproteins.[52]

The most common method is ultracentrifugation, as used in early exosome studies[41], where these vesicles precipitate at equivalent g-forces to 10,0000g [47]. In addition to the traditional methods, there is the development of commercially isolation kits that involve a decrease in the solubility of EVs in solutions of hydrophilic polymers, such as Polyethylene Glycol (PEG).[59] These methods are usually simple, fast, and scalable; and do not requires ultracentrifuges, which makes this method most attractive for clinical research.[51,60,61]

Nevertheless, there are disadvantages that include the precipitation of the proteins on the outer

membrane of EVs along with contaminating proteins of non-EV origin, which could interfere with analysis of the sample by mass spectrometry, proteomic analysis, RNA assay. [62–64]

Table 1.3 Commonly used EV isolation methods and their principle as well as advantages and some challenges.[47,65]

Isolation method	Principle	Advantages	Challenges
Polymer-based precipitation	Reduction of EVs' aqueous solubility in the presence of PEG	Fast; Simple	Low purity Protein Contaminations Precipitant interferences
Differential Ultracentrifugation	Sedimentation under high centrifugal forces based on density and particle size	Common EV sub-fractioning	EV aggregation Possible loss of function
Density Gradient Ultracentrifugation	Based on buoyant density in a density gradient under high centrifugal forces	Common EV sub-fractioning; High purity	Gradients may interfere with EVs' activity Possible loss of function Time consuming
Ultrafiltration	Based on the size of different particles using membrane filters	High concentration	Aggressive Bias towards pressure-resisting EVs
Size Exclusion Chromatography	Based on the size: penetration of smaller particles into the pores of a matrix material during elution through a column	High purity; Removal of soluble proteins	Low yield Need of further concentration steps
Immunoaffinity	Based on EV phenotype: Capturing different EVs owing to specific molecules present on their membranes	Fast; High purity	Low yield Expensive Bias towards known markers containing EVs

- **Identification and Characterization**

There are typically two different types of analyses performed on the isolated vesicles: physical and chemical/biochemical/compositional analysis. Physical analysis, which quantifies the number of EVs in a sample volume and their size distribution or/and confirms EV structure, can be done e.g. by nanoparticle tracking analysis (NTA), dynamic light scattering (DLS), transmission electron microscopy (TEM), scanning electron microscopy (SEM) and tunable resistive pulse sensing (tRPS). The chemical/biochemical/compositional analysis is typically done via staining, immunoblotting, or omics analysis, and gives information regarding the content and the origin of the isolated vesicles.[50,51]

Currently the OMICS technologies, including genomic, transcriptomic, proteomic and metabolomic, are alternative methods to obtain a molecular profiling of EVs and, consequently, to create a database of protein, lipid and metabolite contents of EVs.[55] Liquid chromatography (nanoscale or ultra-high performance)–electrospray ionization tandem mass spectrometry (LC/ESI–MS/MS) is the most popular and versatile analytical technique to study the molecular contents of EVs.[66,67] Vibrational spectroscopy represents an interesting approach to explore the EVs whole molecular composition in a highly sensitive and specific mode, as conducted for characterizing diverse biofluids. Furthermore, the technique it is rapid and economic to apply, representing therefore an interesting technique to be applied routinely as pointed in the following sections.[68]

1.2.4. **Mesenchymal Stem Cell-derived Extracellular Vesicles**

The interest for the therapeutic applications of EVs has exponentially increased as these microparticles may reproduce the effects of parent cells. Besides the soluble factors produced by MSCs, EVs have been identified as important players of the paracrine activity and thus as a part of MSC secretome.[65] In fact, EVs could mediate the immunomodulatory effects of MSCs. For example, the injection of human UCB-MSCs may cause tumor spreading and consequently tissue ossification in animal models. Exosomes derived from MSCs have the reform relevant functionality but minimizing the concerns about the direct use of cells (i.e. MSCs).[69]

EVs can be regarded as signalosomes in that it is multifunctional signaling complexes for controlling crucial cellular and biological functions.[53] An example for this multifunctionality is the roles of exosomes derived of AT-MSCs that include to induce the proliferation of human dermal fibroblasts and promote their mobility; to inhibit the differentiation of T cell; to promote angiogenesis of human umbilical vein endothelial cells; to protect osteocytes from apoptosis by suppression/expression of genes; to promote neurite outgrowth.[70] In addition, EVs secreted by human-MSC carry hyaluronan on their surface which can interact with proteins and proteoglycans of extracellular matrix to maintain tissue homeostasis and contribute to extracellular matrix remodeling and tissue healing.[65]

MSCs release EVs differently depending on external stimulation, suggesting that this process is regulated by cross-talk between MSCs and their surrounding microenvironment.[71] In fact, the EVs' composition may be modified as well as their functional proprieties in conditions such as hypoxia and inflammation. Moreover, MSCs from different sources have been shown to have distinct EVs composition.[72]

Characterization of MSC-derived EVs revealed the presence of the transmembrane proteins CD107, CD63, CD9 and CD81, also the expression of MSC phenotypic markers, such as CD29, CD73, CD44 and CD105.[73,74] MSC-EVs are enriched with miRNAs, which are selectively sorted into EVs and protected from degradation. The release of MSC-EVs allows cells to communicate with other adjacent or distant cells by transferring miRNAs and other biologically active molecules into recipient cells via endocytosis and/or fusion. The effects of MSC-EVs are dependent on the profiles of their miRNAs, which regulate the expression of multiple target genes and participate in various cell signaling processes.[75]

Thus, MSC-derived EVs have innate therapeutic potential for driving tissue regeneration. They can induce angiogenic programs in quiescent endothelial cells, suppress apoptosis and stimulate cell proliferation, deliver immunomodulatory signals as well as recruit and reprogram cells that are required for tissue regeneration[53], as can be seen in the **figure 1.5**.

Furthermore, EVs are a promising source of biomarkers for various diseases and represent interest for noninvasive or minimally invasive diagnosing, assessment of antitumor therapy efficiencies, and disease prognosis.[76] The advantages of EVs as biomarkers and/or source of

biomarkers in relation to the direct analysis of the tissue, include: EVs are easily accessible (non-invasive way) and amenable to functional and molecular analysis; analysis of circulating EVs would represent a “liquid biopsy” with the advantage of not requiring the partial or total removal of tumors to get information about their molecular genetics landscape and allowing repeated analyses over time.[77]

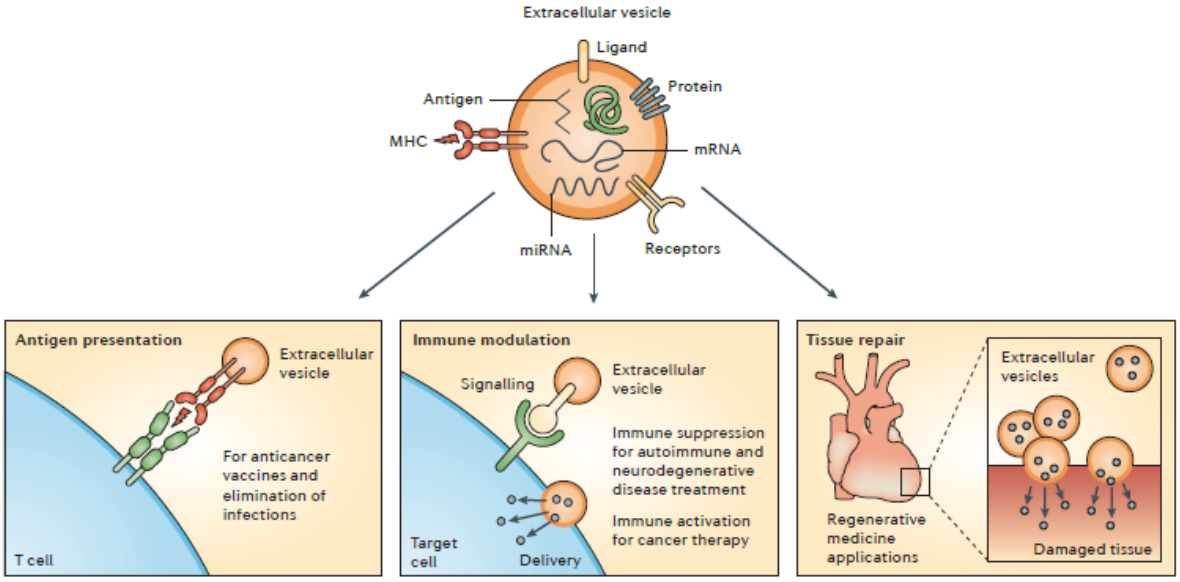

Figure 1.5 Extracellular vesicles as therapeutic agents. They have immunomodulatory effects including the antigen transfer and presentation for anticancer vaccines and elimination of infections by priming specific $CD8^{+}T$ cells; modulation of immune responses in a desired direction either by antigens events; tissue repair can depend on the exosome transfer of growth factors, soluble proteins, bioactive lipids and genetic material, such as miRNA. [53].

1.3. Infrared Spectroscopy

There is a need for fast, simple, label-free and reliable methods for EV characterization, were spectroscopy methods have attracted attention for that due to the speed and precision of the sample analysis, providing diagnosis of various diseases in an early-stage.[68] Infrared (IR) spectroscopy is a candidate for that since it is provides solution, for example, for problems associated with colorimetric assays used in protein determination/characterization. In fact, these assays are based on indirect detection of a secondary reaction, whose signals change over time. Thus, the protein signal also changes, and its quantification is compromised. In contrast, the stability of the IR signal over time as well as the compatibility with detergents and reducing agents, make IR-based quantitation a more convenient, flexible, universal approach to measuring e.g. protein levels in complex mixtures.[78]

1.3.1. Concepts of Infrared Spectroscopy

Spectroscopy is defined as the study of electromagnetic radiation with matter and of properties that vary with frequency or wavelength. Depending of the radiation involved and of the interaction's nature between radiation and matter, there are different types of spectroscopy, such as atomic, ultraviolet and visible, Raman and infrared spectroscopy. The principal detection methods in spectroscopy are based on *absorption* (when matter absorbs the emitted radiation); *emission* (when radiation is emitted by matter); *reflection* (when the radiation emitter by a source reflects on matter); among others.[79]

Transmission spectroscopy is the oldest and most straightforward IR method. This technique relies upon IR radiation absorption at different wavelengths, and can be applied to liquid, solid or gaseous samples[80] There are two other modes: Transflection and Attenuated Total Reflectance (ATR). The first is based on the absorption of IR radiation after transmission through the sample, reflection off the substrate and transmission back through the sample. The second operates on the principles of total internal reflection.[81]

The different types of spectroscopy techniques in function of the electromagnetic radiation are summarized in **figure 1.6** where the IR region is highlighted with corresponding values of wavelength, wavenumber, frequency and energy. IR region covers a wavelength range between 700 nm and 1 mm that results in different vibration or rotation modes of atoms in a molecule, depending of spectral region and physical phases of molecule.

The IR region may be subdivided into three regions defined as near-IR (NIR) at a wavenumber between 1350 and 4000 cm^{-1} where the highest portion is associated with overtones and combinations of bond vibrations; mid-IR (MIR) at a wavenumber between 4000 and 400 cm^{-1} that focus fundamental vibrations; and far-IR (FIR) at a wavenumber between 400 and 10 cm^{-1} that it is the lower energy region in the spectrum and used for rotational spectroscopy.[82]

Radiation Type	γ-Rays	x-rays	Ultraviolet	Visible	Infrared	Microwaves	Radiowaves
Molecular Effects	Ionization		Electronic transitions		Molecular vibrations	Rotational motion	Nuclear spin transitions

	NIR	MIR	FIR
Wavelength (μm)	0.78 – 2.5	2.5 – 25	25 – 1000
Wavenumber (cm^{-1})	13500 – 4000	4000 – 200	200 – 10
Frequency (THz)	120 – 384	12 – 120	0.3 – 0.05
Energy (eV)	0.5 – 1.59	0.05 – 0.5	0.0012 – 0.05

Figure 1.6 The electromagnetic radiation effect on molecules and the three regions from infrared region (near-IR, mid-IR and far-IR). (adapted from[83,84])

1.3.2. **Molecular Vibrations**

IR spectroscopy is a form of vibrational spectroscopy, where the irradiation leads to the sample vibrational motions.[85] For a nonlinear polyatomic molecule with N atoms, there are 3N-6 degrees of freedom, or 3N-6 fundamental vibrations of the molecule atoms or normal modes (*infrared active*). Examples of "*infrared inactive"* molecules are homonuclear diatomic molecules (e.g., O2, H2, N2) and monoatomic molecules, composed of only one type of atom (e.g., Ar, He, Ne). [86]

The absorb radiation occurs in the IR region when two conditions are satisfied: first, there must be coincident (resonance) among the frequencies of the IR radiation and vibration of the chemical bond of molecule; second, the natural vibration must cause change in the electric dipole moment during vibration, *i.e.*, the energy is absorbed by the molecule and the molecule is promoted to an excited state.[87]

Different functional groups absorb radiation at different wavenumber ranges and thus originate characteristic spectral peaks and reveal information of most chemical bonds within the molecules.[88] Functional groups can be associated with characteristic infrared absorption band, which correspond to the fundamental vibrations of the functional groups, as summarized in the **Table 1.4.**

Table 1.4 Short summary of some of the important vibrational frequencies within the MIR region of the electromagnetic spectrum (ν, stretching; γ, wagging, twisting, and rocking; as, antisymmetric; s, symmetric). (adapted from [89–91]).

Wavenumber (cm^{-1})	**Functional group**	**Vibrational mode**	**Biochemical component**
X-H stretching (where X is C, O or N): 4000–2500 cm^{-1}			
3400-3300	N-H	ν(N–H)	Amide A: peptide, protein
~3100	N-H	ν(N–H)	Amide B: peptide, protein
2957	C-CH_3	νas(CH_3)	Lipids
2920	–$(CH_2)_n$-	νas(CH_2)	
2872	C-CH_3	νs(CH_3)	
2851	–$(CH_2)_n$-	νs(CH_2)	
Double bonds stretching: 2000–1500 cm^{-1}			
~1655	O=C-N-H	80% ν(CO), 20% ν(CN)	Amide I: peptide, protein
~1545	O=C-N-H	60% γ(N–H), 30% ν(C–N), 10% ν(C–C)	Amide II: peptide, protein
~1740	-CH_3-COOR	ν(C=O)	Phospholipid esters
Fingerprint region (overlapped vibrations): 1500–600 cm^{-1}			
1400-1200	O=C-N-H, CH_3	γ(N–H), ν(C–N), γ(C=O), ν(C–C) and ν(CH_3)	Amide III, protein, collagen, DNA, RNA, phospholipid, phosphorylated protein
~1060, 1050, 1015	C-O	ν(CO)	DNA and RNA ribose
~1095, ~1084	C-O, C-O-H	νs(PO_2–)	DNA, RNA, phospholipid, phosphorylated protein

Molecules vibrate in different ways, each way being a vibrational mode of its own. The IR spectra can contain many different absorptions and not just one per bond. Absorptions can be the result of a change in bond length (*stretching*), or the bond length can stay constant, but the bond angles change about their equilibrium values (*bending*). Stretching can be in-phase (*symmetrical stretching*) or out-of-phase (*asymmetrical stretching*). Bending vibrations can include various movements such as scissoring, rocking, wagging and twisting, as can be seen in **Figure 1.7.** Stretching absorptions usually produce stronger peaks than bending in the infrared spectrum; however, bending absorptions can be useful in differentiating similar types of bonds.[92,93] While the asymmetric vibrations of all molecules are detected, symmetric vibrations (with respect to the symmetrical center of molecule) are usually not detected in infrared (*infrared inactive*).

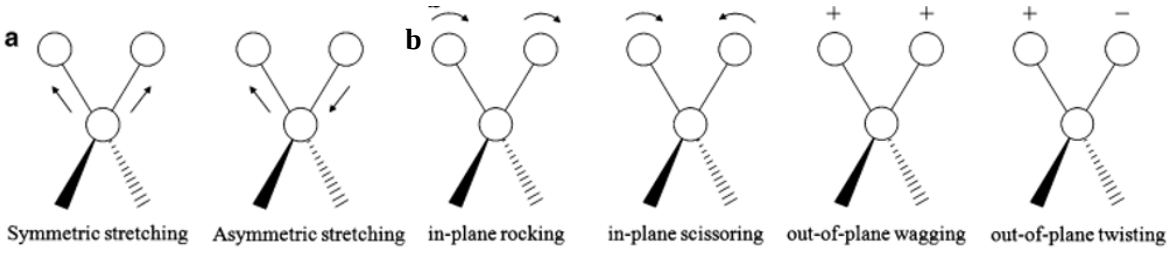

Figure 1.7 Molecular vibration modes of a molecule. Black arrows represent movements in the paper plane while white arrows represent movements out of the paper plane. (adapted from [92]).

In larger molecules, many vibrational modes involve the whole molecule. Some of these molecular vibrations are localized vibrations while others must be considered as vibrations of the entire molecule. Moreover, the more complex a molecule is, the more vibrational modes it has (*i.e*. degrees of vibrational freedom).[79] Various vibrational combinations are possible depending on the mass of the atoms that comprise the molecules, the way their geometry is arranged and the bonding forces between them. Thus, each molecule is unique in their representation on the IR spectrum, as there are no two alike.

1.3.3. **MIR Spectral Analysis**

Many of the IR bands of biological interest occur in the region 4000 and 400 cm^{-1}. This region is better suited to analyze biological samples because the fundamental bands measured with MIR than NIR, as yield a higher intensity and less convoluted spectra. Besides, MIR region is sensitive to the molecular composition of the sample and their microenvironment.[94] MIR spectra can also give information regarding the conformation changes of biomolecules (e.g., protein folding,[94–96] nucleic acids [97–99]).

Typical MIR spectra are approximately divided into four regions generalized as the X–H stretching region (4000–2500 cm^{-1}), the triple-bond region (2500–2000 cm^{-1}), the double-bond region (2000–1500 cm^{-1}) and the fingerprint region (1500–600 cm^{-1}). Finger print region is normally a complex area showing many bands specific to molecular structure of the sample, frequently overlapping each other.[82] For a visual reference of an IR spectrum in MIR region, a resultant spectrum from this work is presented on **figure 4.3 page 33**. To avoid redundancy no spectrum is present in this section. There is an extensive review [89–91] of application of FTIR spectroscopy on biological samples.

1.3.4. **IR equipment**

Historically, IR spectroscopy has been made possible using instruments called spectrometers. These were initially dispersive instruments that made use of prisms made of materials as sodium chloride. This dispersive element would be found within a monochromator. The first conventional dispersive IR spectrometers appeared in the 1940s, although in the 1960s developments in technology made the use of prisms obsolete in detriment of using diffraction gratings. In **Figure 1.8**, it is represented the optical path of a typical IR spectrometer that made use of a diffracting grating. Rudimentary parts of this instrument were a radiation source, a monochromator, and a detector, most frequently in a double-beam setup.[80,100]

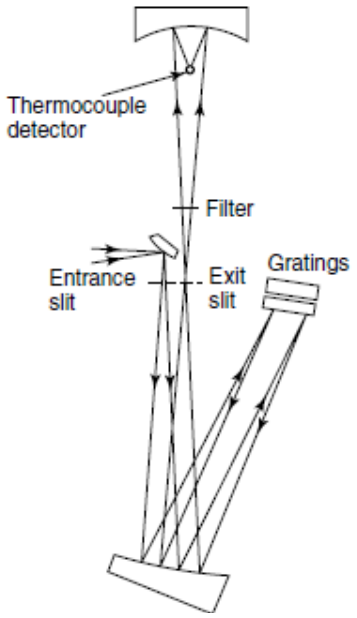

Figure 1.8: Schematic diagram of a double beam IR dispersive spectrometer with a grating monochromator as dispersive element. [80]

In this type of IR spectrometer, dispersion occurs when energy emitted from the **source** and focused on the entrance slit, is collimated onto the gratings, at which point the dispersed IR radiation is separated into the different wavelengths of the spectral range and reflected back to the exit slit, beyond which the thermocouple **detector** can be found. The dispersed spectrum is then scanned across the exit slit by rotating a component inside the monochromator. There was a major problem with this setup as the narrow slits at the entrance and exit of the monochromator limited the wavenumber range of the radiation reaching the detector to one resolution width. Consequently, a whole spectrum needed a long time to be recorded.[80,93] In addition, water plays a very important role in the IR spectrum. As such, atmospheric absorption of CO2 and H2O is taken into consideration in the design of infrared instruments. These limitations of the dispersive instruments are nowadays almost completely overcome by Fourier-Transform infrared (FTIR) spectrometers. For example, FTIR spectrometers provide automatic subtraction of water bands, since the mild drying of biological samples eliminates the excess of water from the system.[101,102]

Thus, the basic and common components of these spectrometers, that are represented schematically in **figure 1.9**, include a source, sample compartment, detector, amplifier, A/D convertor, and a computer. The source generates radiation which passes the sample through the interferometer/monochromator and reaches the detector. Then the signal is amplified and converted to digital signal by the amplifier and analog-to-digital converter, respectively. Eventually, the signal is transferred to a computer in which Fourier transform is carried out.[103]

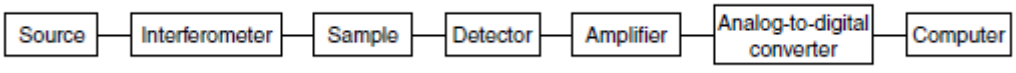

Figure 1.9 Basic components of a spectrometer. Interferometer is represented for the case of FTIR spectrometer. [80]

1.3.5. **Fourier - Transform Infrared (FTIR) Spectroscopy**

The FTIR spectrometer is the invention of the third generation IR spectrometer that marked the abdication of monochromator and the prosperity of interferometer. In fact, the major difference between both IR spectrometers is the Michelson interferometer.[100] It is the first interferometer, built in the 1880s, whose name is the inventor name. Even if modern FTIR spectroscopy equipment's aren't fitted with Michelson interferometers, the basis of operation of other interferometers is very similar.[80,103] The **figure 1.10** shows the setup of a Michelson interferometer.

Its way of working consists of the following. A collimated beam of monochromatic radiation leaves the source and upon reaching an ideal beamsplitter, it is divided into two separate beams. 50% of the incident radiation is reflected to one of the mirrors and the other 50% transmitted to the other mirror, which has a mechanism that allows its control and movement by a few millimeters. The two beams then recombine, and the resulting single beam is transmitted or reflected off the sample.

Given the fact that the two beams cover different distances before being reunited, this results in an interferogram, a signal that is a direct result of the two beams 'interfering' with each other. This signal is then decoded through the mathematical method called Fourier-transform to be able to obtain the final IR spectrum.[80]

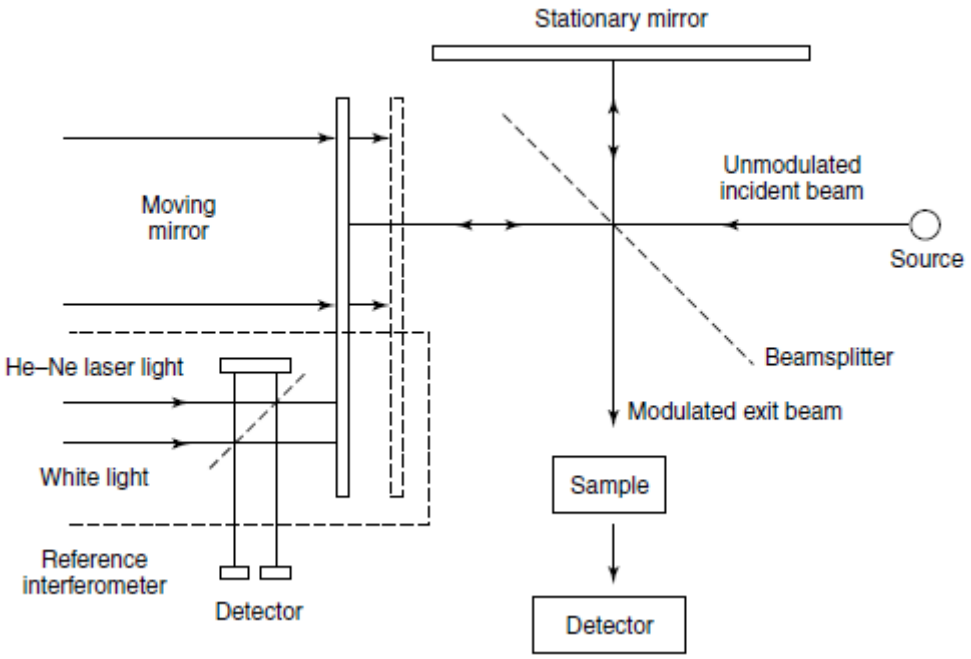

Figure 1.10 Schematic diagram of a Michelson interferometer. It consists of two perpendicularly plane mirrors, one of which is able to travel. A semi-reflecting film (beamsplitter) bisects the plane of these two mirrors. The beamsplitter material is chosen according to the region to be examined (potassium bromide or caesium iodide substrates are used for NIR and MIR regions). [80]

FTIR spectrometers have several prominent advantages, such as those summarized in the **table 1.5**, when compared to dispersive IR spectrometers.

Table 1.5 Advantages of FTIR spectrometers in relation to dispersive spectrometers. [92,103–105]

Advantage	Description
Multiplex (Fellgett)	Since all wavelengths are being measured at the same time, a decrease in the necessary time for spectra acquisition, which may take seconds instead of minutes, and a decrease in noise.
Throughput (Jacquinot)	Since the detectors used are much more sensitive and the optical throughput is much higher, scans are much faster, which results in its coaddition, reducing the levels of noise and, consequently, a higher signal (improved Signal to Ratio (SNR))
Speed	The ability of the mirror to move short distances in a rapid manner, in combination with the SNR improvements by the *Fellgett* and *Jacquinot's* advantages, make it possible to obtain spectra faster (in the order of milliseconds).
Frequency Precision (Conne)	A frequency precision and accuracy of better than 0.01 wavenumbers are achieved. This means that spectra collected can be quantitatively compared whether they were collected five minutes or five years apart.
Constant Spectral Resolution	The resolution of the measured spectrum is the same for all frequencies, not varied throughout the spectrum as is often true with dispersive instruments.
Mechanical simplicity	By having only one moving part (mirror), it is a very simple and easy to maintain equipment, requiring no external calibration.
Availability of powerful software	The sensitivity, speed of spectra acquisition and the precision have seen many companies betting on a wide variety of software that make full use of IR radiation for qualitative and quantitative analysis.

In the other hand, there are some disadvantages regarding to FTIR spectroscopy measurements require clear and detailed protocols describing about how to prepare and dry these samples, since IR is affected by the high absorption of the water and the heterogeneity of liquid or dried samples.[68] Moreover, media parameters, such as culture medium, growth temperature, etc., may cause differences in the spectral obtained. However, this could also be considered an advantage, as it can allow detecting the impact of different conditions in the biological physiology.

1.3.6. **FTIR spectroscopy and its applications**

Nowadays, FTIR spectroscopy has revolutionized infrared spectroscopy and is still evolving.[106] Since its inception, applications for FTIR spectroscopy have seen to increase and they are diverse: identification of microorganisms;[107] analysis of human biofluids on prostate cancer, through the transmission and ATR measurements of dried blood serum on calcium fluoride and films directly deposited on the ATR crystal, respectively;[108109] imaging of protein aggregation in living cells;[110] drug

resistance, using FTIR microspectroscopy to identify IR signatures of drugs actions in leukemic cells exposed to tyrosine kinase inhibitors;[111] online bioprocesses monitoring;[112] characterization of leucocytes;[113] flavonoids analysis, through the IR spectra's analysis of the sulfonic derivatives of quercetin and morin;[114] discovery of diagnostic and prognostic markers in cancer stem cells and other disease situations, like Multiple Sclerosis and Alzheimer's disease;[115116] among others.

- **MSCs and EVs' studies with FTIR Spectroscopy**

In the case of stem cells, the use of vibrational spectroscopy is aimed to search for possible spectral markers for identifying and characterizing these cells in tissues, as well as for monitoring the differentiation process.[117] That is where the most applications of FTIR Spectroscopy in Stem Cells' field focus on. For example, the use of FTIR microspectroscopy, which was supported by principal component and subsequent linear discriminant analysis (PCA-LDA), to discriminate different stages of embryonic stem-derived neural cells differentiation[118]; to identify of murine embryonic stem cells' development status *in situ* through possible changes in their macromolecular content during differentiation.[119] In another study, global structural and compositional changes in BM-MSCs of patients with beta thalassemia major (β-TM) were investigate by ATR-FTIR.[120]

Also, the ATR-FTIR spectroscopy is useful to investigate different subpopulation of EVs from Jurkat T-cell line and there are delicate changes in the spectral features of each subpopulation.[78] Furthermore, there is a patent that combine EVs and ATR-FTIR [121], a method analyses biological fluids collected from patients to form a spectral fingerprint of EVs isolated.

More recently, ATR-FTIR spectroscopy has been applied for the early diagnosis of oral cancer (OC) using computational-aided models, from the evaluation of the characteristics spectra of salivary exosomes from patients.[122] Thus, the most studies concentrate on ATR-FTIR method with few on transmission mode. In a found study, the transmission mode were used to probe the biomolecular changes that occur in monocytes during lipopolysaccharide stimulation as well as that occur as a result in the released MVs.[123]

Only a few studies that contemplate FTIR spectroscopy to analyze MSC-derived EVs, one of them is the FTIR works as a complementary method to investigate whether human UMSC-derived exosomes encapsulated in functional peptide hydrogels could increase the retention and stability of exosomes and improve heart function in a rat myocardial infarction model.[124]

1.4. Spectral Data Pre-Processing and Multivariate Analysis

Data analysis comprises pretreatment of spectra (to correct variation related with spectra acquisition; to reduce and correct for interferences such as overlapping bands, baseline drifts, scattering) [125] and further comparison by multivariate data analysis tools (to interpret more complex data and to handle the large data set).

Next it will be displayed a short theoretical introduction of the techniques used in this work.

1.4.1. **Pre-Processing**

The data can be appreciated to identify the presence of biased patterns or anomalous behaviors. This can be made by various forms depending on the type of data, such as by visual inspection of spectra; by Hotelling's T^2 versus Q residual charts using only the mean-centered spectra; SNR, measuring the signal at both amide I region (1620-1690 cm^{-1}) and noise in the signal-free region (1800-1900 cm^{-1}), further excluding spectra below a minimum value, among others.[126]

Atmospheric Correction

The presence of MIR absorbing molecules in the laboratory atmosphere, like H_2O and CO_2, is a well-known drawback of IR spectroscopy because the spectral contribution of atmospheric gases can hinder the accurate identification and quantification of target analytes.[127] Thus, in the most software, a reference spectrum and a sample spectrum are analyzed and transformed into a ratio spectrum without any H_2O and CO_2 bands, i.e., they are eliminated from spectra at various characteristic absorbance wavenumber like around the 2400 cm^{-1} region.

Baseline Correction

Spectral baselines can be distorted due to scattering, absorption by the supporting substrate, changing conditions during data collection or the variableness by instrumental factors. There are different methods for this correction which objective is to minimize unwanted spectral offsets, broad baseline distortions, positive or negative slopes, and other baseline effects in vibrational spectra.[128] Scattering and Rubber-band Correction are the two principal methods. Both divide spectra in n ranges of equal size (n being the number of baseline points). While the last one stretches the spectra down such that the minimum y-value of each spectral range of interest is used to fit a convex polygonal line (a rubber-band), which is then subtracted from the original spectrum, in the first one this rubber-band is created in such a way that at each point the slope of the baseline must be negative for an absorvance-like spectrum.[129]

Normalization

Normalization is used to minimize the effects (shifting and scaling effects) of source power fluctuations, scattering, variations in sample thickness and in sample quantify among others. The result of normalization is a spectrum which is scaled and offset correct at the same time.[125,128] However, the normalization might hide signal differences between samples at important bands, such as amide I and amide II; it also may introduce non-linearities.[126]

The methods can be grouped in two: a first group relating to the simpler normalization methods that only require the information from the spectrum; a second group where more complex normalization methods require reference spectra are comprised. Methods of the first group include,

the Peak Normalization, which scales spectra regarding a chosen peak or band, usually Amide I band, at around 1650 cm^{-1}, among others. Methods of the second group include, for example, the Multiplicative Scatter Correction (MSC), which deals with multiplicative scattering effects in reflectance spectroscopy. These unwanted scatter effects are removed from the data matrix prior to data modelling, by estimation of the correction coefficients (additive and multiplicative) and correction of the recorded spectrum.[130]

Derivatives

Derivatives are used to enhance spectral information, allowing to reveal some of the information that would be otherwise hidden in a spectrum. First derivative is used to enhance the **resolution of peaks.** The second derivative is helpful for more complex spectra where it can help to **resolve overlapped bands**, allowing to reveal peaks of interest. Thus, the second derivative is essential in the search of differences between groups or clusters, contributing for the selection of suitable peaks and searching for biomarkers. Although, derivatives reduce the signal in the transformed data and amplify the noise. This issue of noise amplification is minimized with Savitzky-Golay (SG) derivative, a derivative of the fitted polynomial at each point (with a chosen number of window points – fitting).[131]

1.4.2. Multivariate Data Analysis

Samples can be classified according to their IR spectrum by using qualitative analysis techniques based on pattern recognition methods. As well, quantitative analysis are well-suited in that it allows to know with precision and to what extent samples differ from each other.[81]

In qualitative analysis, the classification techniques can be divided into unsupervised and supervised methods. The first, that include principal component analysis (PCA) and hierarchical cluster analysis (HCA), among others, that doesn't require a prior sample knowledge. It can be used to get an overview of the of the complexity, heterogeneity and similarity of the dataset. And as well to control reproducibility of the measurements, and to check for outliers.[107]

In the second method, such as linear discriminant analysis (LDA), samples are identified from a classification model that was generated on a training set of samples with known categories. An assessment of the model performance was then executed by comparing the true categories with the predicted classifications of validation (test) samples.[81] The main disadvantage of these supervised methods is their dependency on labeling data. When the data set has many observations, it is very unwieldly to label each and every one of these observations. To solve this problem, unsupervised and supervised methods are often used in conjunction.[125]

The aim of multivariate analysis in this context is the extraction of most important features in the FTIR spectra of samples of different origin for further clustering and classifications according to distinct compositional characteristics. It requires algorithms that reduce the dimensionality of the

spectral information into a few key components allowing interpretation with minimal loss of information.[121]

Principal Component Analysis

PCA is used to reduce a set of variables into a smaller set of orthogonal and independent principal components (PCs) in the direction of maximal variation. It reduces the dimensionality and retains the most significant information for further analysis. PCs are defined as variance-scaled vectors in the variable space. The first PC demonstrates the maximum variance in the data and the second PC illustrates the largest residual variance along a direction orthogonal to PC1 and so forth. The higher-order PCs are progressively thought of as noise directions which accounts for noise component. Although the most variance is described indeed by the first two PC, the PC conjugations that best separate a given dataset in separate clusters may not be found in the two main PCs.

Each PC can be represented as a linear combination of the n unit vectors of the variable space. Each PC is also called a "loading" and a loading spectrum contains a variety of peaks, positive and negative. The coefficients in the linear combination that represent the PC indicate the contributions of each variable (wavenumber) in the original variable space. This represents the spectral variation in the dataset.[125,132]

Hierarchical Cluster Analysis

HCA is used to clustering different groups. There are mainly two different approaches in HCA: a *bottom up* approach (agglomerative HCA) and a *top down* approach (divisive HCA). In the first, it starts with all of the observations (spectra) in one cluster and then proceeds to split (partition) them into smaller clusters according to the variation in the spectra data sets. First, a distance matrix is calculated which quantifies the similarity of the spectra. Next, the two most similar spectra with the smallest inter-spectral distance, are determined. These spectra are combined to form a new cluster. The spectral distances between all remaining spectra and the new cluster are then recalculated. A new search for the two most clusters in then initiated. These objects are merged and again, the distance values for the newly formed cluster are determined. This procedure is performed n-1 times until only one cluster remains. In the second, the process starts with a single cluster and ends up with the same number of clusters as the number of observations in the data set. At every step, a chosen cluster is split in two based on a particular criterion. [125,133] The dendrogram is the main graphical tool of HCA. It is a tree-like display, in which the objects are clustered along the y-axis and the distance at which the cluster was formed is found along the x-axis.

Chapter 2: Study's objective and Tasks

The present study is a continuation from a previous one where it was observed that the molecular profile of BMMSCs-derived EVs, as analysed by FTIR spectroscopy, varies with the medium composition used to culture the cells, the MSC donor and the conditioned days. The main objective of this thesis is to further evaluate the influence of different sources of MSC (adipose tissue, bone marrow and umbilical cord matrix) on the molecular profile of EVs analysed by FTIR spectroscopy. To achieve this goal, the following tasks were defined.

- Conduct the expansion of MSCs and the production of MSC-derived EVs from 9 donors of three sources (adipose tissue, bone marrow and umbilical cord matrix) (3 donors/source) with XF or serum-contain medium;
- Isolate EVs from the conditioned medium with a commercial kit. Since the reagent kit strongly absorbs in the MIR region, the protocol of isolation of MSC-derived EVs will be optimized to minimize the presence of the reagent kit interference on isolated EVs;
- Characterize isolated EVs, MSCs and conditioned media by FTIR spectroscopy;
- Evaluate the effect of MSC sources, donors and culture media composition on the EV, MSC and conditioned media molecular profile.

Chapter 3: Materials and Methods

This work is divided in two major sections. The first one is the culture of MSCs and the production and isolation of MSC-derived EVs; and the second consist of analysis by FTIR spectroscopy and statistical evaluation.

3.1. Biological Assays

3.1.1. MSCs Culture and MSC-derived EVs Production

For this work, nine donors of MSCs, three of each source (AT, BM and UCM), from 5 passages, were use: M83A15, M86A15, M79A15 (BM-MSCs), L090724, L090602, L090403 (AT-MSCs), #2, #6 and #78 (UCM-MSCs). Additionally, for an initial test, the donor L140311 from AT-MSCs was used.

The human MSC used in this study are part of the cell bank of the Stem Cell Engineering Research Group (SCERG), iBB-Institute for Bioengineering and Biosciences at Instituto Superior Técnico (IST). Cells were stored in liquid nitrogen inside cryogenic vials (approximately 1mL) containing cell suspension in the appropriate growth media supplemented with 10% Dimethyl Sulfoxide (DMSO).

To start the MSCs culture, cryovials (containing cells from passage 2) were removed from liquid nitrogen, quickly placed in a 37ºC water bath for a short period (1-2 minutes) and when almost all the cell suspension reached a liquid state, transferred into a laminar flow hood. Then the contents of each vial were diluted in 5 mL of Dulbecco's Modified Eagle Medium (DMEM) supplemented with 20% common fetal bovine serum (FBS). Cells were centrifuged at 1250 rpm, 20ºC for 7 minutes. Then, the supernatant was discarded, the pellet was resuspended in DMEM supplement with 10% FBS and transferred into a T-flasks.

MSCs from three sources were expanded in two media: DMEM supplemented with 10% fetal bovine serum - MSC qualified (FBS) (further designated as DMEM10%FBS) and Stem Pro® MSC SFM XenoFree medium supplemented with 1% (v/v) of GlutaMAX™-I CTS™ and 1% (v/v) of Anti-mycotic-Antibiotic (*Amphotericin B, Penicillin, Streptomycin*) (further designated as XF).

MSCs were plated in Falcon tissue culture flasks of 25 cm^2 (T-25) and 75 cm^2 (T-75) in DMEM10% FBS (corresponding to passage 3 in **figure 3.1**) at a cell density of 3×10^3 cells/cm^2 and then incubated at 37ºC and 5% CO_2 in a humidified atmosphere (SANYO, CO2 incubator). The culture medium was exchanged from 3 to 3 days and the cell passage was performed when cells achieved a confluence of 70-90%. In total, two passages were done (from passage 3 until to passage 5). The following **figure 3.1** shows the outline of MSCs expansion. In passage 4, cells were plated in two T-75, one in DMEM10% FBS and the other in CellBind® Surface cell culture flasks in XF. In the next passage, passage 5, each of these T-flasks were duplicated, *i.e.*, MSCs plated in DMEM10% FBS were

transferred to other two T-75 in DMEM10% FBS and the same happened to the cells that were in XF, thus obtaining four T-75 for each donor (two in DMEM10% FBS and other two in XF). In total, there were 36 samples.

The passaging process was performed as follows. The exhausted medium was removed and saved in a Falcon tube for later. The cell layer was washed with a volume of 3-4 mL (T-25) and 5-6 mL (T-75) of phosphate-buffered saline (PBS) solution to remove any remnants of media which could inhibited future dissociative agent. This last one, Trypsin 0.05% for cells cultured with DMEM10%FBS and TrypLE™ Select Enzyme (10x) for cells cultured with XF, was added to the T-flask (2.5 mL for T-25 and 5 mL for T-75) and the cells were incubated at 37ºC for 3 minutes. After incubation, the culture flasks were observed under a microscope to make sure the process of dissociation led to a complete cell detachment. If cell detachment was confirmed, exhausted medium was added (twice the volume of DMEM10%FBS; if TrypLE™ was used as a dissociative agent, it was added an equal volume of exhausted medium) to neutralize the dissociative agent. The cell suspension was transferred to a Falcon tube and centrifuged at 1250 rpm for 7 min. After centrifugation, the supernatant was discarded, and the pellet was resuspended in 4 or 5 mL of culture medium.

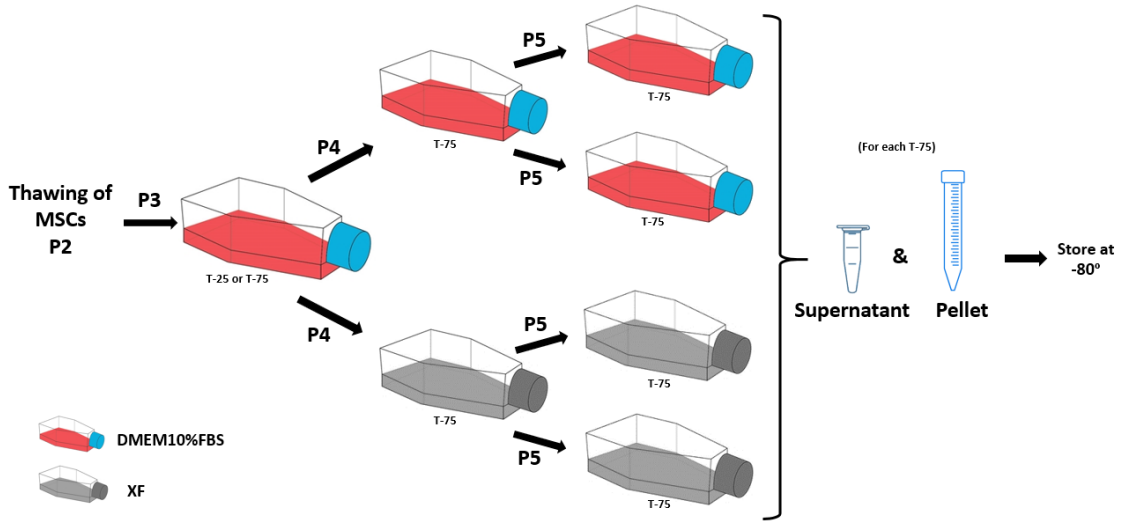

Figure 3.1 Outline of MSCs expansion. It is a process example for a sample from a donor. After the thawing process, where cells from passage 2 were thawed, the cell passage was performed when cells achieved a confluence of 70-90%. Initially (P3), the cells were plated in T-flasks with DMEM10%FBS and the next passage (P4) they were divided in two culture medium, XF and DMEM10%FBS. In the last passage (P5), the cultured cells in each culture medium were duplicated. After 48H of conditioning, the conditioned medium and the cells were collected and stored at -80ºC. For each MSC's source, there were three donors and for each them four T-flasks with cultured cells (two of each culture medium).

Cell number and viability were determined using the trypan blue exclusion method. 10 µL of cell suspension was mixed with 10 µL of 0.1% trypan blue stain, and 10 µL of the previous mixture was placed inside the hemocytometer's counting chamber. Viable (unstained cells) and dead (blue-strained cells) cells were identified and counted under an optical microscope. After counting, MSCs were replated at two T-75 at an appropriate cell density.

When cells reached approximately 100% confluence, the exhausted medium was removed and

10 mL of XF (for cells grown with XF) or DMEM Basal (for cells grown with DMEM10%FBS) was added to each well to be conditioned. After 48H of incubation, conditioned medium was collected to a Falcon tube and kept at 4ºC for later.

Flasks were washed with 4 mL of PBS and a dissociative agent StemPro® Acutase® for cells cultured with DMEM and TrypLE™ Select Enzyme (10x) for cells cultured with XF, was added. Then, the flasks were incubated for 5 minutes. To inactivate the dissociation, 4 mL of PBS or DMEM10%FBS NOT MSC was added to the flask with XF or DMEM, respectively. The cell suspension was transferred to a Falcon tube and centrifuged at 1250 rpm 20ºC for 7 min. The supernatant was discarded, and the pellet was resuspended in 5 mL of PBS. While the cell number was determined, cells were centrifuged again, discarding the supernatant. The pellet was stored at -80ºC.

Finally, the conditioned medium was centrifuged for 30 minutes at 2000 rpm 4ºC to remove cells debris. The pellet was discarded, and the supernatant was transferred to another Falcon tube and stored at -80ºC.

3.1.2. **Isolation of MSC-derived EVs**

MSCs-derived EVs were isolated from conditioned media with Total Exosome Isolation Reagent Kit (from cell culture media) from Life Technologies®. Three procedures, as described in the **Table 3.1**, were conducted in order to optimize the EVs' purification. These procedures are variants of the following protocols (**Table 3.1**):

I) A protocol developed in a previous work[134] that was based on the protocol of the kit to isolate EVs[135];

II) A protocol used in the small-scale preparation of filamentous bacteriophage by single PEG-precipitation[136].

III) A protocol that combines the I and II protocols.

Table 3.1 Three protocols used to isolate MSCs-derived EVs and their steps.

<table>
<tr><th>Protocol I</th><th>Protocol II</th><th>Protocol III</th></tr>
<tr><td colspan="3">500 µL conditioned medium + 250 µL purification kit</td></tr>
<tr><td>The Mixture was vortexed and incubated at 4ºC overnight;</td><td colspan="2">The Eppendorf with mixture was inverted (nor vortexed) and incubated at 4ºC overnight;</td></tr>
<tr><td colspan="3">Sample was centrifuged at 10000g for 1 hour at 4ºC;
Supernatant was gently discarded;
Intermediate washing step by gently adding 50 µL of PBS 0.01M;</td></tr>
<tr><td rowspan="2">Pellet resuspended in 50 µL of PBS;</td><td>-</td><td>Sample was centrifuged at 14000g for 5 min at 4ºC;
Supernatant discarded;
Pellet resuspended in 120 µL of PBS;</td></tr>
<tr><td colspan="2">The Eppendorf was incubated at ice bath for 1 hour;
Sample was centrifuged at 13000g for 2 min at 4ºC;
EVs were in supernatant;</td></tr>
<tr><td colspan="3">EVs were immediately analysed by FTIR spectroscopy</td></tr>
</table>

3.2. MIR Spectral Acquisition

The isolated EVs were submitted to serial dilutions in PBS: 1:1, 1:2, 1:4, 1:8, 1:16 and 1:32. Conditioned media were analyzed without performing any dilution. Concerning the analysis of the homogenates of cells, its dilution degree (in PBS) were predicted considering the following analysis of a test sample: the number of cells present before the freezing process and the absorbance at 1650 cm^{-1} of the cell's homogenate. With the aim of an absorbance value between 0.1 and 0.5 and considering the number of cells in all the cell's samples, the dilution degreed in PBS was estimated in order to achieve the target absorbances. Cells from donor L140311 from AT MSC source in DMEM medium was used to determinate these dilution degreed predictions. The **table 3.2** summarizes the cell's samples that were submitted to a dilution degree.

Table 3.2 Cell's donors submitted to a dilution degree per source and per culture media.

MSCs Source	XF medium	DMEM medium
BM	M86A15; M79A15	-
AT	L090602; L090724; L090403	L090602
UCB	#2; #6; #78	#2; #78

From each of the previous samples (at specific dilutions degrees), 25 µL were transferred to a 96-wells Si micro-plate and then dehydrated for about 2.5 h, in a desiccator under vacuum. If samples were not well dehydrated after this time, they were left for an additional 30 minutes, to ensure a complete dehydration.

Spectral data was collected using a FTIR spectrometer (Vertex 70, Bruker) equipped with an HTS-XT (Bruker) accessory. Each spectrum represented 64 coadded scans, with a $2cm^{-1}$ resolution,

and was collected in transmission mode, between 400 and 4000 cm^{-1}. The first well of the 96-wells plate did not contain a sample and the corresponding spectra was acquired and used as background, according to the HTS-XT manufacturer.

3.2.1. Spectra Multivariate Pre-processing and processing methods

OPUS software was used to transfer the spectral data acquired from the spectrometer. Atmospheric and baseline correction was performed by OPUS (Bruker), whereas normalizations, derivatives and varied multivariate analysis techniques, such as PCA and HCA were done by The Unscrambler® X (CAMO), according to **table 3.3**.

Table 3.3 Description of Pre-Processing methods used in this work.

Method	Description
Baseline Correction	Rubber-band method
Normalization	Normalization to amide I
1st and 2nd derivatives	2nd order polynomial, with a Savitzky-Golay filter and a 15-points window
PCA	Cross-Validation method. Singular Value Decomposition Algorithm. Number of PCs: the software's default of seven or four (depending of samples dimension). Combinations of pre-processing methods: • atmosphere correction; • atmospheric and baseline correction; • atmospheric and baseline correction as well as normalization to amide I; • atmospheric and baseline correction as well as multiplicative scatter correction; • atmospheric and baseline correction as well as first derivative; • atmospheric and baseline correction and normalization to amide I as well as first derivative; • atmospheric correction and second derivative.
HCA	Linkage method: Complete linkage Distance measure: • Spearman's rank correlation; • Kendall's Tau distance measure; • Chebyshev distance; • Bray-Curtis distance.

3.2.2. **Analysis of ratios of spectral peaks**

Ratios of spectral peaks were determined based on spectra pre-processed with atmospheric and baseline correction and first derivative. To evaluate possible differences in these selected ratios between the groups of experiments appropriate hypothesis test were performed at significance level of 5%. To compare two independent groups (DMEM vs XF) t-tests or Wilcoxon-Mann-Whitney tests were applied in accordance with the samples dimension come or not from populations with normal distributions. Due the fact the two populations presented less than thirty (n = 18 for each) observations, the Kolmogorov-Smirnov test was applied to evaluate the normal distribution of populations.

For populations with normal distribution, the parametric t-test was used; when at least one of the samples didn't come from a population with normal distribution, the nonparametric test Wilcoxon-Mann-Whitney was conducted.

Chapter 4: Results and Discussion

4.1. Expansion of Mesenchymal Stem Cells (MSCs)

After initial passages, MSCs from different sources (BM-MSCs, AT-MSCs and UCM-MSCs) were used. All these cells became relatively homogeneous and showed a similar fibroblast like (elongated spindle) morphology. In **figures 4.1 A, B and C** are shown microscopic images of, BM-MSCs, AT-MSCs and UCM-MSCs, respectively, cultured in DMEM in passage 5 (P5). The BM-MSCs were larger than the others. The AT-MSCs were very similar to the BM-MSCs.

There were some shape's differences between MSCs cultured with DMEM and XF medium. As can be seen in **figures 4.1 D, E and F,** where BM-MSCs, AT-MSCs and UCM-MSCs, respectively, cultured in XF medium are represented, it is observed that MSCs in XF had a smaller and compact morphology than MSCs cultured in DMEM. Furthermore, there was a higher cell growth in the XF culture medium (**table 4.1)**. It is observed that while the cells from BM source possesses the lowest cell density in both culture media, the UCM-MSCs presented the highest density (**table 4.1**).

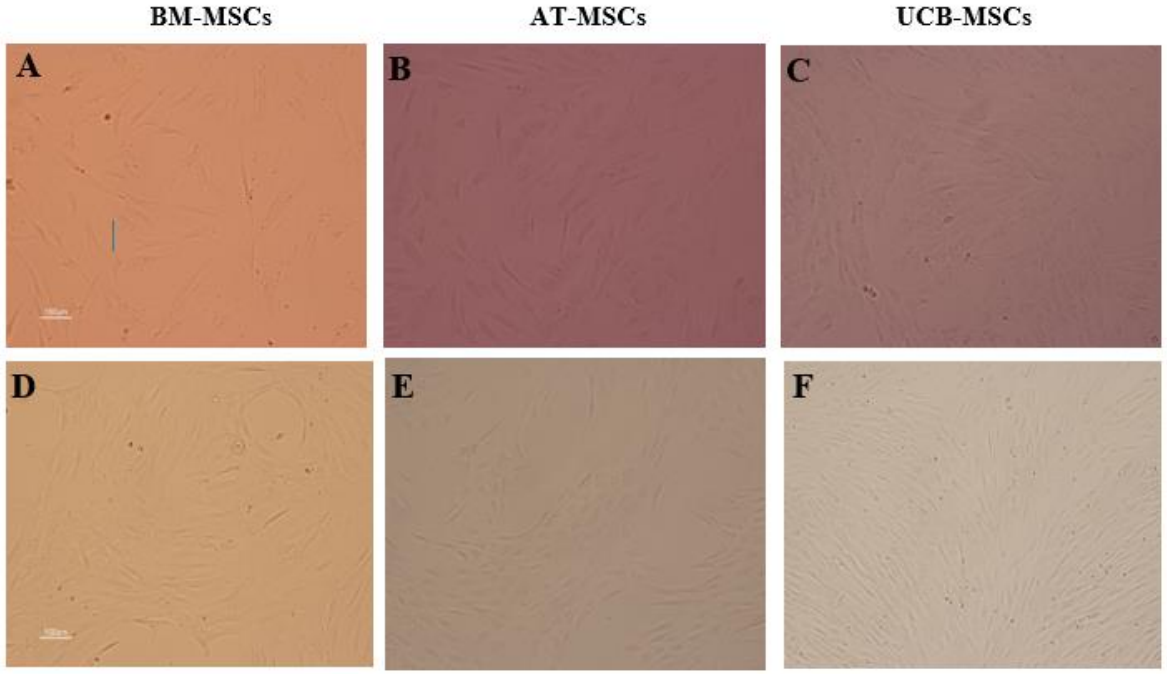

Figure 4.1 Microscopic images (scale bar = 100µm) of donor M86A15 from BM-MSCs, donor L090403 from AT-MSCs and donor #2 UCB-MSCs for passage 5 in DMEM10%FBS (A,B,C) and XF (D,E,F). Amplification: 100x

Comparing the number of days that were required to reach the conditioning period (**table 4.1**), *i.e.*, to achieve 100% cell confluency, cells from AT showed the shortest culture period, whereas BM and UCM-MSCs took longer to grow and could be cultured longer. During cell expansion, abnormalities occurred in some cultures.

Table 4.1 Number of MSCs, in resuspended volume of 5 mL, per of donor's samples in XF and DMEM10%FBS culture media, as well as the number of days from passage until to conditioning media

Source	Donor	#T75	Count Cells		Days from Passage 3 to conditioning	
			XF	**DMEM10%FBS**	**XF**	**DMEM10%FBS**
BM	M83A15	I II	527 k 689 k	272 k -	22	22
	M86A15	I II	1.2 M 1.7 M	544 k 611 k	24	20
	M79A15	I II	3 M 2.87 M	689 k 739 k	11	19
AT	L090724	I II	3.98 M 6.36 M	500 k 544 k	11	9
	L090602	I II	2.8 M 2.2 M	1.4 M 1.48 M	11	11
	L090403	I II	2.73 M 2.03 M	739 k 872 k	15	15
UCM	#2	I II	3.47 M 3.8 M	1.86 M 2.3 M	15	15
	#6	I II	3.44 M 3.86 M	711 k 633 k	17	22
	#78	I II	4.73 M 4.07 M	1.17 M 1.19 M	21	27

As it is possible to observe in **figure 4.2 A,** BM-MSCs from donors M79A15 expanded with XF medium, grew in island instead of a monolayer. This problem might have happened due to a non-uniform T-flask coating which did not allow a homogeneous cell distribution.for the complete homogeneity. It might have also been due to the cells themselves. In an attempt to solve this issue, the defined substrate CELLstart™CTS™ (used for attachment and expansion of human stem cells in STEMPRO® MSC SFM), was replaced by CellBIND® Surface cell culture flasks (used when there are growth difficult conditions) in subsequent cultures.

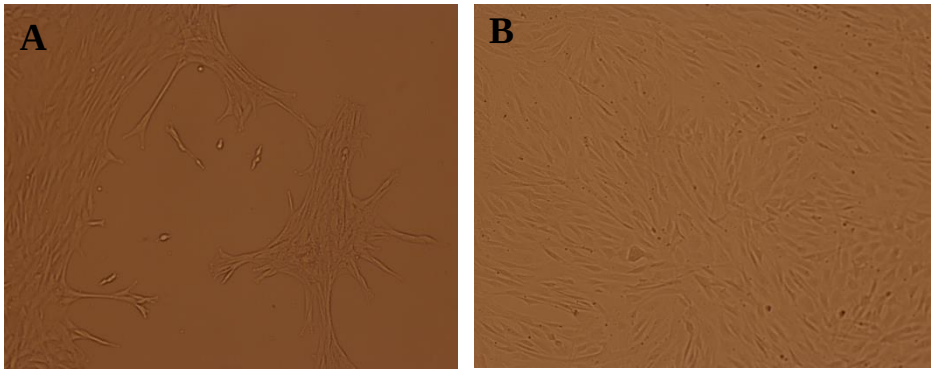

Figure 4.2 Microscopic images (scale bar =100um) of donorM79A15 from BM-MSCs, for passage 5 in XF medium, evidencing an abnormal (A) and a typical (B) cell growth. Amplification: 100x

However, in some cases, with CellBIND® this abnormality occurred as well, which indeed lead to believe that the underlying problem is indeed due to the cells. The **table 4.2** shows the type of culture flasks as well as the substrate used in each donors' expansion.

Even though there were some abnormalities observed in the T-flask, that did not stop some cells from growing, such as represented in **figure 4.2 B** and thus were used in the production of EVs.

Table 4.2 Type of culture flasks and substrates used per of donor's samples in XF medium.

Source	Donor	#T75	Substrate/culture flask
BM	M83A15	I II	CellBIND®
	M86A15	I II	CellBIND®
	M79A15	I II	CELLstart™CTS™
AT	L090724	I II	CellBIND®
	L090602	I II	CELLstart™CTS™
	L090403	I II	CellBIND®
UCB	#2	I II	CellBIND®
	#6	I II	CellBIND®
	#78	I II	CellBIND®

4.2. Optimization of the EVs isolation process to minimize the reagent kit signal on the spectra

There is a strong affinity of the reagent of the purification kit to EVs and, consequently, a polymeric layer around them is formed, as observed by Lee *el al* [137]. These researchers isolated exosomes from human ovarian cell lines with the same purification kit used in this work as well as ultracentrifugation (UC), observing that the adsorption of this reagent on EVs will result on a FTIR spectra reflecting mostly this reagent and not the EVs, according to our own observation (**figure 4.3 A**).

Figure 4.3 B represents spectra of EVs from donor F81A08 from BM-MSCs cultured in XF medium obtained by diverse isolation protocols based on the kit, showing a signal mostly from the reagent kit, as obtained by Lee *el al* [137]. However, it was observed that a high dilution degree (between 8 to 32) of the isolated EVs in PBS, leads to the reagent kit desorption, and consequently on a signal mostly from EVs (**figure 4.3 B**), in accordance to the previous observations conducted by Pereira *et al* [134]. This last author observed that the spectra of EVs obtained by ultracentrifugation with the spectra of EVs obtained by the isolation and diluted in PBS between 16 and 32, were very similar. Thus, to characterize EVs obtained by the isolation kit by FTIR spectroscopy, it is necessary to conduct a high dilution in PBS.

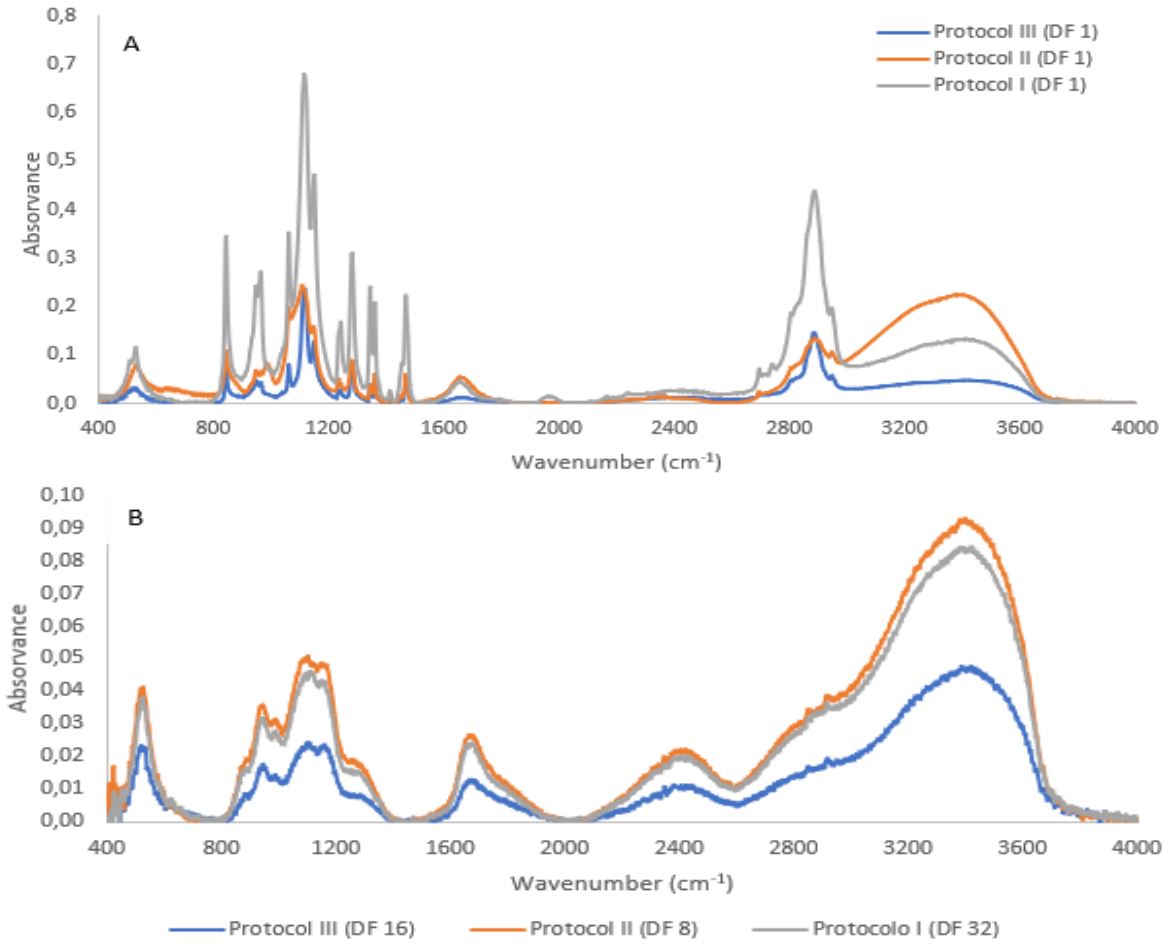

Figure 4.3 Spectra pre-processed with atmospheric and baseline correction from BM MSC-derived EVs from donor F81A08 in XF medium, purified with the protocol I (grey line), protocol II (orange line) and protocol III (blue line) at dilution factors of 1 (A), or at dilutions factors of 32, 8 and 16 (B), respectively.

To minimize the dilutions factors while maximize the spectral signal due to EVs, in the present work, it was evaluated three different protocols for EVs isolation based on the kit, as described in **Subsection 3.1.2.** For all the protocols, the isolated EVs were diluted in PBS at dilution factors (DFs) of 1, 2, 4, 8, 16 and 32. On this experiment, samples from BM MSC donor F81A08 cultured in XF medium were used.

In the 3 protocols, at a DF of 1 the spectra-signal is mainly due to the kit polymer (**Figure 4.3 A**). Were after dilution with PBS, the signal is mainly due to EVs, possibly due to desorption of the polymer kit from EVs (**Figure 4.3 B**). The minimum dilution to achieve the EVs spectral signal, while minimizing the polymer signal, was of 32, 8 and 16 for protocol I, II and III, respectively. At these dilutions, the spectra present a pattern similar to the one obtained for EVs purified with ultracentrifugation (UC), i.e. without the use of the purification kit, as presented in Pereira *et al* [134].

For example, the peak at around 3400, 2400 and 1600 cm^{-1} are the most intense and common in the spectra from EVs purified by UC. The most intense peaks on a spectrum that reflect the reagent kit are the 2800 cm^{-1} and between 1000 and 1200 cm^{-1}. The **figure 4.4 A and B** represent the spectra of EVs isolated by protocols I to III and after DF between 8 to 32 and obtained from MSC culture in XF (**figure 4.4 A)** or DMEM (**figure 4.4 B**) media. On these figures, the media spectra are also represented (yellow line).

The main differences between the three protocols, were extra centrifugations on protocol II and III in relation to protocol I, aiming to precipitate more kit polymer, and consequently to reduce the polymer presence on the final EVs. Therefore, protocols II and III indeed resulted in a less adsorption of the kit polymer to EVs, leading to lower DF to minimize the signal of the reagent kit on the spectra. Most probably, the extra centrifugation step on the protocol III lead to a less yield of EVs, resulting in a lower EVs signal than protocol II. Therefore, the apparent best protocol was protocol II. In the remaining of this work, if not stated otherwise, all the EVs were purified by this protocol II.

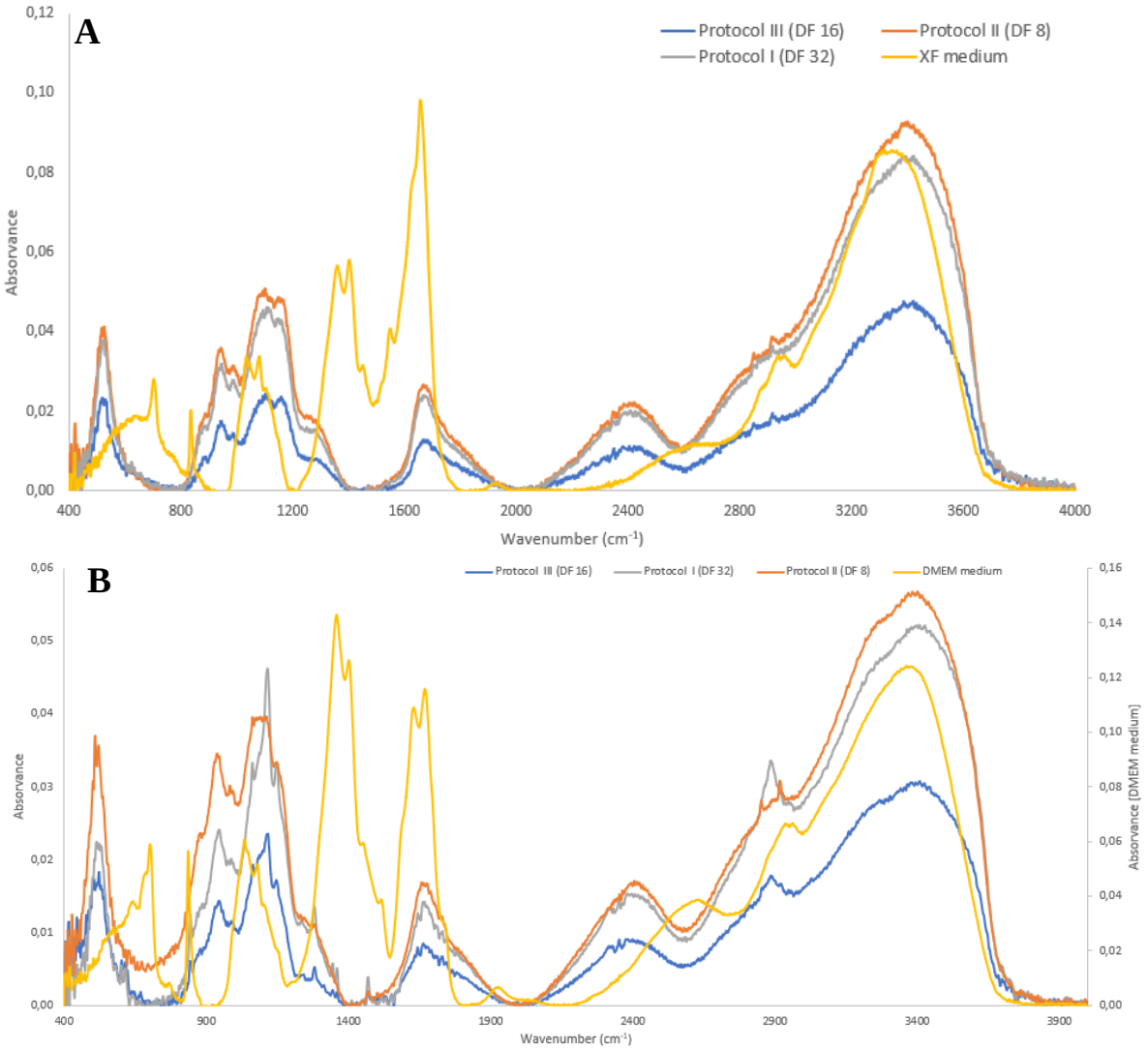

Figure 4.4 Spectra pre-processed with atmospheric and baseline correction from (A) XF medium not submitted to any isolation protocol (yellow line) and BM MSC-derived EVs from donor F81A08 in XF medium, isolated with protocol I (grey line), protocol II (orange line) and protocol III (blue line) after DF of 32, 8 and 16, respectively; from (B) DMEM medium not submitted to any isolation protocol (yellow line) and AT MSC-derived EVs from donor L090411 in DMEM. medium, purified with protocol I (grey line), protocol II (orange line) and protocol III (blue line) after DF of 32, 8 and 16, respectively.

Since the specific molecular composition of different samples may affect the EVs isolation and consequently the polymer kit adsorption, it was evaluated the effect of the DF of 8, 16 and 32 for all EVs isolated by protocol II in on the PCAs score-plots. As observed in Pereira *et al* [134], the media composition (XF vs DMEM) affects the EVs molecular profile. For that, it was evaluated which DF lead to best discrimination on the PCA score-plot between EVs spectra produced by MSC in XF in relation to EVs spectra produced in MSC culture in DMEM media. In this evaluation, it was simultaneously studied the effect of diverse pre-processing methods.

It was conducted seven different pre-processing methods as described in **table 3.3.** These methods minimized interferences due to physical characteristics as light scattering, while deconvolute spectral bands by derivatives. Normalization was also conducted as pre-processing method to minimize the effect of EVs quantity on the PCA. From the pre-processing methods evaluated, the following two resulted in the best cluster separation between EVs produced in XF from EVs produced in DMEM media:

- Atmospheric and baseline correction and normalization to amide I;
- Atmospheric and baseline correction coupled to first derivative.

For simplicity, **figure 4.5** represent PCA scores plots of the raw spectral data (no-processing) and the two best pre-processing methods referred of EVs produced in DMEM (represented by blue) and XF (represented by red) for the three dilution factors. The PCA with spectra without pre-processing (**figure 4.5 A, B, C**), from EVs with a DF 8 resulted in score plot without no separation of clusters and from EVs with both DF 16 and 32, there are some samples more grouped between each other in function of the culture media, thought a dispersion of samples in general is observed, namely EVs samples cultured in XF.

When two pre-processing methods are used (**figure 4.5 E, F, H, I)**, some clusters separation continues to be observed. Although, with atmospheric and baseline correction and normalization to amide I, EVs samples cultured in XF are more grouped between each other, still they are not complete apart from the samples obtained in DMEM. With atmospheric and baseline correction coupled to first derivative, a dispersion of samples is more manifest, specifically for DF 32 due to the low signal-to-noise ratio which is inherent to a higher dilution factor. In contrast, for scores plots from processed EVs samples for DF 8 (**figure 4.7 D, G)**, unexpected results were observed, since there is no separation between EVs samples cultured in both media, annulling the possibility to use the DF 8, most probably still due to some interference from the polymer kit. Thus, the DF 16 was ideal for the analysis presented in the following chapters, except for the **subchapter 4.3.1** were the effect of EVs with multiple dilution factors on culture media and MSC sources was studied.

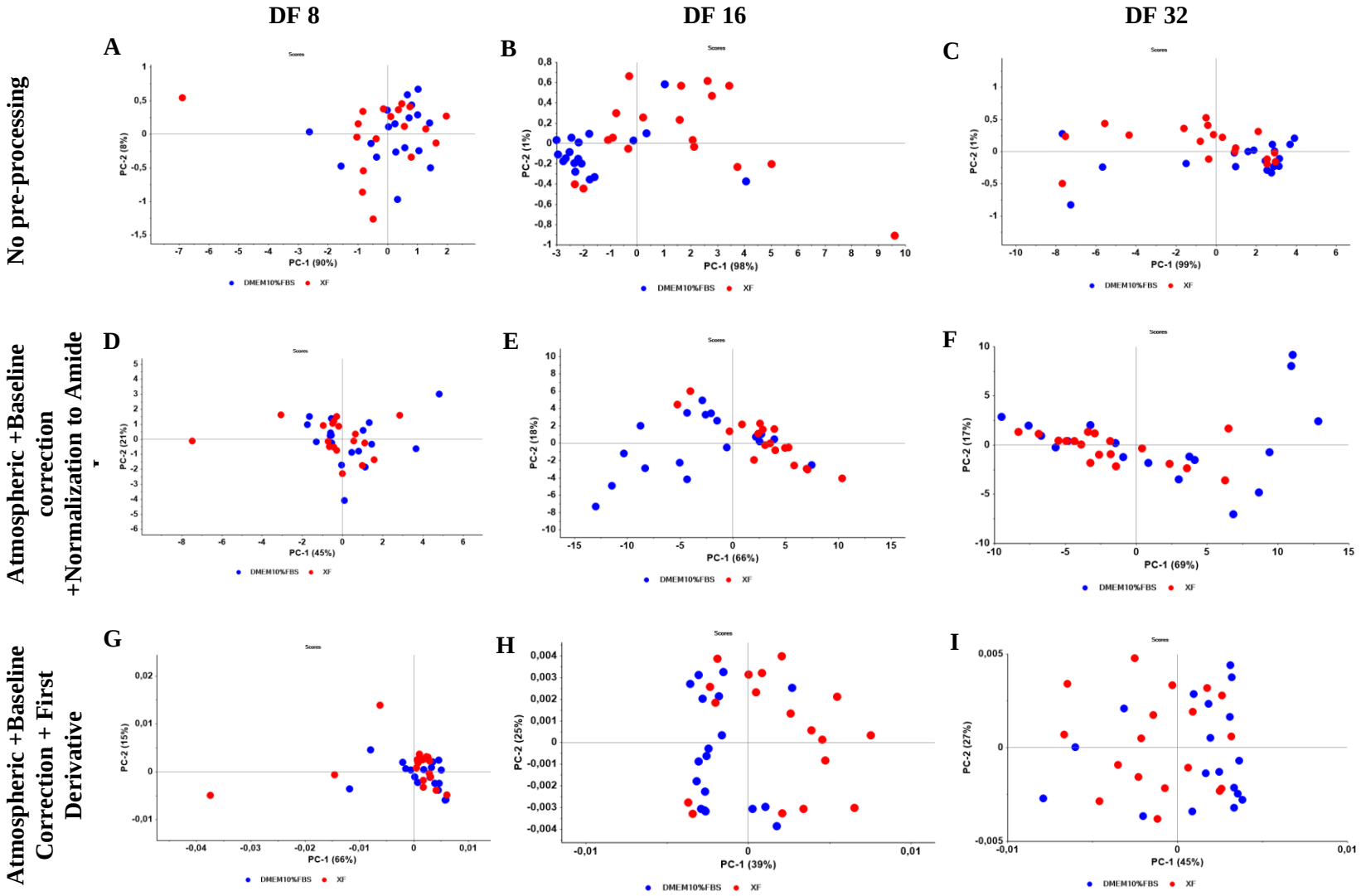

Figure 4.5 PCA for spectra of EVs purified with the purification kit (protocol II) for dilution factors of 8 (A, D, G), 16 (B, E, H) and 32 (C, F, I), with no processing, atmospheric and baseline correction as well as normalization to amide I, atmospheric and baseline correction as well as first derivative pre-processing. Representation of DMEM in blue and XF in red.

4.3. Effect of the Medium Composition, MSC source and MSC donor on EVs Molecular Characteristics

In this and the following subchapters, the effect of different culture media (DMEM and XF), MSC sources (bone marrow, adipose tissue and umbilical cord matrix) and donors were evaluated by PCA of spectra of EVs purified, using a DF of 16 in PBS, with exception of **subchapter 4.3.1**.

On **subchapter 4.3.1**, with the goal to evaluate if for some samples a different DF would be better than 16, it was evaluated the effect of using a dilution degree that maximised the EVs signal while minimising the polymer reagent signal. The DF selected per each sample is described in **table 4.3**. In **Chapter 4.3.2**, a similar data processing was conducted as in **chapter 4.3.1** but with a DF of 16 for all EVs samples.

Table 4.3 The corresponding dilution factor to the spectral data used from each sample

Source	Donor	DMEM medium	XF medium
BM MSC	M79A15	8	8
			16
	M83A15		8
	M86A15		
AT MSC	L090403	8	8
		32	
	L090602	8	16
	L090724		8
			16
UCM MSC	#2	8	8
		32	
	#6	8	
		16	16
	#78	8	8
			32

For the results that have been considered more relevant, besides the PCA, a Hierarchical Clustering Analysis (HCA) was conducted. In general, no outliers were removed because these biological samples are limited in quantity (only duplicates per donor). Nevertheless, in some cases, the removal of possible influential samples and potential outliers was tested.

4.3.1. **Effect of culture media and MSC sources on EVs molecular profile, based on EVs at different DF**

Figure 4.6 represents PCA of the raw spectral data of isolated EVs (from conditioned media of XF and DMEM) and pre-processed by:

- Atmospheric and baseline correction and normalization to amide I;
- Atmospheric and baseline correction and first derivative;
- Atmospheric correction and second derivative.

In general, there were some spectra pre-processing that apparently resulted in the grouping of EVs from a defined media, as observed with spectra pre-processed by atmospheric and baseline correction and normalization to amide I (**Figure 4.6 C**) and atmospheric and baseline correction and normalization to amide I coupled to first derivative (**Figure 4.6 E**). However, the corresponded HCA (**Figures 4.6 D and F**) did not reveal any relevant separation between EVs obtained from MSC culture in these two different media (XF and DMEM). In consequence, there were no visible clustering of EVs spectra in function of MSC source (**figure 4.7**).

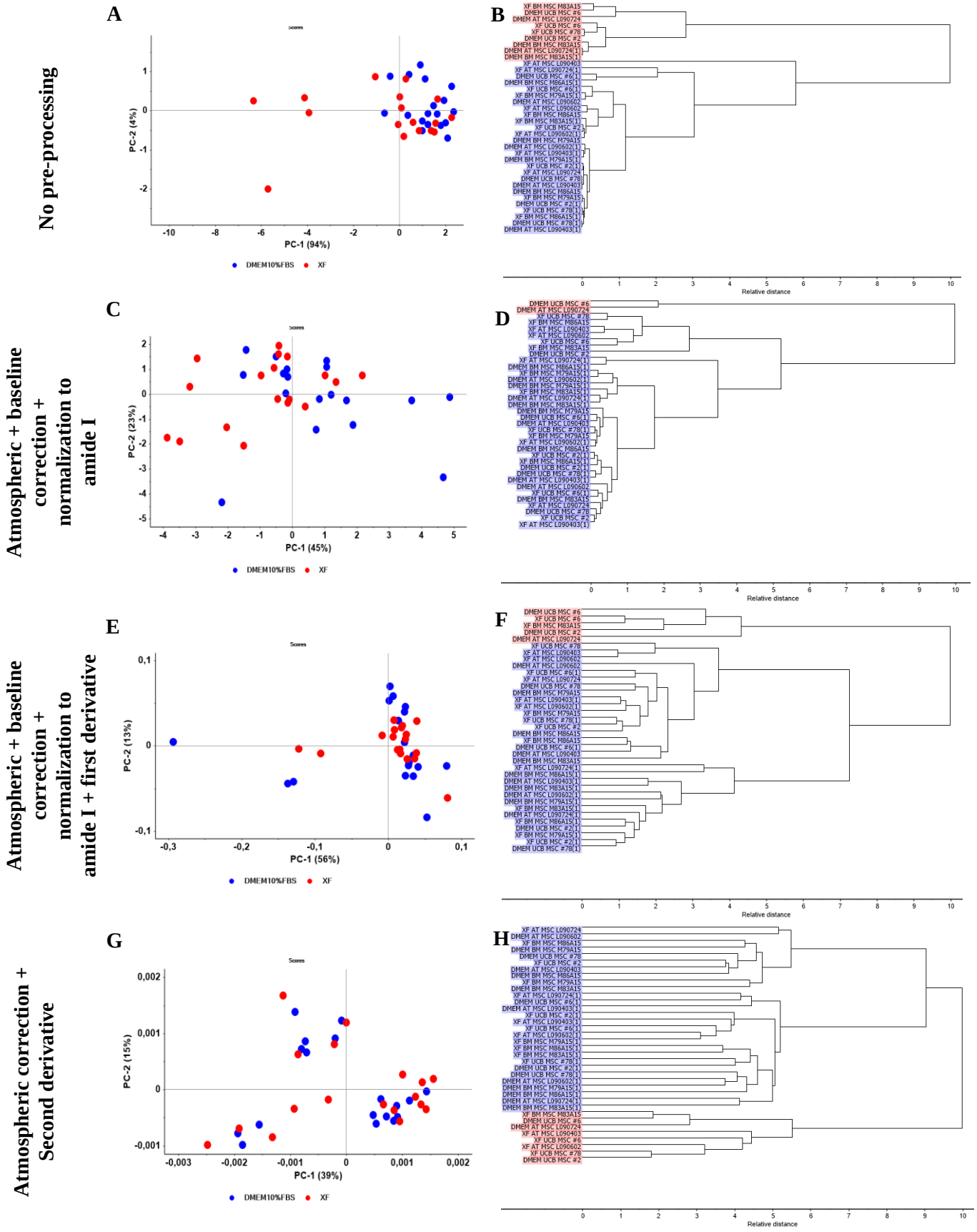

Figure 4.6 PCA for EVs spectra diluted at different DF with no processing (A), atmospheric and baseline correction coupled to normalization to amide I (C), atmospheric and baseline correction and first derivative (E), atmospheric correction and second derivative (G) pre-processing. Representation of DMEM in blue and XF in red. The respective HCAs (B, D, F, H) (Spearman's rank correlation) are represented. Each sample is represented by culture media, MSC source, donor number and number of duplicated.

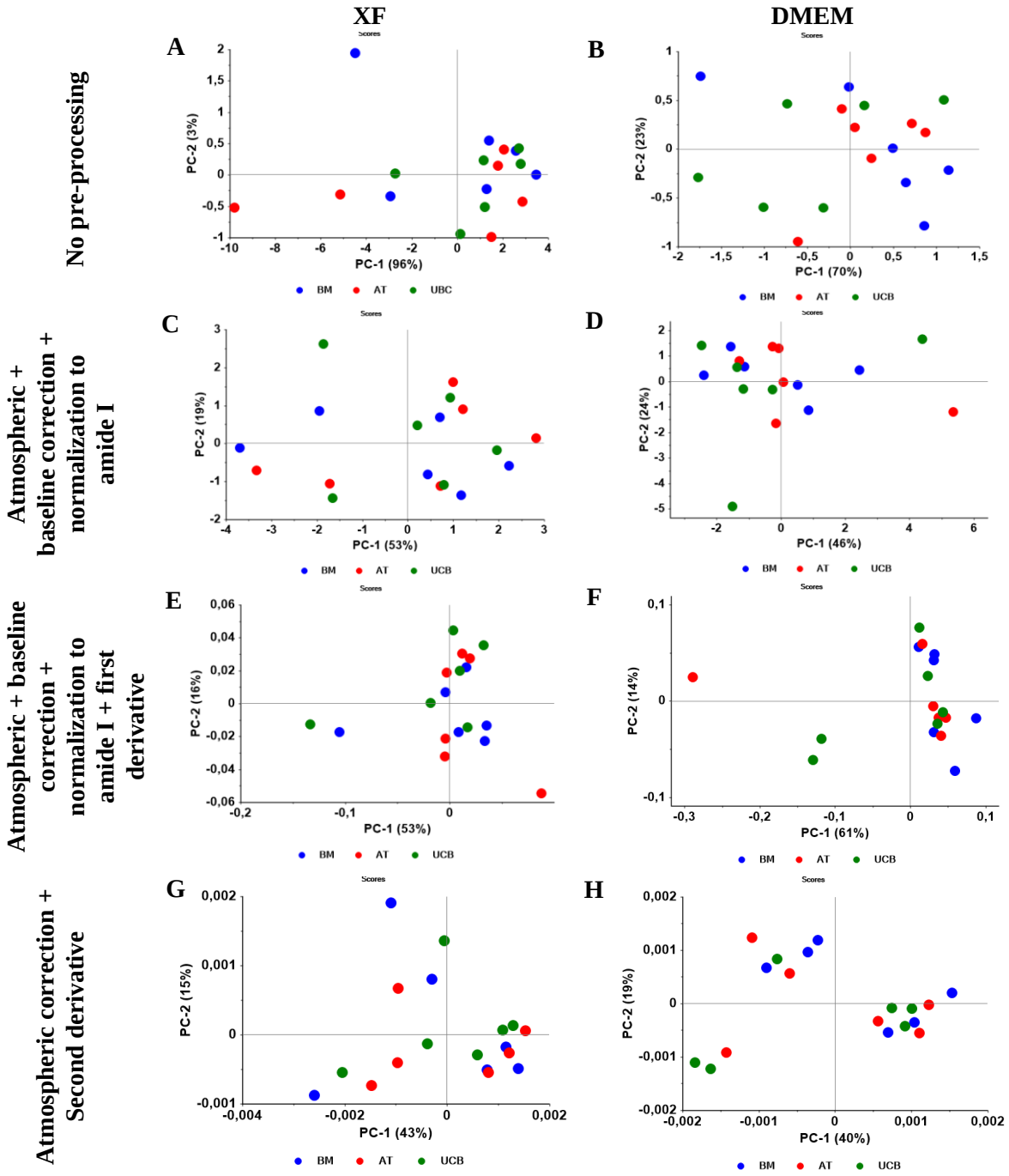

Figure 4.7 PCA for EVs spectra diluted at different DF from three MSCs sources, BM (represented in blue), AT (represented in red) and UCM (represented in green), in XF and DMEM medium with no processing (A,B), atmospheric and baseline correction coupled to normalization to amide I (C,D), atmospheric and baseline correction and first derivative (E,F), atmospheric correction and second derivative (G,H) pre-processing.

4.3.2. **Effect of culture media on EVs molecular profile, based on EVs at DF of 16**

Figure 4.8 represents PCAs of raw spectral data and of spectra pre-processed by atmospheric and baseline correction and first derivative. It was observed in the PCA score plot that EVs spectra grouped apparently according to the media used to culture MSC, i.e. the media used for MSC culture affects the EVS molecular profile. It was also observed a higher dispersion of EVs data when XF (in red) was used, i.e. the molecular profile variability of XF is apparently higher than when using DMEM.

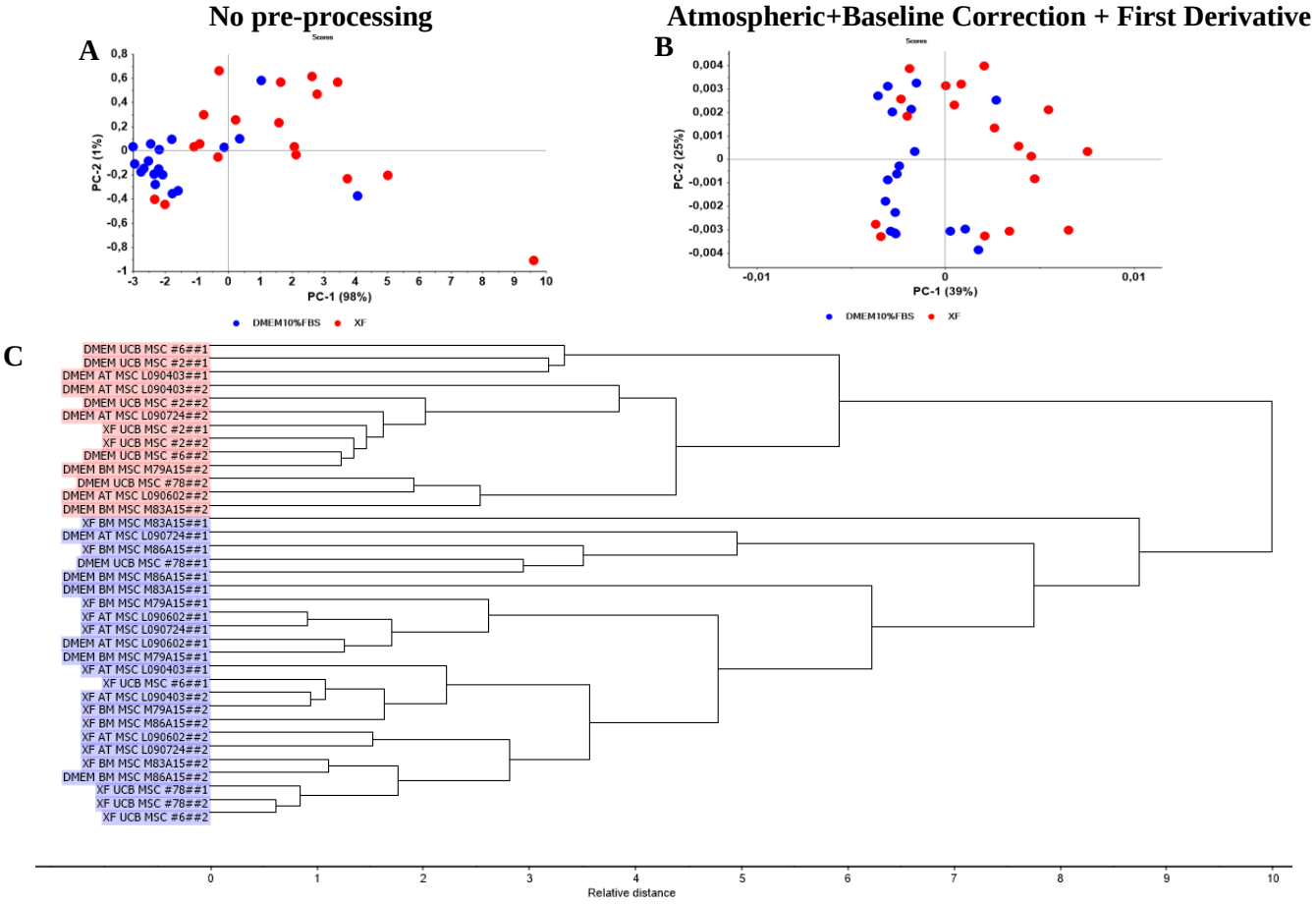

Figure 4.8 PCA for EVs spectra in DMEM and XF media (for DF 16) with no-processing (A) and pre-processed with atmospheric and baseline correction and first derivative(B). Representation of DMEM in blue and XF in red. HCA (C), with Spearman's rank correlation, where in general DMEM samples are represented in red and XF samples in blue. Each sample is represented by culture media, MSC source, donor number and number of duplicated.

The HCA, based on spectra pre-processed with atmospheric and baseline correction and first derivative (**figure 4.8 C**), corroborates this result, as 61% of EVs produced in DMEM and 89% of EVs produced in XF were correctly classify. The misclassification of samples could result from specific characteristics of MSC donors, as two samples of XF in DMEM's cluster are from the same donor (from UCM MSC donor #2), while the seven purified EVs in DMEM were from BM and AT MSCs.

In resume, it was observed that the composition medium affects the EVs chemical profile and consequently the culture medium is a relevant parameter that should be considered when producing EVs for human therapy.

4.3.3. **Effect of MSC Sources on the EVs molecular profile, based on EVs at DF of 16**

To better evaluate how the MSC source affects EVs chemical characteristics, EVs produced by MSC cultured in DMEM and XF medium were evaluated separately. From all pre-processing spectra of EV produced in DMEM, in general, none PCA showed clusters separated by MSCs source (**figure 4.9 B, D, F, H and J**). The exception to this was EVs from BM MSCs (in blue and circled by a black line in **figure 4.9 D and F**).

EVs from UCM MSCs cultured in XF medium (in green and circled by a black line) are also closer to each other in the PCA score plot than EVs from other donors (**figure 4.9 C**). In XF, EVs from BM MSCs (in blue) are more dispersed than EVs from AT MSCs (in red). Thus, for EVs produced in XF medium, apparently its chemical variability from a defined source, increases in the following order: **UCM to, AT to BM MSCs.**

In resume, EVs from UCM MSCs in XF and EVs from BM MSCs in DMEM present a specific and chemical composition in relation to the one obtained from other sources and medium.

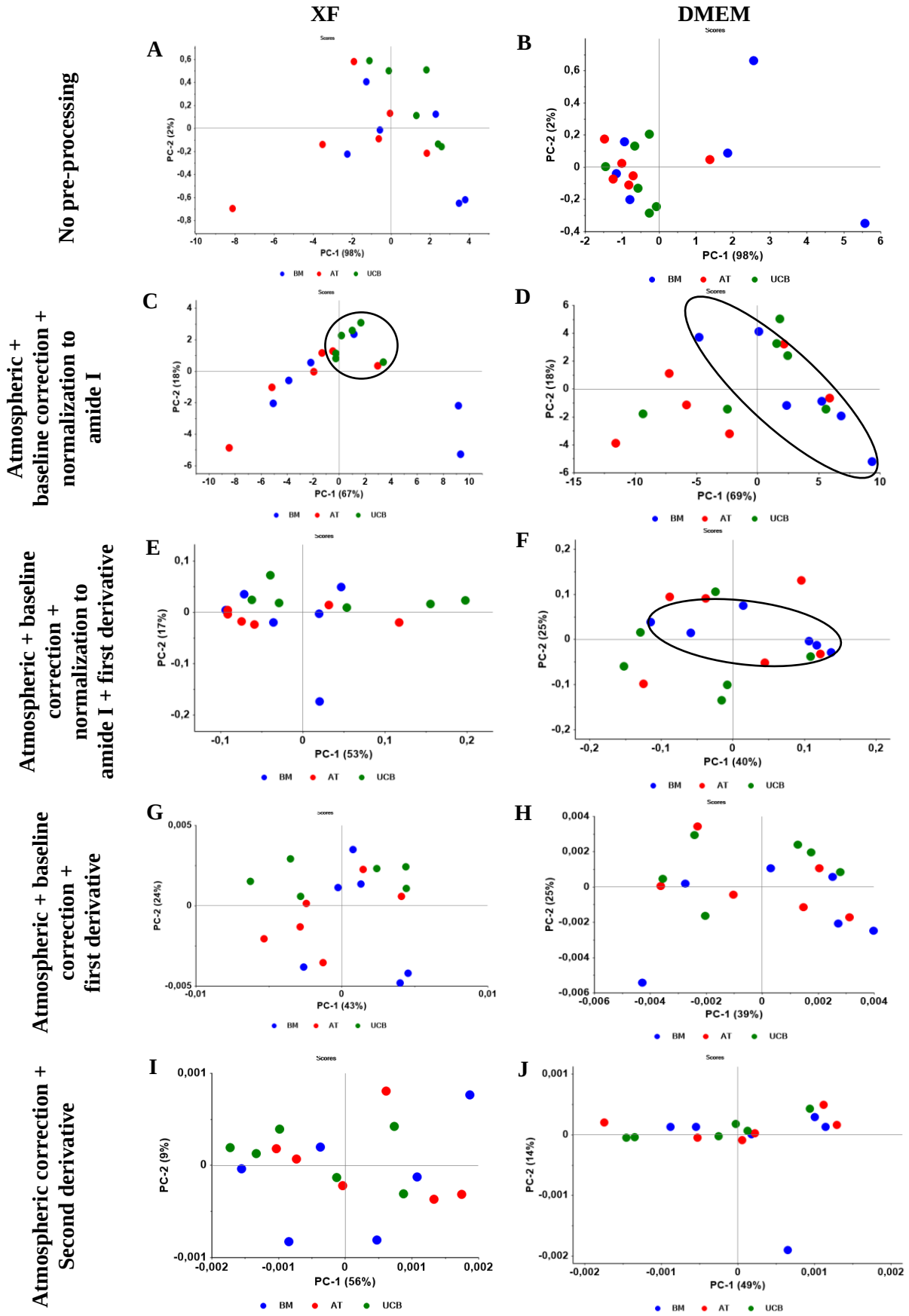

Figure 4.9 PCA for EVs spectra from three MSCs sources, BM (in blue), AT (in red) and UCM (in green), in DMEM and XF medium (for DF 16) with no processing (A,B), atmospheric and baseline correction coupled to normalization to amide I (C,D), atmospheric and baseline correction coupled to normalization to amide I and first derivative (E,F), atmospheric and baseline correction and first derivative (G, H) and atmospheric correction and second derivative (I,J) pre-processing.

4.3.4. **Effect of the MSC donor on the EVs molecular profile, based on EVs at DF of 16**

To better evaluate how the chemical composition of EVs depends of the MSCs donors, EVs from each of the sources (BM, AT and UCM) produced in DMEM and XF medium were evaluated separately (**figures 4.10, 4.11 and 4.12**).

Through the analysis of **figure 4.10 C and D,** within BM MSCs sources in both culture media, the donor M83A15 (in red) seem to result in EVs with a different molecular profile relatively to the other donors since these processed data were more distant in the score plots from EVs from other donors. In fact, PC2 separates samples of this donor from at least one of the other donors. The two replicas of all donors were distant from each other, which means that they presented a high variability. Neither HCA based on linkage method and distance measure corroborate these observations.

With non-processed spectra (**figure 4.10 A**), it was possible to observe a separation (by PC1) between EVs of donor M79A15 (in blue) and donor M83A15 (in red) in XF medium, which corroborated by distinct clusters in HCA (**figure 4.10 G**).

For AT MSCs in DMEM (**figure 4.11 B and D)**, with non-processed spectra was possible to observe a separation between EVs of donors L090724 (in red) and L090602 (in green), probably since no-processing takes account the quantity factor. In XF medium (**figure 4.11 A and C)**, PC1 separates EVs samples of the donor L090403 (in blue) from the remaining, i.e. presented a different molecular profile in relation to EVs from donors L090724 and L090602. This was confirmed by HCA **(figure 4.11 E)**, where replicas of donor L090403 formed a cluster (in blue) and donors L090724 and L090602 formed another cluster (in green and red).

For EVs from UCM MSCs source, in DMEM medium (**figure 4.12 D),** samples of donor #78 (in blue) separated from other donors, while in XF medium (**figure 4.12 C)** samples of donor #2 (in red) separated from the other donors. In fact, by HCAs, donor #78 (evidenced in both **figures 4.12 F and E**), formed a sub-cluster even though divided by other donors, which means that this donor #78 presents a similar chemical composition to other donors. For donor #2 in XF medium, its replicas were grouped which indicates that EVs from them present a lower variability.

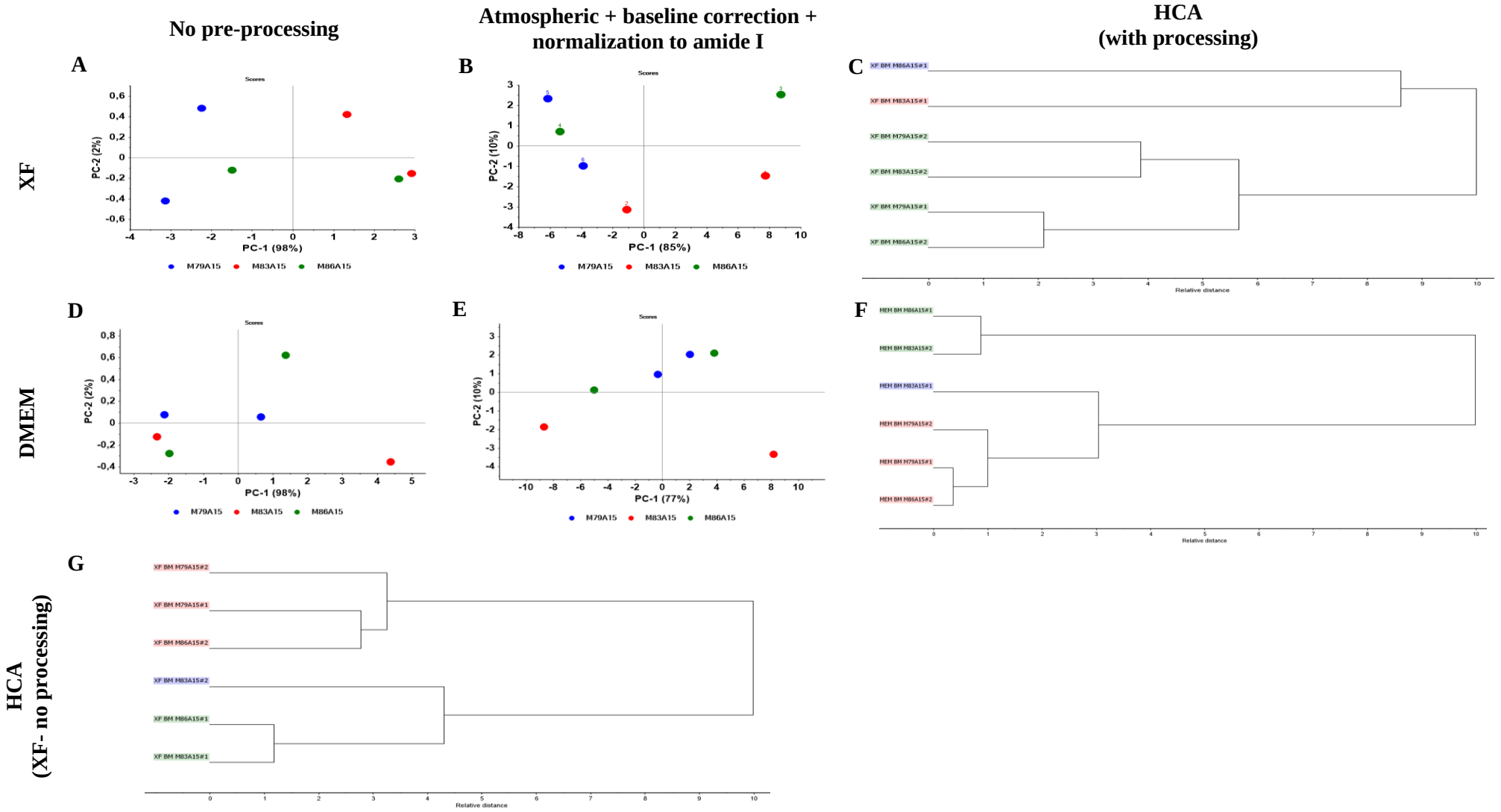

*Figure 4.10 PCA for EVs spectra from **BM MSCs** in XF (A and B) and DMEM (D and E) medium, considering MSCs donors: M79A15 (represented in blue), M83A15 (represented in red) and M86A15 (represented in green), with no processing; and atmospheric and baseline correction as well as normalization to amide I. The respective HCA (C, F, G) with Chebyshev distance, are represented. Each sample is represented by culture media, MSC source, donor number and number of duplicated.*

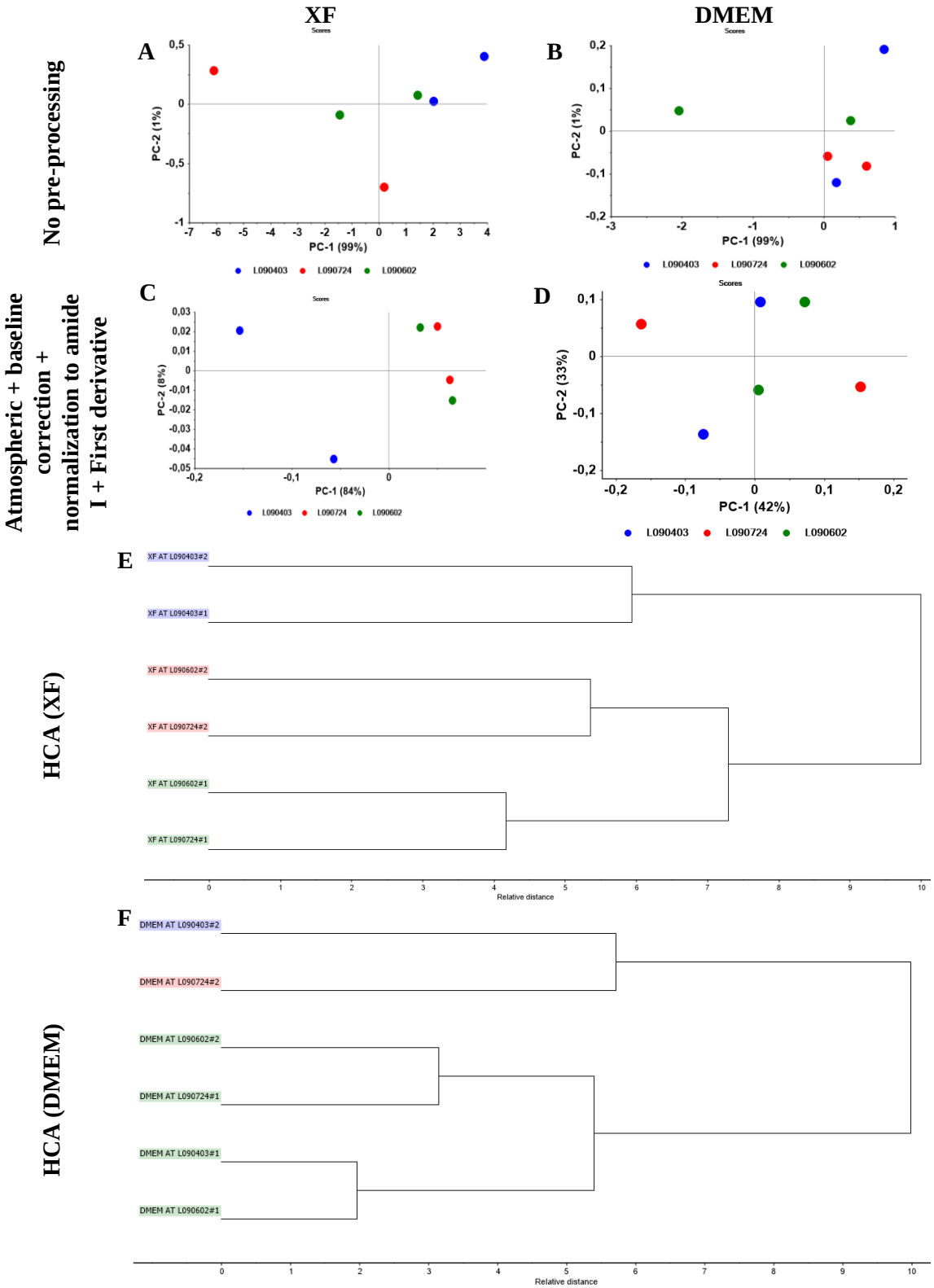

*Figure 4.11 PCA for EVs spectra from **AT MSCs** in XF (A, C) and DMEM (B,D) medium, considering MSCs donors: L090403 (represented in blue), L090724 (represented in red) and L090602 (represented in green), with no processing; and atmospheric and baseline correction as well as first derivative. The respective HCAs (E, F) (Kendall's Tau distance measure and Squared Euclidean distance) for atmospheric and baseline correction couplet to first derivative are represented. Each sample is represented by culture media, MSC source, donor number and number of duplicated.*

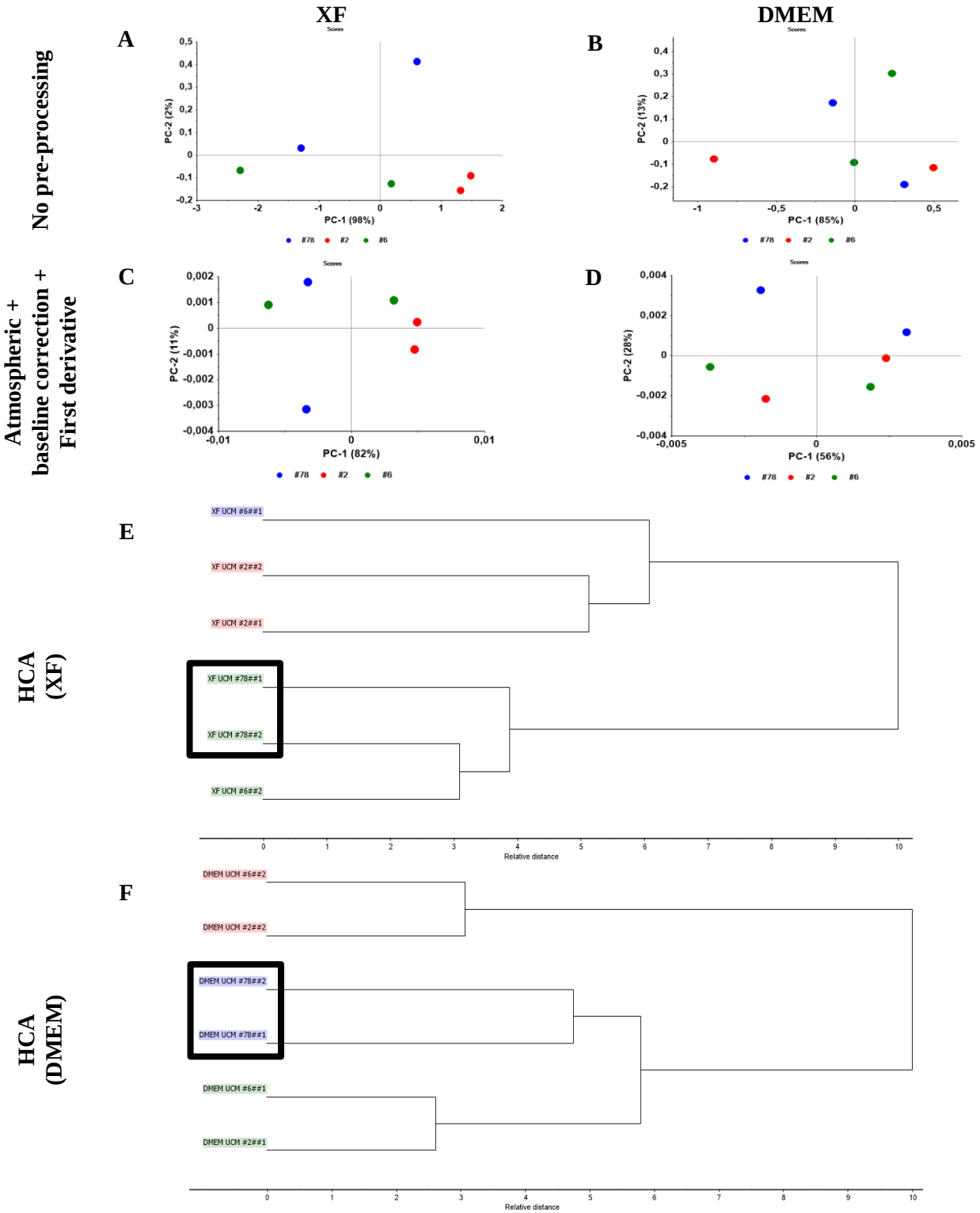

*Figure 4.12 PCA for EVs spectra from **UCM MSCs** in XF (A, C) and DMEM (B,D) medium, considering MSCs donors: #78 (represented in blue), #2 (represented in red) and #6 (represented in green), with no processing; and atmospheric and baseline correction as well as first derivative. The respective HCA (Kendall's Tau distance measure and Chebyshev distance) for atmospheric and baseline correction as well as first derivative (E, F) is represented. Samples of donor #78 were evidenced. Each sample is represented by culture media, MSC source, donor number and number of duplicated.*

In general, it was observed for the three MSC sources on both culture media, a high dispersion of EVs in the PCA score plot in function of donors. This could result from the high variability observed between replicas of each donor. The few exceptions were donor M79A15 from BM MSCs cultured in both culture media; donor L090724 from AT MSCs cultured in both culture media; donor #2 from UCM MSCs cultured in XF medium.

In resume, from this analysis, it was observed that EVs molecular profile depends of the culture media, in some cases of the MSC source and donor. However, the present study presents a high variability of EVs replicas per experiment, probably still due to adsorption of the polymer reagent. Would be highly desirable to increase the number of biological replicas per donor in order to obtain a more reproductible result.

4.3.5. **Ratios of spectral peaks for discrimination EVs produced in DMEM from EVs produced in XF media**

From the analysis of the loading diagrams of PCA, it is possible to define the spectral regions that contributed most for the cluster separation in the score-plot. Every single variable in spectra has a loading on each PC. This reflects how much the individual variable contributes to that PC and how well the PC considers the variation contained in a variable. Variables with large loadings (large positive and negative peaks presented in loading vectors plots) in early components (PC1 and PC2) are the ones that vary the most, *i.e.*, they are the variables that are responsible for the greatest differences between the samples. Thus, it is possible to infer the most significant spectral regions (wavelengths) that contribute to discrete of the chemical characteristics of EVs.

For the analysis of the loading diagram, it was considered the PCA based on spectra pre-processed by atmospheric and baseline correction and first derivative (**figure 4.8 B**), were its PC1 separates EVs produced in DMEM from EVs produced in XF medium. **Figure 4.13** represents the loading vector for this PC1.

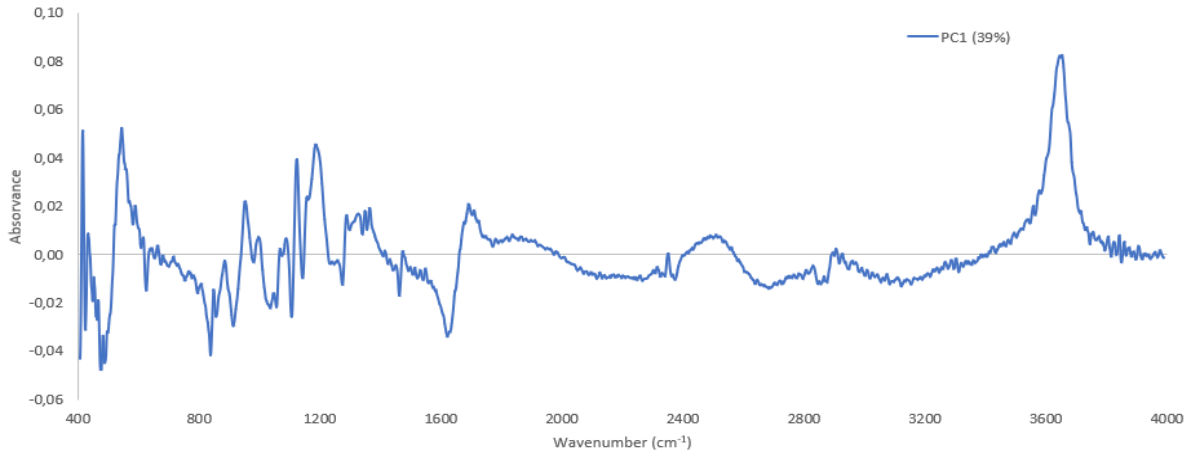

Figure 4.13 Loadings for PC1 for EVs spectra as represented in figure 4.8, with 39% variance

The relevant spectral regions that contribute to the separation of EVs were: a band at 3656 cm^{-1} which may be attributed to N-H groups from amides; 1694 cm^{-1} which corresponds to Amide I band from proteins; between 1289 and 1367 cm^{-1} which can be corresponded to many vibrations of groups in amide III; 1190 and 1124 cm^{-1} which can be attributed to RNA ribose; 956 cm^{-1} which is attributed to stretching vibrations from PO groups in phosphorylated proteins; and 545 cm^{-1} correspond the other vibrations on fingerprint region.

Ratios of derivatived absorvance were determined by considering the target peak identified previously with a reference peak. This reference peak was determined for defined regions, as 400 - 1000 cm^{-1}, 1000 – 1995 cm^{-1}, 2700 – 4000 cm^{-1}, by comparing the average first derivative spectra of EVs obtained in DMEM in relation to average first derivative spectra of EVs obtained in XF medium. The peaks that were maintained were considered as reference (**figure 4.14**).

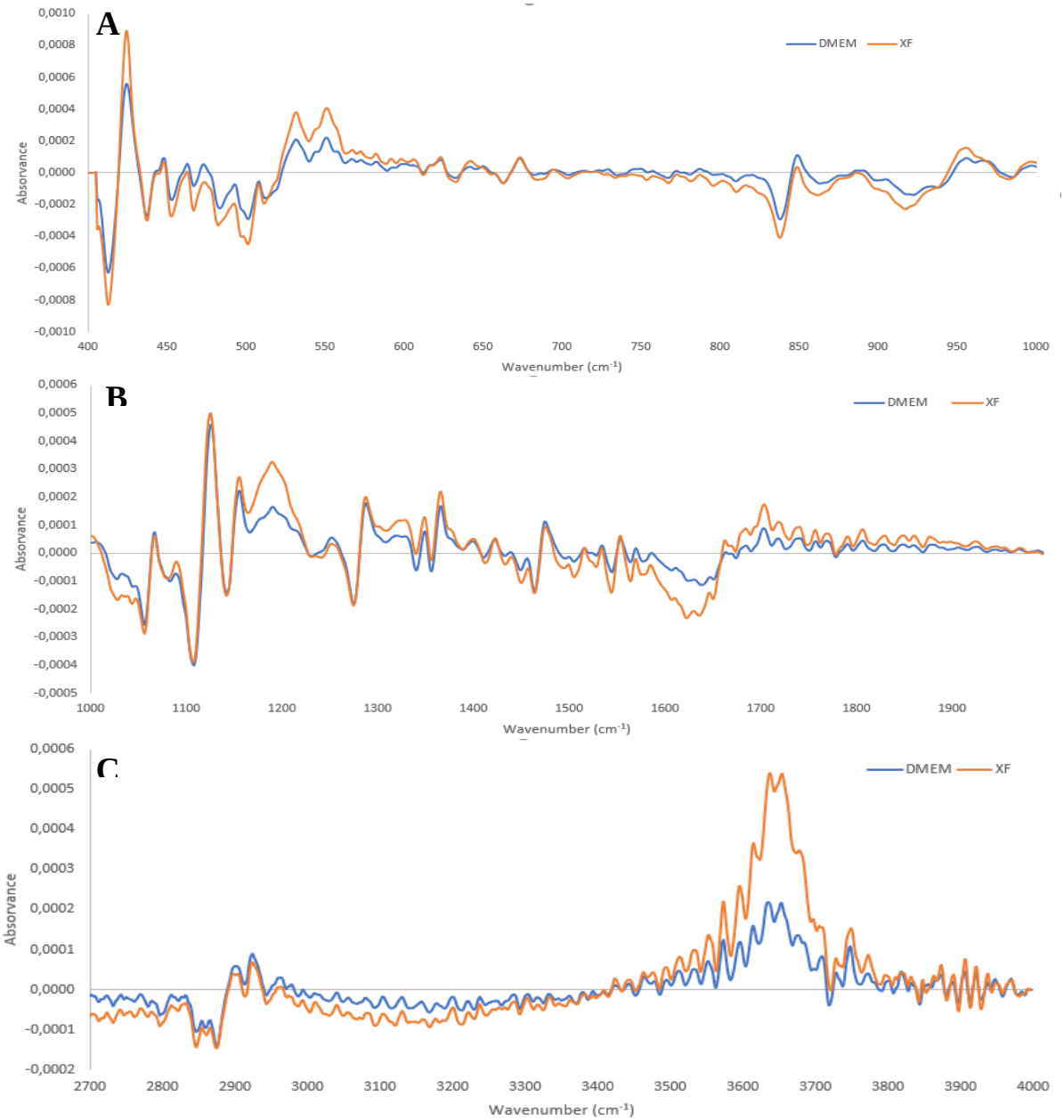

Figure 4.14 Average EVs spectra (pre-processed with atmospheric and baseline correction and first derivative) obtained in DMEM (in blue) and average EVs spectra obtained in XF (in orange) medium. (A) 400 - 1000 cm^{-1}, (B) 1000 – 1995 cm^{-1}, (C) 2700 – 4000 cm^{-1}. For simplicity, absorvance represents derivatived absorvance.

Since this method used is time-consuming, only 16 derivatived absorvance ratios were determined. For future work, applying an automatic method is essential to enable the analysis of thousands of variables as well as the analysis the other conditions studied in this work.

Ratios are represented by letter "A" to derivatived absorvance and the respective wavenumber. For exemplify, A1289 corresponds to the derivatived absorvance at 1289 cm^{-1}. The following derivatived absorvance ratios (obtained through the visualization of spectra in **figure 4.14**), that were attributed to diverse functional groups and biomolecules, were considered:

A3653/3465 A3638/3465	Ratios between regions of NH groups from proteins.
A2904/2926 A2904/2866	Ratio between methyl and methylene groups in lipids.
A1694/1554	Ratio between Amide I and NH, CN and CC groups from proteins.
A1694/1475	Ratio between Amide I and CH_3 or CH_2 from proteins and lipids.
A1694/1288	Ratio between Amide I and phosphate groups.
A1554/1067	Ratio between Amide II and phosphate groups.
A1425/1475	Ratio between methyl and methylene groups in lipids and proteins.
A1366/1475	Ratio between CH_3 in phospholipids and CH_3 or CH_2 present in lipids.
A1191/1126	Ratio between esters and RNA ribose.
A1157/1126	Ratio between carbohydrates and RNA ribose.
A1157/1066	Ratio between carbohydrates and phosphate groups.
A1126/1066	Ratio between RNA ribose and phosphate groups.
A1090/1252	Ratio between phosphate groups.
A958/675	Ratio between fingerprint regions.

To be able to evaluate if these ratios were statistically different, an appropriate hypothesis test (t-test or Wilcoxon-Mann-Whitney test) and considering the significance level of 5%, was applied (**table 4.4**).

Table 4.4 Average values and standard deviations of spectral derivatives absorbance ratios of purified EVs (DF 16) in DMEM and XF medium, and the p-value of appropriated statistical test (t-test or Wilcoxon-Mann-Whitney test), regarding the comparison of the average values between DMEM and XF group. Significant derivatived absorvance band ratio is highlighted in bold.

Spectral Ratios	**p-value (α = 0.05)**	**DMEM**		**XF**	
		Average	Standard Deviation	Average	Standard Deviation
A3653/3465	0.901	0.42	0.069517	0.42	0.086874
A3638/3465	0.444	0.53	0.072505	0.55	0.087648
A2904/2926	**0.038**	**1.13**	**0.186798**	**1.02**	**0.045094**
A2904/2866	**0.001**	**1.15**	**0.074919**	**1.08**	**0.043512**
A1694/1554	0.197	3.02	0.8167401	2.68	0.592963
A1694/1475	0.079	3.46	3.14281	4.54	2.28536
A1694/1288	**0.000**	**1.01**	**0.340824**	**1.46**	**0.364828**
A1554/1067	0.152	0.24	0.126475	0.30	0.180200
A1425/1475	**0.029**	**0.63**	**0.346824**	**0.36**	**0.367581**
A1366/1475	**0.013**	**1.41**	**0.532564**	**1.01**	**0.280175**
A1191/1126	0.949	0.62	0.12695	0.63	0.105241
A1157/1126	0.120	0.84	0.111\61	0.89	0.063446
A1157/1066	**0.003**	**1.23**	**0.22763**	**1.03**	**0.090259**
A1126/1066	**0.009**	**1.51**	**0.48992**	**1.15**	**0.130168**
A1090/1252	**0.037**	**2.04**	**0.420877**	**2.40**	**0.568487**
A958/675	0.058	0.07	0.05625	0.04	0.04866

Eight peak ratios distinguish EVs in DMEM from EVs in XF medium: A2904/2926 (p-value 0.038), A2904/2866 (p-value 0.001), A1694/1288 (p-value 0.000), A1425/1475 (p-value 0.029), A1366/1475(p-value 0.013), A1157/1066 (p-value 0.003), A1126/1066 (p-value 0.009) and A1090/1252 (p-value 0.0376), indicating the possible effect of the medium type (**figure 4.15**).

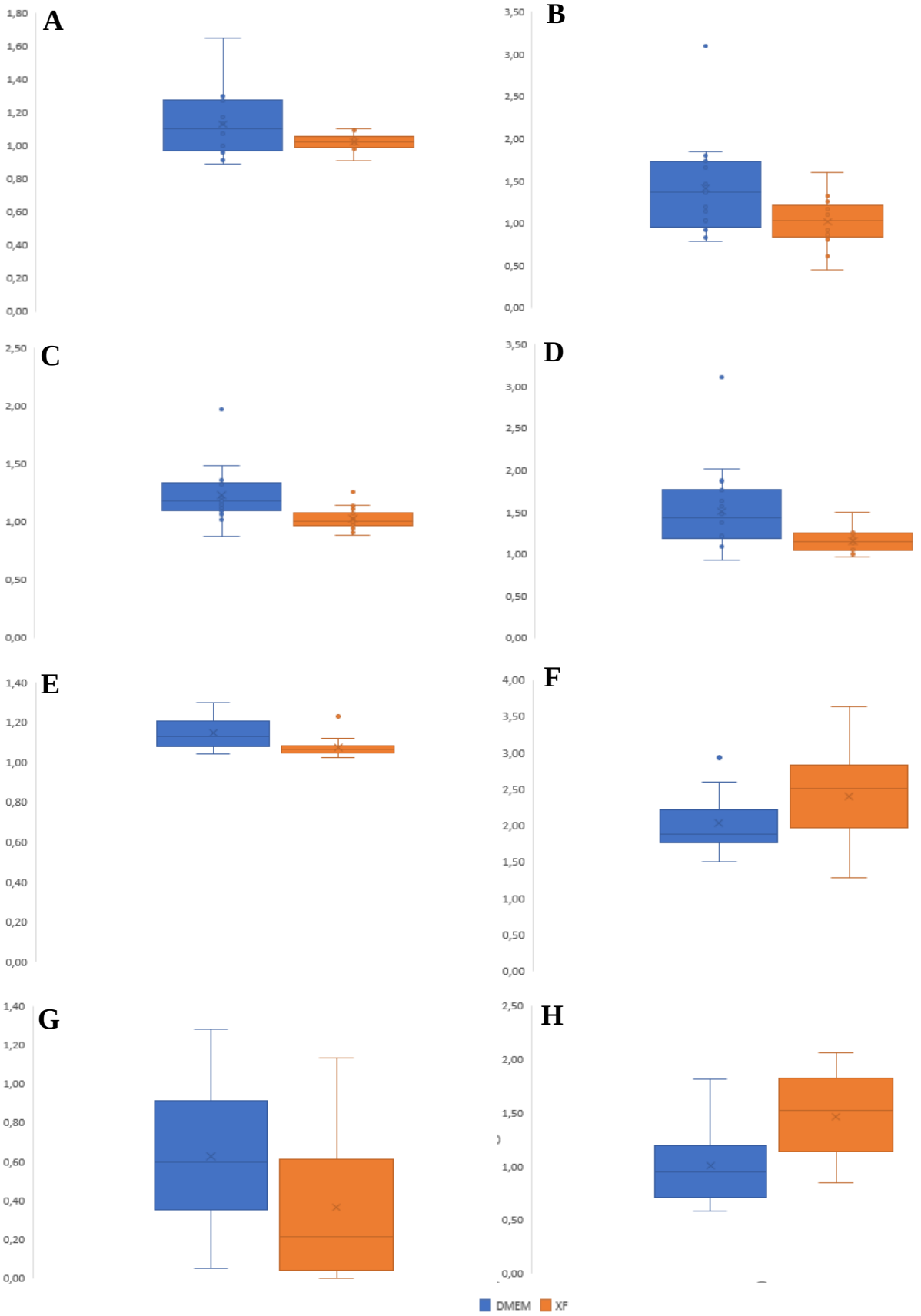

Figure 4.15 Boxplots representing the median and the other quartiles of the spectral ratios A2904/2926 (A), A1366/1475 (B), A1157/1066 (C), A1126/1066 (D), A2904/2866 (E), A1090/1252 (F), A1425/1475 (G) and A1694/1288 (H) for EVs produced in DMEM (blue) and in XF (orange) medium.

4.4. Effect of the Medium Composition, MSC source and MSC donor on Mesenchymal Stem Cells and Conditioned Media Molecular Characteristics

Cells, stored as pellets, and conditioned media before purification were also analyzed by FTIR spectroscopy. In the **Figure 4.16** is represented the FTIR spectra from the MSCs (represented in blue) conditioned media (represented in green) and purified EVs (represented in orange) from AT MSC donor L090403 for replica 1 in DMEM and XF medium.

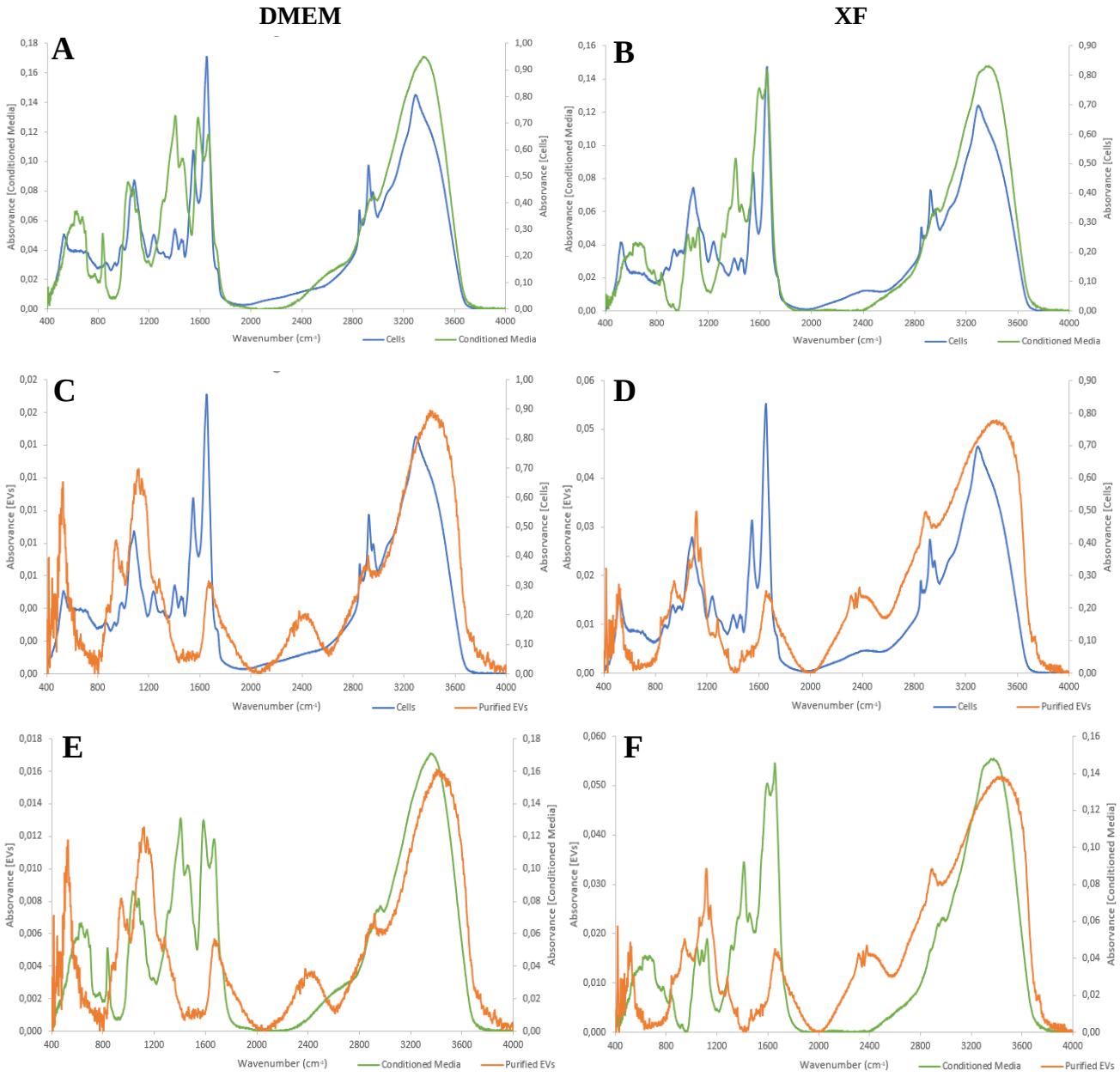

Figure 4.16 Spectra pre-processed with atmospheric and baseline correction from conditioned media (represented in green), cells (represented in blue) and purified EVs (represented in orange) from AT MSC donor L090403, replica 1, in DMEM (A, C, E)) and XF (B, D, F) medium.

The relevant common spectral bands between cells and conditioned media are: the peak at around 1089 cm^{-1} related with phosphate groups, in DMEM (**figure 4.16 A**) and the peak at around 1652 cm^{-1} attributed to Amide I from proteins, in XF medium (**figure 4.16 B**).

Cells spectra possess peaks more defined than conditioned media, such as the most intense peak at 1652 cm^{-1} already mentioned; 2928 and 2857 cm^{-1} corresponding to the absorption of CH_2 and CH_3 groups of lipids; 1551 cm^{-1} which corresponds to Amide II from proteins; and a peak at the fingerprint region at 539 cm^{-1}. In relation to conditioned media spectra, it has intense peaks at 1589 cm^{-1} which corresponds to Amide II; 1472 and 1416 cm^{-1} corresponding to bending vibrations of CH_3 and CH_2 groups of lipids and proteins; 1322 cm^{-1} corresponding to Amide III from proteins; three peaks, 1041, 1105 and 1047 cm^{-1} which correspond to phosphate groups; and a peak at the fingerprint region at 840 cm^{-1}. For simplicity, the EVs profile is not describe, since it was already performed in the previous subchapter.

Comparing the FTIR spectra from isolated EVs and cells (**Figure 4.16 C and D**) and conditioned media (**Figure 4.16 E and F**), the common spectral bands between them are the peak at around 3400 cm^{-1}, which is attributed to N-H group stretching (in both culture media) and the peaks in the range 2850-2970 cm^{-1}, corresponding to the absorption of CH_2 and CH_3 groups of lipids (for conditioned media versus purified EVs).

In addition, visualizing the profiles of cells, EVs and conditioned media from AT MSC donor L090403 for replica 1 in XF and DMEM medium (**figure 4.17 A, B and C**, respectively), it is possible to observe that for three cases, in both media, the profiles were very similar, except in the relative intensities of Amide I and II bands for conditioned media (**figure 4.17 C**).

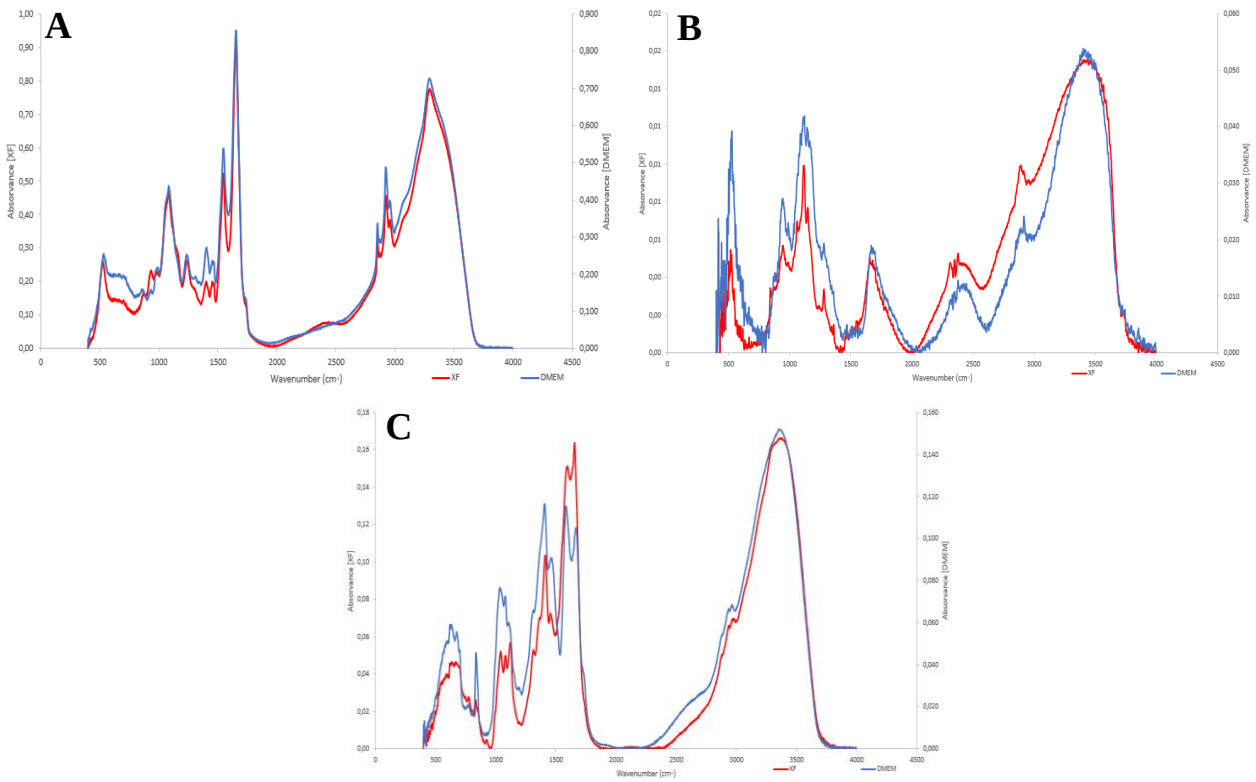

Figure 4.17 Spectra pre-processed with atmospheric and baseline correction from cells (A), purified EVs (B) and conditioned media (C) from AT MSC donor L090403, replica 1, in DMEM (represented in red) and XF (represented in blue) medium.

In order to visualize the cells' profile from different sources in the same media, **Figures 4.18 A and B** represent FTIR spectra from cells and conditioned media, respectively, in DMEM medium, from BM MSC donor M79A15 (blue line), AT MSC donor L090724 (red line) and UCM MSC donor #2 (grey line) for replica 1.

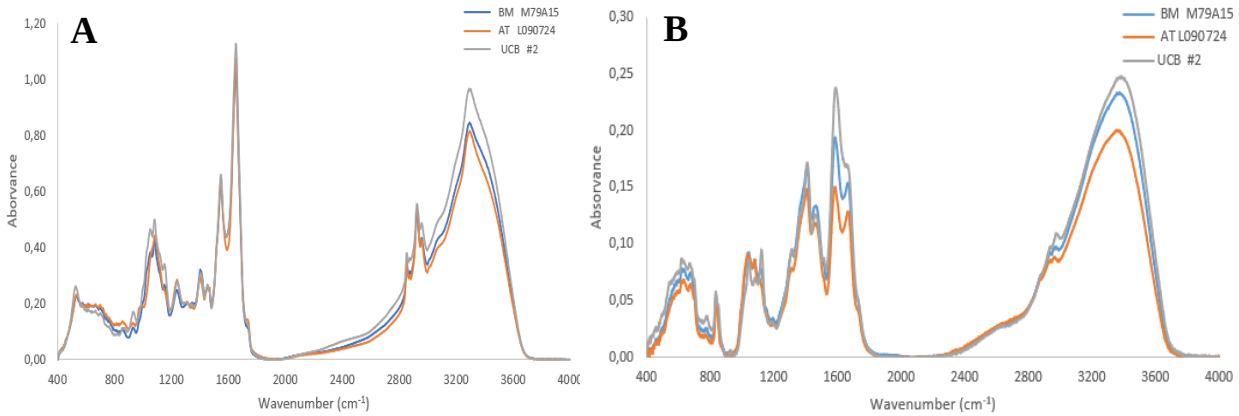

Figure 4.18 FTIR spectra pre-processed with atmospheric and baseline correction from cells (A) and conditioned media (B) in DMEM medium, from BM MSC donor M79A15 (blue), AT MSC donor L090724 (red) and UCB MSC donor #2 (green).

It was possible to observe that the MSC's profile from three sources is very similar, existing slight differences regarding the relative's intensities of bands in general. Although, for conditioned media there are more evident differences, namely in the relative intensities of Amide I and II bands. These observations are generalized for all cell's samples, both is DMEM and XF medium but not for conditioned media, since in both media, some conditioned media's samples, from any MSCs source, present Amide I and II bands with the same intensity, and others present a difference between these two peaks, as can be seen in **figure 4.17.**

The following subchapters contain the same workflow that was conducted to EVs spectra in **chapter 4.3**, which encompasses evaluating by PCAs of conditioned media and cells spectra after testing the same combinations of spectra pre-processing methods. The study was also complemented by HCA when appropriated. For both, cells and conditioned media, the best spectra pre-processing were the atmospheric and baseline correction and normalization to amide I as well as first derivative.

4.4.1. **Effect of the culture media on the cells and conditioned media molecular profile**

Figure 4.19 A and B represent PCAs of non-processed spectra of MSCs and conditioned media, respectively. PCAs with cells and conditioned media spectra pre-processed by atmospheric and baseline correction and normalization to amide I as well as first derivative are represented in **Figure 4.19 C and D**, respectively.

In all PCA score-plots, it was observed that MSCs in DMEM medium (in blue) are more dispersed in the score plot than samples in XF medium (in red) (**figure 4.19 A and C**). Thus, MSCs molecular profile depends of the media were where cultivated. Furthermore, MSCs cultured in XF medium present a more homogeneous molecular profile between them, when compared to MSC cultured in DMEM.

The HCA of MSC pre-processed spectra (**figure 4.19 E)** corroborated the PCA observations, as a nearly perfect separation of clusters between the MSC grown on the two media were achieved: 100% and 89% of MSCs cultured in DMEM and XF medium were correctly classify. There were two misclassified cell's samples of XF medium from the same source (UCM MSC) but different donors (#78 and #6). These two samples correspond to label numbers 35 and 33 in PCA score plot, which supported this misclassify since both samples are more distant from the XF's cluster. Furthermore, the cluster distance of MCS cultured in XF was lower than the distance of associated to DMEM, corroborating that MSCs cultured in XF media are more similar between them than MSC cultured in DMEM.

The PCA score plot of conditioned media spectra also showed two data clusters in function of media type (XF versus DMEM medium), were DMEM conditioned media data presented a higher dispersion in the score plot than XF data (**figure 4.19 B and D**). Therefore, and as observed with MCSs, XF medium samples presented a more homogenous molecular profile between them than DMEM conditioned media samples. These observations were corroborated by HCA (**figure 4.19 F**), were all XF media spectra were classified in a different cluster from the DMEM media spectra. Furthermore, the cluster distance of the XF conditioned media cluster is lower (i.e. they are more homogenous) than the distance for the DMEM conditioned media cluster.

In resume, the molecular profile of conditioned media was according to the molecular profile of MSCs, were cells cultured on XF medium presented a more homogenous molecular composition than cells cultured in DMEM. Consequently, XF conditioned media also presented a more homogenous molecular profile than DMEM conditioned media samples.

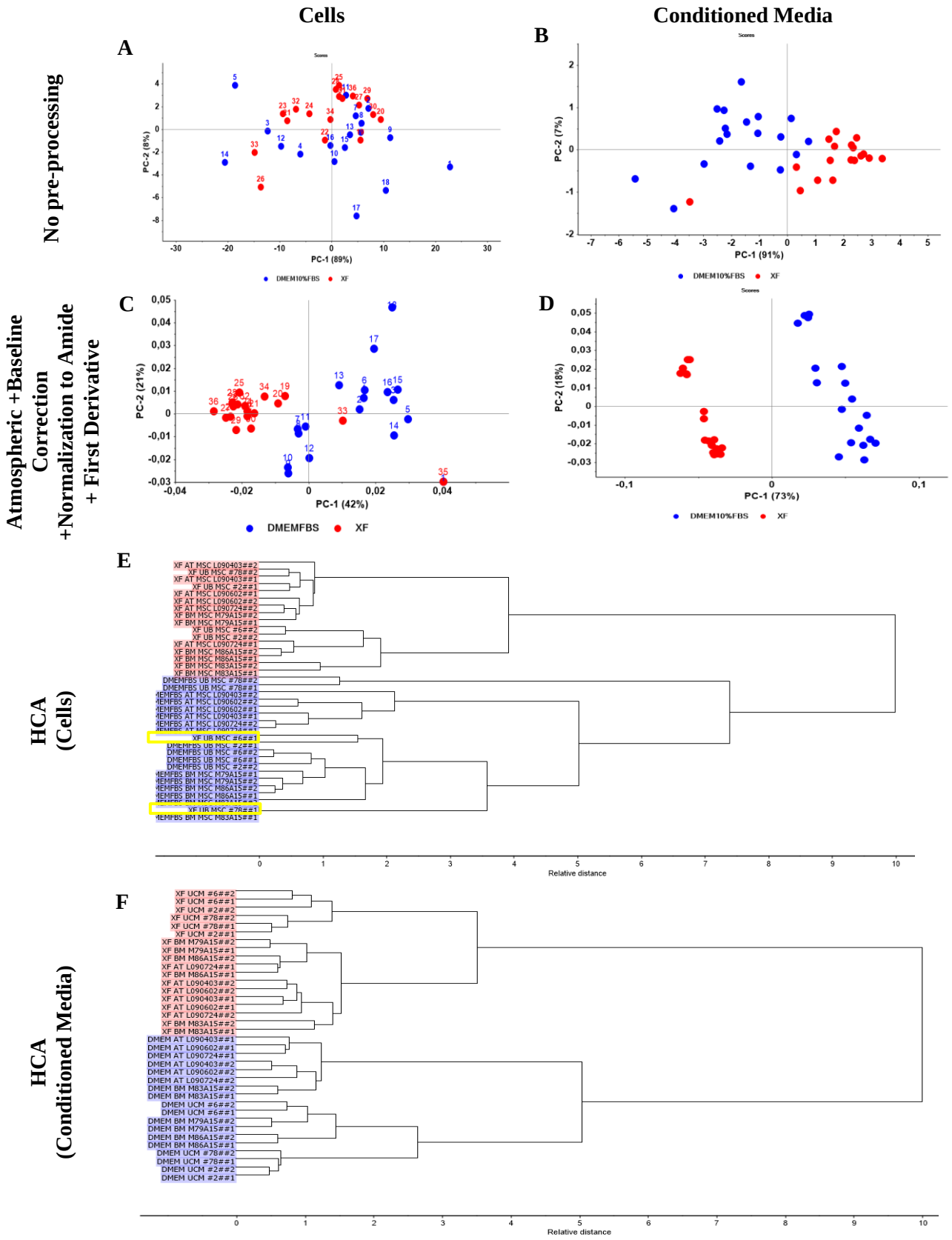

Figure 4.19 PCA for cells (A, C) and conditioned media (B,D) with no processing, atmospheric and baseline correction as well as normalization to amide I as well as first derivative pre-processing. Representation of DMEM in blue and XF in red. The respective HCA (Spearman's rank correlation distance) for cells (E) and conditioned media (F) are represented. In general, in HCA, representation of DMEM in red and XF in blue. Each sample is represented by culture media, MSC source, donor number and number of duplicated.

4.4.2. **Effect of the MSC Source on the cells and conditioned media molecular profile**

To evaluate how the MSC source (BM, AT and UCM) affects cells and conditioned media chemical characteristics, data associated to the two types of media were evaluated separately (**figures 4.20 and 4.21**). The PCA and HCA will be discussed based on pre-processed spectra, as this shown the best results in relation to analysis conducted with non-processed spectra.

In relation to conditioned media, it was observed either in DMEM, either in XF media, the data cluster (in the PCA sore plot and HCA) in function of the MSC source. Therefore, the MSC source affected the molecular profile of the conditioned media, independently of the media type (**figure 4.20 D, F and figure 4.21 D, F**). This effect is clearer in the XF media, were cluster of a defined MSC source data are closer together and apart from other sources. Interestingly, PC1 separates samples of AT and BM from UCM samples. This was observed either in DMEM either in XF medium, corroborating that MSC source influences the MSC metabolism and consequently the conditioned media.

It was observed that samples of DMEM conditioned media from AT MSCs source (in red), seem to present more a homogeneous chemical composition between them, since they are closer from each other than the remaining samples from other MSC sources (**figure 4.20 D**). This was confirmed by HCA (**figure 4.20 F**), where all these samples were included in the same cluster (in red). Two samples from BM MSCs (in blue) were closer to samples from AT MSCs. By HCA, these samples divided the same sub-cluster (in red), which means that they have a similar chemical composition. A high dispersion of remaining sources (UCM MSCs in green and BM MSCs in blue) was observed. Furthermore, by HCA, two samples from UCM MSCs were similar chemically to the others of BM MSCs since they are part a same sub-cluster (in blue). For samples XF medium conditioned (**figure 1.21 D**) samples of the UCM MSCs source (in green) separated from the remaining, i.e. presented a different molecular fingerprint in relation to AT and BM MSCs sources that were similar between them. This was confirmed by HCA **(figure 4.21 F)**, where samples of UCM MSCs source formed a cluster (in red) and AT and BM MSCs sources formed another cluster (in green and red).

Some of the above observations were not so visible in the MSC spectra. Cells cultured in DMEM medium showed some distinct molecular profiles in function of the source, especially cells from AT presented a distinct cluster either in PCA score plot either in the HCA (**figure 4.20 C and E**). Cells cultured in XF medium did not clustered according to MSC source (**figure 4.21 C and E**). It was expected that MSCs metabolism is dependent of the XF medium, as observed in XF conditioned media. A possible justification for this observation is that the cells quantity needs to obtain a spectrum with a good signal-to-noise ratio was determined based on cells grown on in DMEM medium. Ideally, this should have been also based on cells cultured in XF medium.

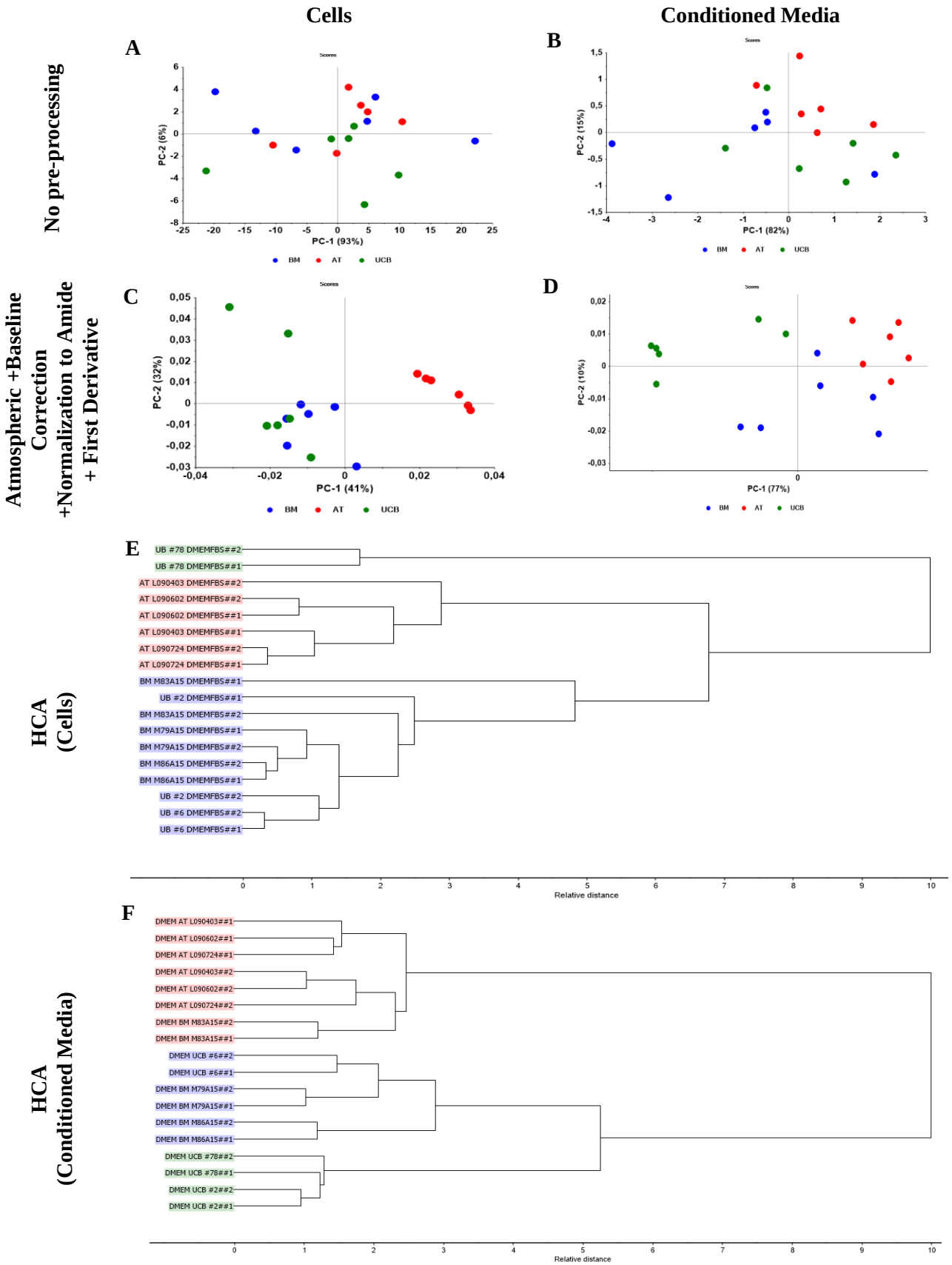

*Figure 4.20 PCA scores for cells spectra and conditioned media spectra from three MSCs sources, BM (represented in blue), AT (represented in red) and UCM (represented in green), in **DMEM medium** with no processing (A), atmospheric and baseline correction as well as normalization to amide I as well as first derivative (B). The respective HCA (Spearman's rank correlation distance) for cells (E) and conditioned media (F) for are represented.*

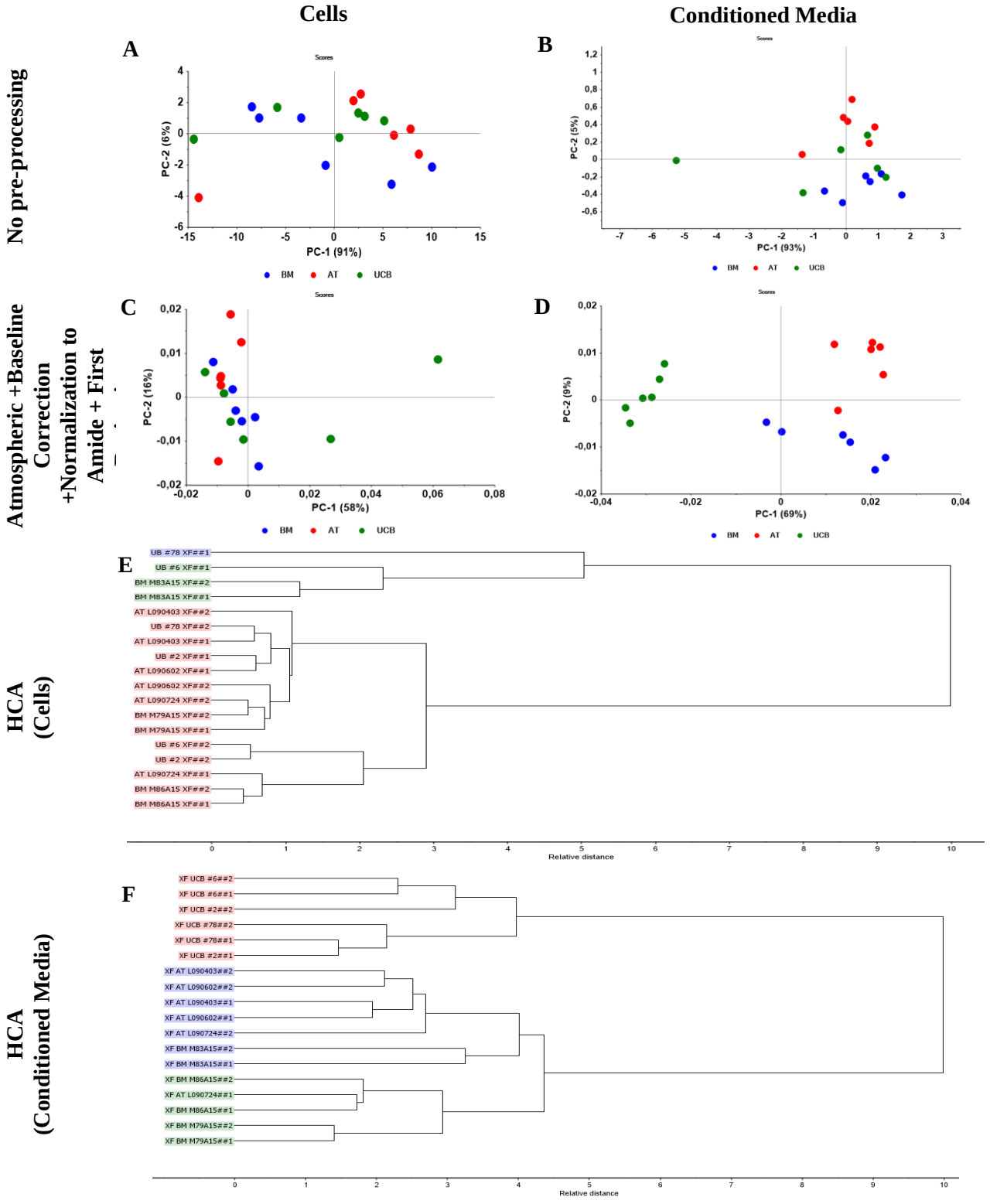

*Figure 4.21 PCA scores for cells spectra and conditioned media spectra from three MSCs sources, BM (represented in blue), AT (represented in red) and UCM (represented in green), in **XF medium** with no processing (A), atmospheric and baseline correction as well as normalization to amide I as well as first derivative (B). The respective HCA (Spearman's rank correlation distance) for cells (E) and conditioned media (F) for are represented.*

In fact, it is observed a higher variability between spectra of MSCs cultured in XF medium (**figure 4.22 A, B and C**) and in DMEM medium (**figure 4.22 E, F and G**). The majority of MSC spectra has

a maximum absorvance higher than 0.5, reflecting the impact of the variability of MSCs donors on MSC growth, and consequently the estimation of DF should have been conducted, even for each MSC culture.

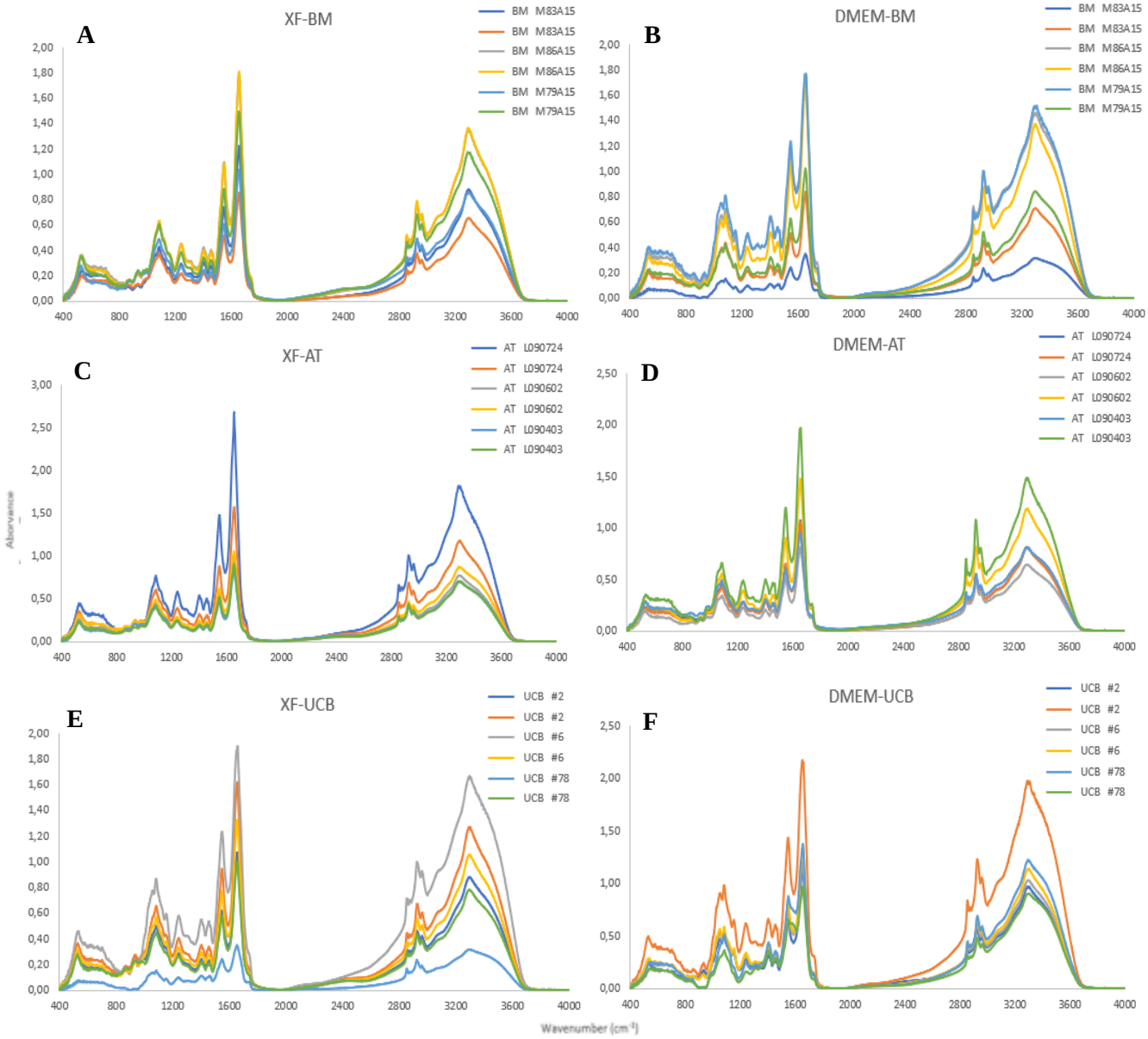

Figure 4.22 Spectra pre-processed with atmospheric and baseline correction from MSCs from BM, AT and UCM sources cultured, in XF (A, C, E)) and DMEM (B, D, F) medium. Donors are represented in different colors.

4.4.3. **Effect of the MSCs Donor on cells and conditioned media molecular profile**

The effect of the MSCs donors in the molecular composition of MSCs and conditioned media was evaluated separately for each of the sources (BM, AT and UCM) produced in DMEM and XF media. **Figures 4.23, 4.24 and 4.25** represent PCA score plots, each for MSCs source in a defined medium and in function of the MSCs donor. The PCA and HCA will be discussed based on pre-processed spectra, as this shown the best results in relation to analysis conducted with non-processed spectra.

In general, it was observed either in MSCs, either in conditioned media, that there was always some separation of samples in function of the MSC donor, independently of the source and the culture medium used.

In relation to conditioned media, it was observed either in DMEM, either in XF media data clusters (in the PCA score plot and HCA) in function of the MSC donor. Therefore, the MSC donor affected the molecular profile of the XF or DMEM conditioned media. Within AT and UCM sources, this effect is clearer in XF conditioned media than in DMEM conditioned media, were cluster of each MSC donor data are closer together and apart from other donors.

Within BM source, in both conditioned media (**figure 4.23 C and D**), it was observed that the replicas of each donor seem to group which indicates that conditioned media from each MSCs donor present a lower variability. Interestingly, PC1 separates samples of M86A15 and M79A15 from M83A15 samples. This was observed either in DMEM either in XF conditioned medium and corroborated by HCAs (**figure 4.23 F and H**), where the donor M83A15 formed a cluster (in blue) and other donors formed another cluster (in red and green). Furthermore, the cluster distance of the donors from DMEM conditioned media cluster is lower (i.e. they are more homogenous) than the distance for the donors from XF conditioned media cluster.

Within AT source, samples of DMEM conditioned media were more dispersed in PCA score plot (**figure 4.24 C**). This is corroborated by HCA (**figure 4.24 H**), where none donor replicas were defined by a unique cluster. However, if the samples of donor L090403 (in green) are removed, PC2 separates samples of remaining donors. For XF conditioned media (**figure 4.24 D**), PC1 separates samples of donor L090724 (in blue) from other donors, as can be verified by a unique cluster formed by this donor (in blue and red) in HCA (**figure 4.24 F**). The other donors were more chemically similar between them since incorporated same cluster (in green).

Within UCM source, DMEM and XF conditioned medium from donor #6 (in green) presented a lower variability between replicas and were separated from other donors (**figures 4.25 C and D**). This is supported by HCA where the donor formed a different cluster (**figures 4.25 F and H**), which corroborate the different molecular composition of this donor in relation to the other donors.

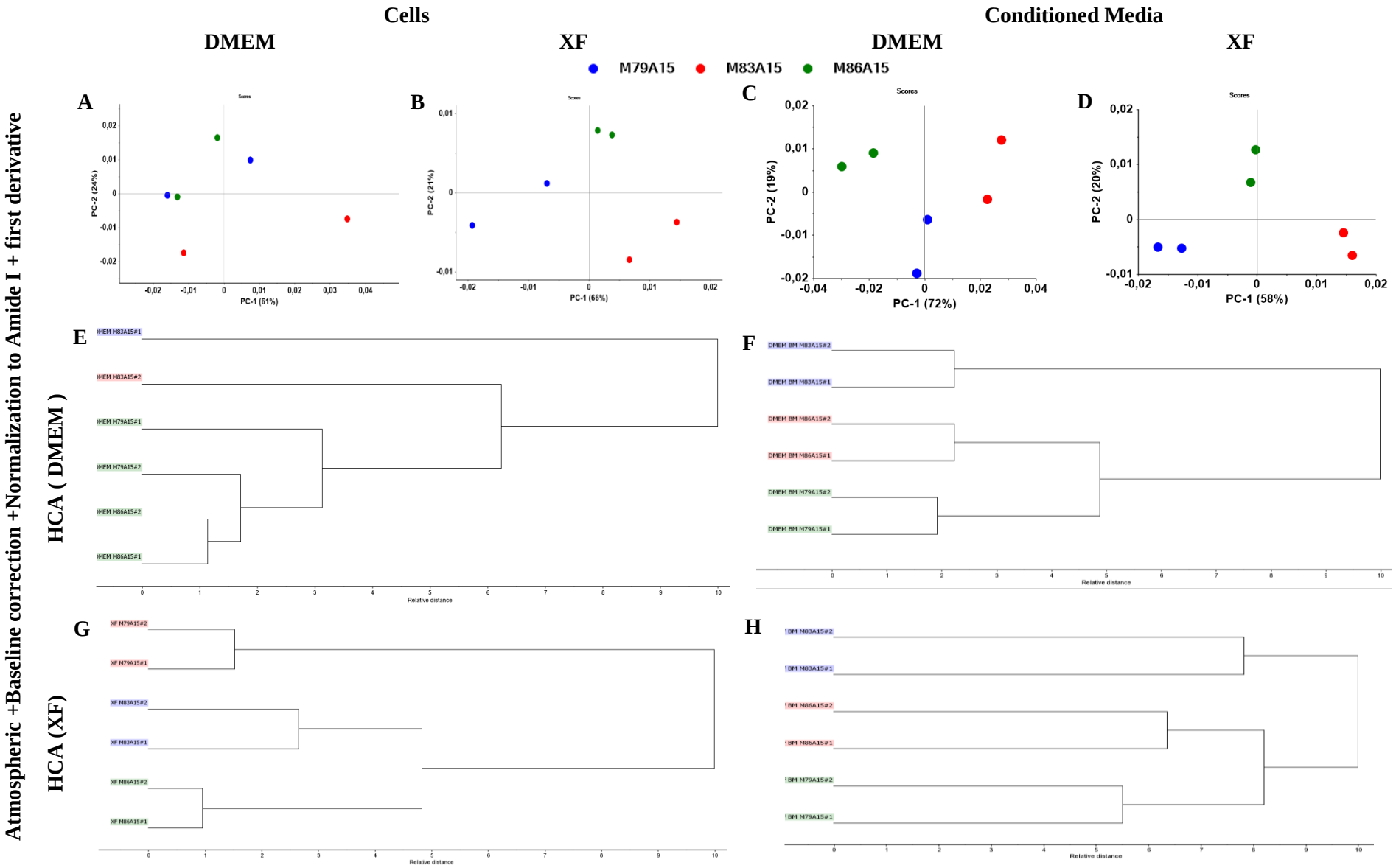

*Figure 4.23 PCA for cells and conditioned media spectra from **BM MSCs** in XF and DMEM medium, considering MSCs donors: M79A15 (represented in blue), M83A15 (represented in red) and M86A15 (represented in green), with no processing; and atmospheric and baseline correction as well as normalization to amide I and first derivative. (A, B, E, G) - PCAs of Cells cultured in DMEM and XF medium and corresponding HCAs. (C, D, F, H) - PCAs of DMEM and XF conditioned medium and corresponding HCAs. All HCAs with Spearman's rank correlation distance.*

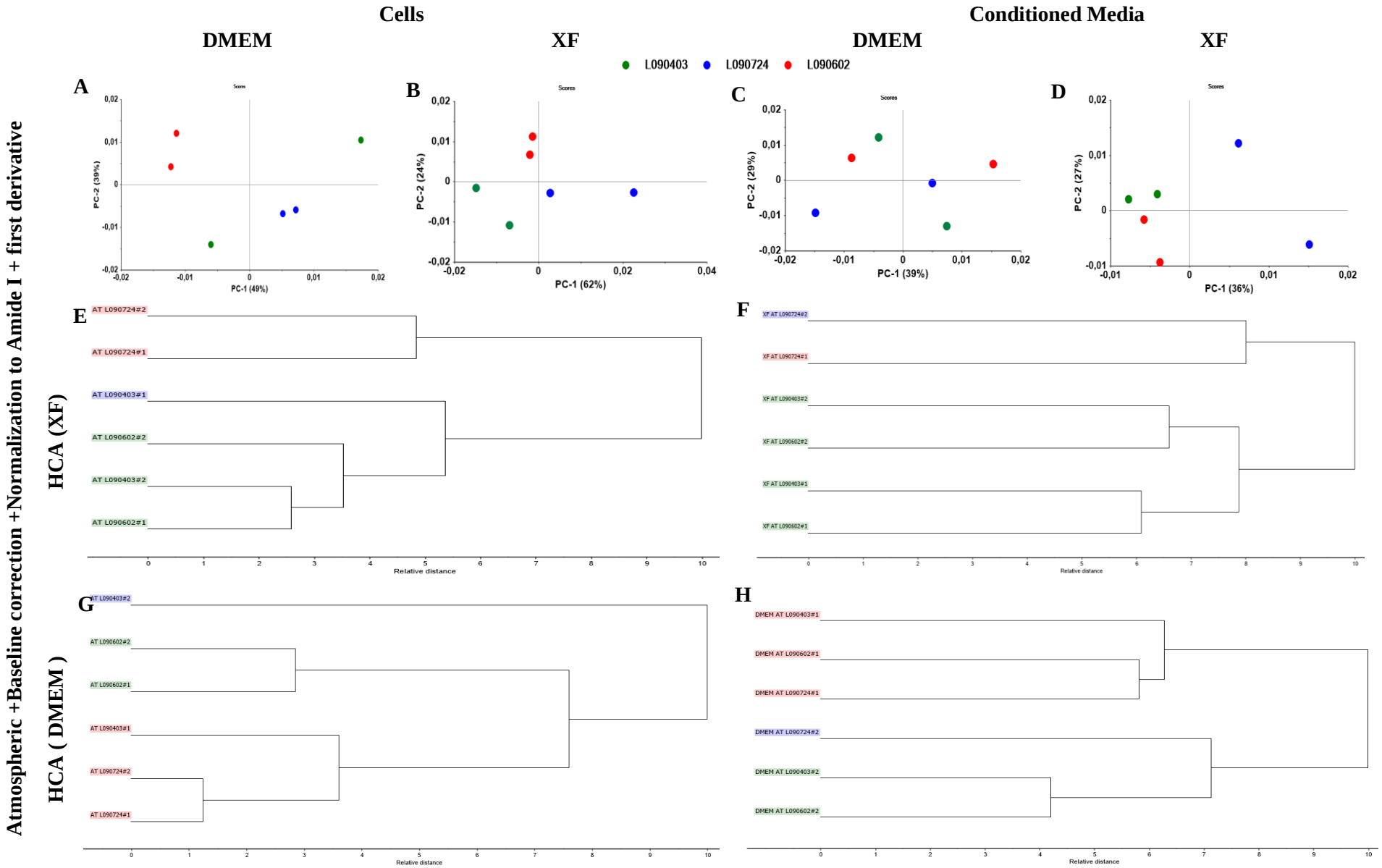

*Figure 4.24 PCA for cells and conditioned media spectra from **AT MSCs** in XF and DMEM medium, considering MSCs donors: L090403 (represented in blue), L090724 (represented in red) and L090602 (represented in green), with no processing; and atmospheric and baseline correction as well as normalization to amide I and first derivative. (A, B, E, G) - PCAs of Cells cultured in DMEM and XF medium and corresponding HCAS. (C, D, F, H) - PCAs of DMEM and XF conditioned medium and corresponding HCAS. HCAs with Spearman's rank correlation distance or Kendall's Tau.*

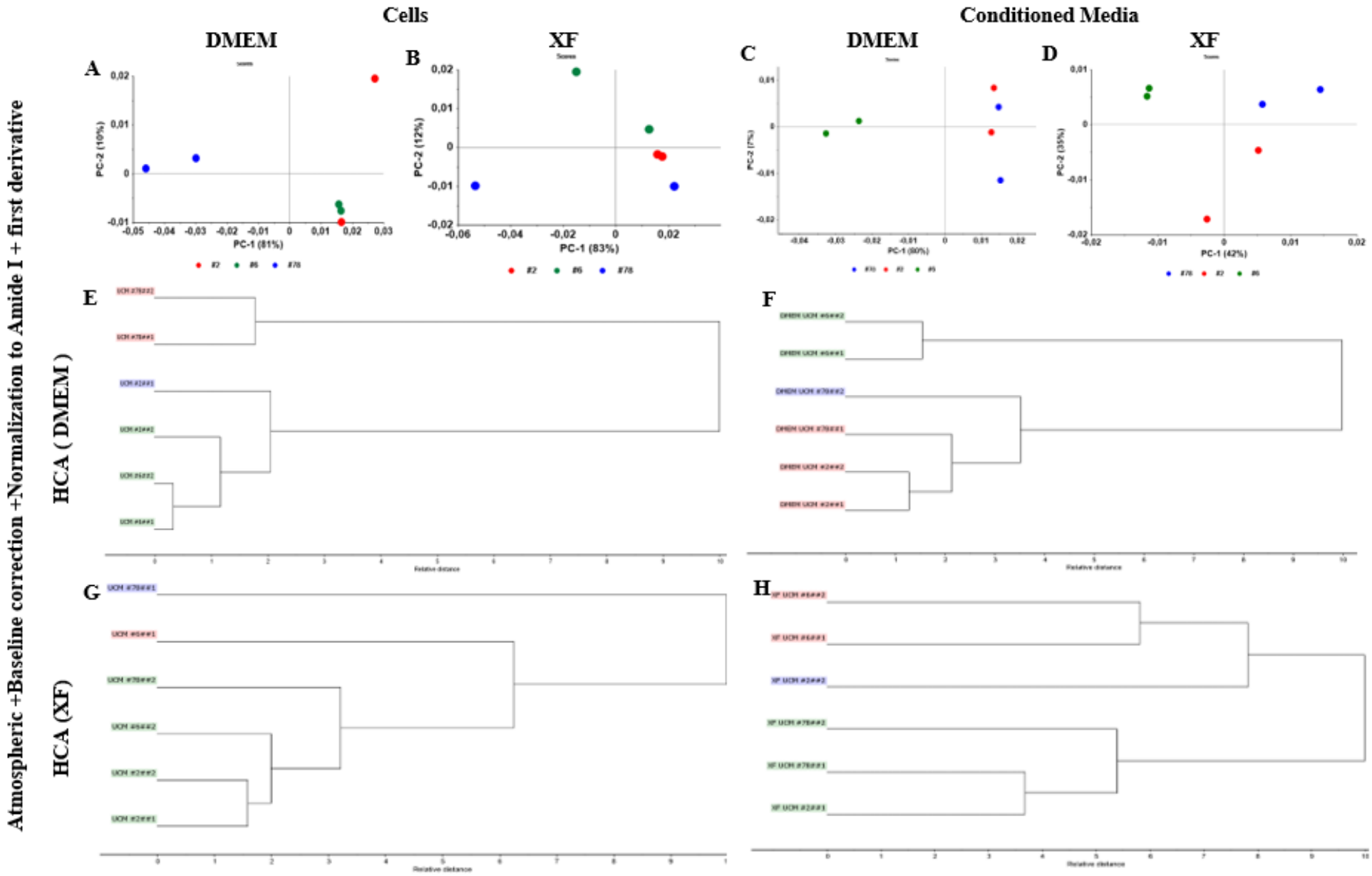

*Figure 4.25 PCA for cells and conditioned media spectra from **UCM MSCs** in XF and DMEM medium, considering MSCs donors: : #78 (represented in blue), #2 (represented in red) and #6 (represented in green) with no processing; and atmospheric and baseline correction as well as normalization to amide I and first derivative. (A, B, E, G) - PCAs of Cells cultured in DMEM and XF medium and corresponding HCAS. (C, D, F, H) - PCAs of DMEM and XF conditioned medium and corresponding HCAS. All HCAs with Spearman's rank correlation distance.*

In relation to MSCs spectra, some observations were identical to conditioned media. Interestingly, as observed in samples of DMEM conditioned media from AT source, if the MSC samples of donor L090403 (in green) are removed, PC2 separates samples of remaining donors (**figure 4.24 A**).

Cells from BM cultured in DMEM medium (**figure 4.23 A**) showed some distinct molecular profiles in function of the donor: donor M83A15 (in red) present a different cluster in PCA score plot, where PC2 separates samples of this donor from remaining donors. Donors M79A15 (in blue) and M86A15 (in green) have a similar molecular profile, which it was corroborated by HCA (**figure 4.23 E**). Within UCM source, MSCs cultured in DMEM medium, PC1 separates samples of donor #78 (in blue) from other donors (**figure 4.25 A**), as can be verified by a cluster formed by this donor (in red) in HCA (**figure 4.25 E**). Cells cultured in XF medium from donor #2 (red) presented a lower variability either in PCA score plot (**figure 4.25 B**), either in HCA (**figure 4.25 G**).

In summary, as observed for EV donor's samples, there is no pattern among replicas of each donor in general. Although, in the following donors, respective replicas present a lower variability between them:

For cells:

- Donor M86A15 from BM MSCs cultured in XF medium;
- Donor L090602 from AT MSCs cultured in both media;
- Donor L090724 from AT MSCs cultured in DMEM medium;
- Donor #2 and #6 from UCM MSCs cultured in XF and DMEM medium, respectively.

For conditioned media:

- Donor M86A15 from BM MSCs for both conditioned media;
- Donors M83A15 and M79A15 from BM MSCs for XF conditioned medium;
- Donor #6 from UCM MSCs for both conditioned media;
- Donor #2 from UCM MSCs for DMEM conditioned medium.

The molecular profile of conditioned media and MSCs samples depended on the MSCs donor and source and the type of media. For a specific conditioned media or MSCs and relative to a defined MSC source, there were donors that presented distinct characteristics from the others, which indicates that conditioned media or MSCs from these specific source and donor presented a specific molecular profile.

4.4.4. **The spectral regions that discriminates MSCs at different cultured media and conditioned media between them**

To infer the most significant spectral regions that contribute to discriminate data in the analysis of the previous chapters the loadings of the PC that best separate the data clusters were considered. This was conducted to evaluate the spectral regions that discriminated MSC in function of the cultured media and DMEM vs XF conditioned medium. In both cases, it was considered the loading of PC1 (**figures 4.26 A and B**).

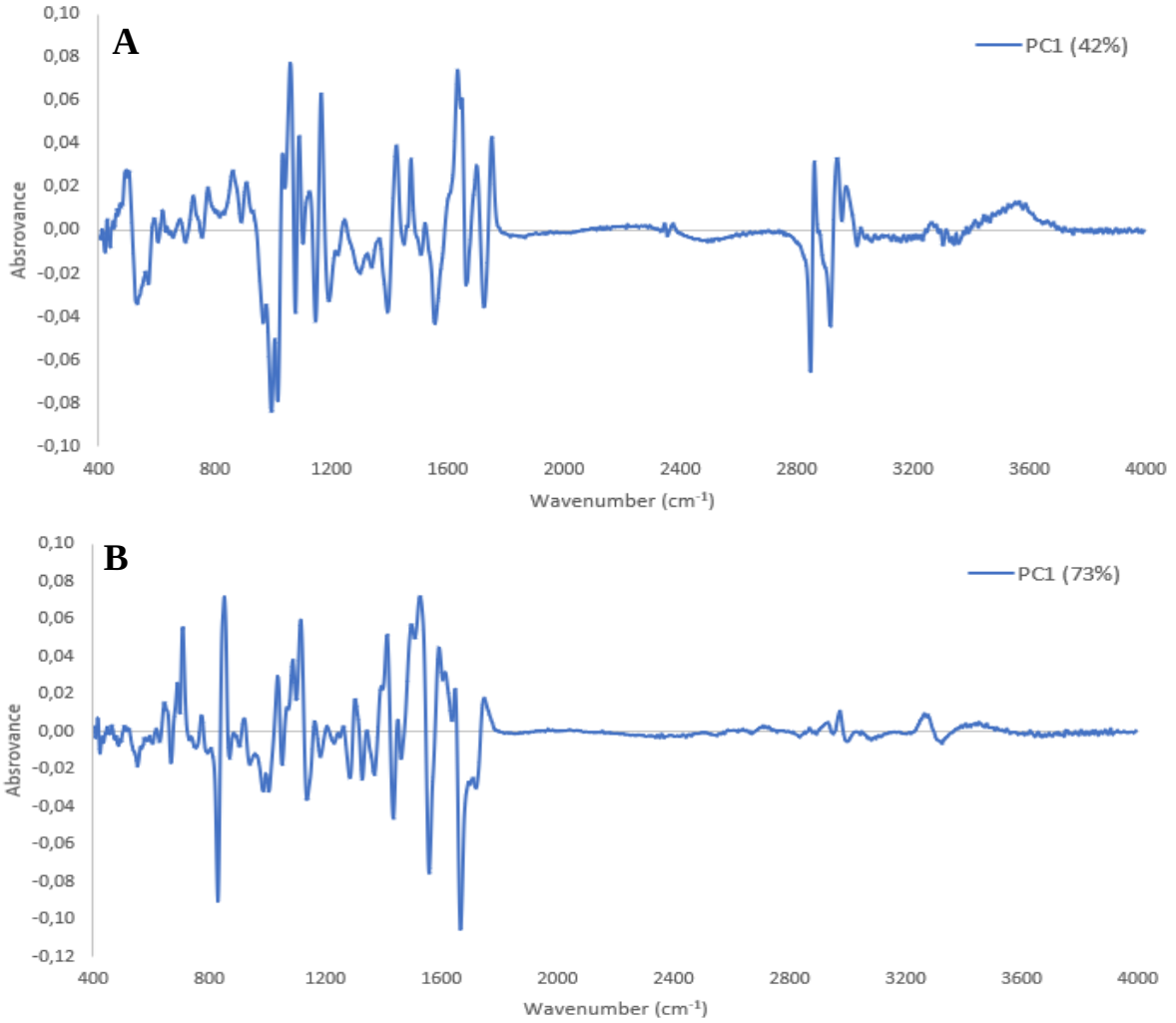

Figure 4.26 PC1 loadings for cells spectra cultured in XF and DMEM media (A) with 42% variance and for DMEM and XF conditioned media spectra (B) with 73% variance.

For cells, the most relevant peaks were at 867 and 912 cm^{-1}, which can be attributed to stretching vibrations from COP groups in phosphorylated proteins; 1059 and 1089 cm^{-1}, which corresponds to CO stretching vibrations from DNA and RNA ribose; 1166 cm^{-1}, the most intense peak, which can be attributed to RNA ribose; between 1426 and 1471 cm^{-1}, which may be attributed to bending vibrations from lipids and proteins; 1635 cm^{-1}, which correspond to Amide I band from proteins; 1702 and 1722 cm^{-1}, which corresponds to CO stretching vibrations from phospholipid esters; 2860, 2940 and 2976 cm^{-1}, which they are present in lipids and associated with the symmetrical and

asymmetrical stretching vibrations of CH_3 and CH_2 groups.

In relation to conditioned media, the most important peaks that contribute for discrimination appear at 853 cm^{-1}, which can be attributed to stretching vibrations from COP groups from phosphorylated proteins; 1037 and 1089 cm^{-1}, which corresponds to CO stretching vibrations from DNA and RNA ribose; 1116 cm^{-1}, which corresponds to CO stretching vibrations from DNA and RNA ribose; 1305 and 1398 cm^{-1}, which can be associated with the wagging vibrations of CH_3 and CH_2 groups in phospholipids, fatty acids, triglycerides; 1413 cm^{-1}, which may be attributed to bending vibrations of CH_3 from lipids and proteins; 1529 cm^{-1}, the most intense peak which corresponds to stretching vibrations of CC groups from Amide II peptides and proteins; 1648 cm^{-1}, which corresponds to Amide I band from proteins.

4.5. Prediction of the quantity of EVs and Cells produced and the Metabolic Profile of Conditioned Media

Considering that, in the present work, the spectra was acquired from dehydrated films, it is expected that the Beer-Lambert´s Law is not applicable, as its assumptions are for diluted solutions. However, diverse authors observed that in dehydrated films, there are also, in defined conditions, a direct proportion between absorvance and the analyte that absorbs. To predict the quantity of EVs from whole spectra, it was considered the sum the absorvances of all wavenumbers. The average between the absorvances of two biological replicas of donors and the respective standard deviation were determined as represented in **figure 4.27**. This type of analysis was also conducted with spectra from MSC and from conditioned media. For cells, DF and respective number of cells of each donor (represented in **table 4.1**) was considered, and consequently the final obsorvance values is theoretically proportional to the mass of MSC.

The quantity of EVs produced (**figure 4.27 A**) in XF medium, in general, is higher than in DMEM. This is in accordance with the lower absorvances obtained in the spectra from DMEM medium and with the higher cell growth in the XF culture medium (**table 4.1**), since more cells mean more EVs secreted by them. However, donor M83A15 is an exception, whom the result obtain in DMEM is higher than XF medium. While in DMEM donors from BM-MSCs source have the highest absorvances and relatively with the same quantity of EVs produced between donors; in XF, donor L090724 from AT-MSCs source presents the higher production of EVs.

In relation to the cells (**figure 4.27 B**), there are no pattern between donors from the same source in both culture media. For donors from AT source (in red) in DMEM, the absorvance per number of cells does not differ much, which it is accordance with the homogeneous molecular composition between them observed in previous chapters.\ The lower value is observed with donor #78 from UCM source in XF, which corresponded to its localization in the PCA scores plots: further away from the other samples. The higher production of cells is observed in donor L090724 from AT source in XF medium, which it is in accordance with the higher EVs produced with this donor.

In case of conditioned media (**figure 4.27 C**), it was observed an opposition result relative to EVs produced: in general, the highest absorvance are presented in DMEM conditioned medium, especially with donors from BM source (in blue). However, donor #78 from UCM-MSCs is an exception, were a higher value was observed in XF than in DMEM medium. In DMEM, the absorvances between donors from AT and UCM-MSCs sources do not differ much. The same is observed in XF between donors from BM and AT-MSCs sources.

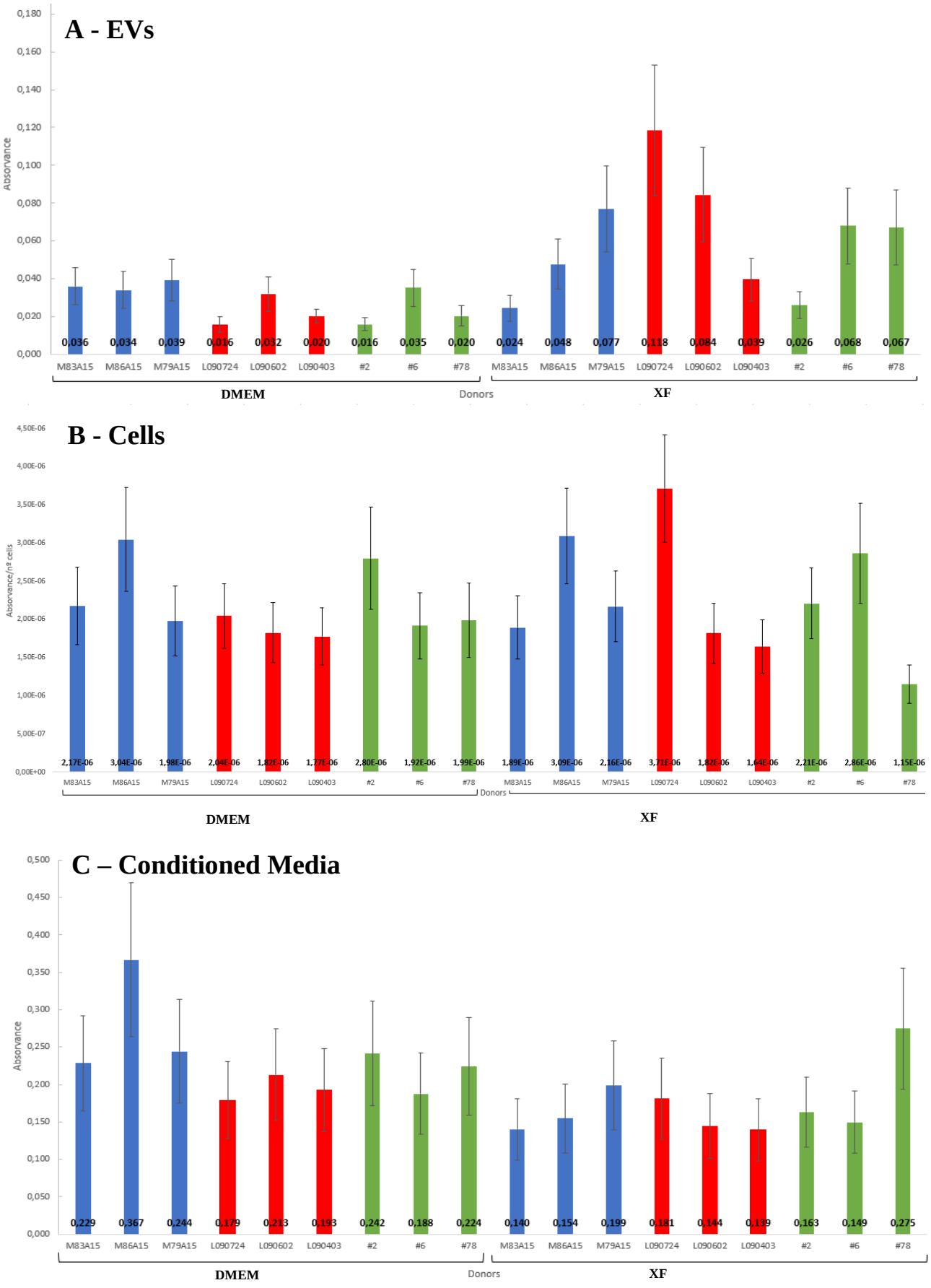

Figure 4.27 Sum of absorvances for whole spetra for EVs (A), cells (B) and conditioned media (C) per MSCs donors produced in DMEM and XF medium. Bars corresponding to BM (in blue), AT (in red) and UCM (in green) sources are represented, respectively, by blue, red and green. The respective absorvance or absorvance per number of cells are represented in each bar.

Chapter 5: Conclusions and Future Work

Considering the theoretically relevance of MSC EVs in human therapies, it is crucial to evaluate the impact of the conditioned media, MSC sources and donors on the EVs chemical profile and biological activity. To conduct this, usually diverse, complex, cost and time-consuming techniques are needed. Therefore, it is relevant to develop new methods that enable this type of characterization in a more simple, high-throughput and economic mode. The FTIR spectroscopy associated to uni- and multi-variate data analysis technique presents characteristics that could enabled to achieve that, as it enables to acquire the molecular profile of biological samples, as MSC, conditioned media and EVs in a highly specific and sensitive mode, but also in a fast, economic and high-throughput way. The present work aimed to evaluate the impact of MSC sources (from adipose tissue, bone marrow and umbilical cord blood), as well as of three donors per source in the molecular profile of EVs. Two types of media were also evaluated (XF versus DMEMFBS). In the present work duplicates of cultures were conducted. As a complementary study, the molecular profile of MSCs and the conditioned media were also studied by FTIR spectroscopy.

To obtain the EVs from conditioned media, an isolation kit was applied. However, the reagent kit adsorbed at the EVs surface, shielding the EVs signal on the spectra, according to other researchers observations as by *Lee et al* [137] and *Pereira et al* [134]. The last researchers observed, however, that higher dilutions of isolated EVs implied a desorption of the kit polymer and consequently on a spectrum mostly due to EVs. In present work, it was evaluated the optimization of the isolation protocol based on that kit, to increase the kit polymer precipitation. Although, highly variable EVs spectra were still obtained. Independently of this high replicas variability, it was possible to observe that the molecular profile of EVs depends of the medium type, where apparently EVs chemical profiles were more homogenous when MSC were cultured in DMEM than in XF medium. Probably due to the polymer interference on the spectra, in general, it was not possible to observe distinct patterns of EVs chemical composition in function of MSC source, with exception of EVs from UCM obtained in XF medium. It was observed an apparent impact of MSC donor on the EVs chemical composition, especially in XF medium. Some donors presented, on the PCA score plots, a distinct cluster from remaining donors either in XF either in DMEM medium, as donor M83A15 from BM, donor L090403 from AT and donor #78 from UCM. These results corroborate the results obtained by *Pereira et al* [134] that observed the impact of different donors from BM on the EVs molecular profile obtained by FTIR spectroscopy.

It was observed molecular profiles of cells and conditioned media patterns according to cultured media (DMEM vs XF). It was observed that MSC presented a more homogeneous molecular profile between them, obtained from different MSC sources and donors, when cultured in XF medium in relation to cells cultured in DMEM medium. This tendency was also observed in conditioned media, i.e., XF conditioned media present a more homogeneous molecular profiles than DMEM conditioned media among different conditions.

The conditioned media molecular profile, both on XF and DMEM, depended from the MSC source and donor. The molecular profile of conditioned media, obtained from different MSC sources and donors, was more homogeneous in XF medium than in DMEM.

The MSCs molecular profile analysis, presented some limitations, as its was obtained from frozen cell pellets and the quantity of cells used to acquire the spectra was not optimized. Consequently, the spectra from XF medium samples had a higher variability and high absorvance values. Even so, it was possible top observe that the MSC molecular profile also depended from the MSC donors. These molecular profiles were more affected by donor when cells were cultured in XF medium in relation to cells cultured in DMEM medium. The differences observed on the molecular profiles in function of the donor were more distinct in the analysis of conditioned media than the analysis of MSCs. It was not possible to observe the effect of MSC source on the molecular profile of cells, with exception for cells from AT in DMEM medium. However, this result is not conclusive since the cell analysis presented limitations.

From the three samples' types studied by FTIR spectroscopy (isolated EVs from kit, frozen cell pellets and conditioned media), the analysis of conditioned media are the ones with the greatest confidence, i.e. with less variability between duplicated cultures, because:

- Conditioned media spectra presented absorvance values more similar between them (with values of absorvance between 0.1 and 0.31 at 1602 cm^{-1}.
- EVs spectra were obtained from higher dilutions, implying either reduced signals. Furthermore EVs spectra still presents the polymer interference, that is also variable from sample to sample.
- The spectra cell analyses were from frozen pellets,and were not optimized considering the cells quantity. Consequently, spectra with highly variable signal to noise ratios were obtained. For example, some cells spectra presented absorvances (at 3400 cm^{-1}) near the unit, implying the saturation of some spectral bands, while other presented absorvance values (to the same spectral band) as low as 0.3.

Based on the PCA and HCA of conditioned media pre-processed spectra, it was possible to observe that the MSC source (BM, AT and UCM) imply different molecular profiles of conditioned media and most probably different EVs molecular profiles. It also was observed that the MSC donor affects the conditioned media molecular profile and most probably the EVs molecular profile. In general, it was observed that XF conditioned media, from different MSC sources and donors, implied a higher homogenous molecular profile than in DMEM based media. It was also observed, that conditioned media profile was also affected by MSC sources and donors. These results were corroborated by observations effectuated with isolated EVs (in special, relatively to the donors) and MSCs (relatively to the culture media, sources and donors).

Based on the present work, there are evidences that point that the molecular profiles of EVs are affected by the media type used for MSC culture, MSC source and donor.

In future, it is crucial to test the use of an alternative EVs isolation procedure, to avoid the EVs FTIR spectra interference by the kit polymer. It is noted that this last suggestion has already been initiated by the present research group. It also is important to optimize the MSC spectra acquisition, to maximize spectra reproducibility and high signal to noise rations. Would also be highly desirable to increase the number of biological replicas per donor. Studies also focusing the biological effect of different EVs molecular profile is also advisable.

Hopefully, the present work contributed to understanding how the medium composition, MSC donors and sources, may affect the MSC and EVs molecular profile, and by this way contributed to a the understand and controlled human therapies based on MSC or its EVs. This is of paramount importance in view of the increasing number of clinical trials with MSCs.

Bibliography

1. Macpherson, C. The accidental discovery of stem cells. (2018). Available at: https://medicalxpress.com/news/2018-05-accidental-discovery-stem-cells.html. (Accessed: 21st August 2019)
2. Niwa, H. Mechanisms of Stem Cell Self-Renewal. in *Essentials of Stem Cell Biology: Third Edition* 81–94 (Elsevier Inc., 2013). doi:10.1016/B978-0-12-409503-8.00007-X
3. Zakrzewski, W., Dobrzyński, M., Szymonowicz, M. & Rybak, Z. Stem cells: past, present, and future. **5,** 1–22 (2019).
4. Amira Ragab EL Barky*, E. M. M. A. and T. M. M. Stem Cells, Classifi cations and their Clinical Applications. *Am. J. Pharmacol. Ther.* **1,** 1–7 (2017).
5. Goldthwaite, C. The Promise of Induced Pluripotent Stem Cells (iPSCs). in *Regenerative Medicine* (ed. Wisnlow, T.) 97–104 (Department of Health and Human Services, 2006).
6. Karagiannis, P. *et al.* Induced pluripotent stem cells and their use in human models of disease and development. in *Physiological Reviews* **99,** 79–114 (2019).
7. Martin, U. Therapeutic application of pluripotent stem cells: Challenges and risks. *Front. Med.* **4,** (2017).
8. Bindu A, H. & B, S. Potency of Various Types of Stem Cells and their Transplantation. *J. Stem Cell Res. Ther.* **01,** 1–6 (2011).
9. Girlovanu, M. *et al.* Stem Cells - biological update and cell therapy progress. *Med. Pharm. Reports* **88,** 265–271 (2015).
10. Bozdağ, S. C., Yüksel, M. K. & Demirer, T. Adult stem cells and medicine. *Adv. Exp. Med. Biol.* **1079,** 17–36 (2018).
11. U.S. National Library of Medicine & National Institutes of Health. ClinicalTrials.gov. (2019). Available at: https://clinicaltrials.gov/ct2/results?term=mesenchymal+stem+cells&phase=23. (Accessed: 23rd August 2019)
12. Itakura, G. *et al.* Fail-Safe System against Potential Tumorigenicity after Transplantation of iPSC Derivatives. *Stem Cell Reports* **8,** 673–684 (2017).
13. Kim, H. J. & Park, J.-S. Usage of Human Mesenchymal Stem Cells in Cell-based Therapy: Advantages and Disadvantages. *Dev. Reprod.* **21,** 1–10 (2017).
14. Prockop, D. J. Marrow stromal cells as stem cells for nonhematopoietic tissues. *Science (80-.).* **276,** 71–74 (1997).
15. Jamnig, A. & Lepperdinger, G. From tendon to nerve: An msc for all seasons. *Can. J. Physiol. Pharmacol.* **90,** 295–306 (2012).
16. Friedenstein, A. J., Afanasyev, B. V, Elstner, E. E. & Zander, A. R. founder of the mesenchymal stem cell concept Maximow and Friedenstein. *www.ctt-journal.com Cell. Ther. Transplant.* **11,** 35–38 (2009).
17. Augello, A., Kurth, T. B. & de Bari, C. Mesenchymal stem cells: A perspective from in vitro cultures to in vivo migration and niches. *Eur. Cells Mater.* **20,** 121–133 (2010).
18. Bianco, P. The great MSC History review. in **2,** 313–319 (2009).
19. Caplan, A. Mesenchymal Stem Cells. *J. Orthop. Res.* 641–650 (1991). doi:10.1016/0009-2614(70)87009-9
20. Murray, I. R. & Péault, B. Q&A: Mesenchymal stem cells - where do they come from and is it important? *BMC Biol.* **13,** 4–9 (2015).
21. Dominici, M. *et al.* Minimal criteria for defining multipotent mesenchymal stromal cells. The International Society for Cellular Therapy position statement. *Cytotherapy* **8,** 315–317 (2006).
22. Shahdadfar, A., Frønsdal, K., Haug, T., Reinholt, F. P. & Brinchmann, J. E. In Vitro Expansion of Human Mesenchymal Stem Cells: Choice of Serum Is a Determinant of Cell Proliferation, Differentiation, Gene Expression, and Transcriptome Stability. *Stem Cells* **23,** 1357–1366 (2005).
23. Li, C. Y. *et al.* Comparative analysis of human mesenchymal stem cells from bone marrow and adipose tissue under xeno-free conditions for cell therapy. *Stem Cell Res. Ther.* **6,** (2015).
24. Oikonomopoulos, A. *et al.* Optimization of human mesenchymal stem cell manufacturing: The effects of animal/xeno-free media. *Sci. Rep.* **5,** 1–11 (2015).

25. Tekkatte, C., Gunasingh, G. P., Cherian, K. M. & Sankaranarayanan, K. 'Humanized' stem cell culture techniques: The animal serum controversy. *Stem Cells Int.* **2011,** (2011).
26. Cimino, M., Gonçalves, R. M., Barrias, C. C. & Martins, M. C. L. Xeno-free strategies for safe human mesenchymal stem/stromal cell expansion: Supplements and coatings. *Stem Cells Int.* **2017,** (2017).
27. Jin, H. J. *et al.* Comparative analysis of human mesenchymal stem cells from bone marrow, adipose tissue, and umbilical cord blood as sources of cell therapy. *Int. J. Mol. Sci.* **14,** 17986–18001 (2013).
28. Berebichez-Fridman, R. & Montero-Olvera, P. R. Sources and clinical applications of mesenchymal stem cells state-of-the-art review. *Sultan Qaboos Univ. Med. J.* **18,** e264–e277 (2018).
29. Brown, C. *et al.* Mesenchymal stem cells: Cell therapy and regeneration potential. *J. Tissue Eng. Regen. Med.* 0–2 (2019). doi:10.1002/term.2914
30. Nagamura-Inoue, T. Umbilical cord-derived mesenchymal stem cells: Their advantages and potential clinical utility. *World J. Stem Cells* **6,** 195 (2014).
31. Hass, R., Kasper, C., Böhm, S. & Jacobs, R. Different populations and sources of human mesenchymal stem cells (MSC): A comparison of adult and neonatal tissue-derived MSC. *Cell Commun. Signal.* **9,** 12 (2011).
32. Mizukami, A. & Swiech, K. Mesenchymal stromal cells: From discovery to manufacturing and commercialization. *Stem Cells Int.* **2018,** (2018).
33. Kim, N. & Cho, S. G. Clinical applications of mesenchymal stem cells. *Korean J. Intern. Med.* **28,** 387–402 (2013).
34. Parekkadan, B. & Milwid, J. M. Mesenchymal Stem Cells as Therapeutics. *Annu. Rev. Biomed. Eng.* **12,** 87–117 (2010).
35. Samsonraj, R. M. *et al.* Concise Review: Multifaceted Characterization of Human Mesenchymal Stem Cells for Use in Regenerative Medicine. *Stem Cells Transl. Med.* **6,** 2173–2185 (2017).
36. Wang, Y., Chen, X., Cao, W. & Shi, Y. Plasticity of mesenchymal stem cells in immunomodulation: Pathological and therapeutic implications. *Nat. Immunol.* **15,** 1009–1016 (2014).
37. Mastrolia, I. *et al.* Concise Review: Challenges in Clinical Development of Mesenchymal Stromal/Stem Cells. *Stem Cells Transl. Med.* (2019). doi:10.1002/sctm.19-0044
38. Rohban, R. & Pieber, T. R. Mesenchymal stem and progenitor cells in regeneration: Tissue specificity and regenerative potential. *Stem Cells Int.* **2017,** (2017).
39. Börger, V. *et al.* Mesenchymal stem/stromal cell-derived extracellular vesicles and their potential as novel immunomodulatory therapeutic agents. *Int. J. Mol. Sci.* **18,** (2017).
40. Bonventre, J. V. Microvesicles from mesenchymal stromal cells protect against acute kidney injury. *J. Am. Soc. Nephrol.* **20,** 927–928 (2009).
41. Johnstone, R. M., Adam, M., Hammond, J. R., Orr, L. & Turbide, C. Vesicle formation during reticulocyte maturation. Association of plasma membrane activities with released vesicles (exosomes). *J. Biol. Chem.* **262,** 9412–9420 (1987).
42. Konala, V. *et al.* The current landscape f the mesenchyal stromal cell secretome: A new paradigm for cell-free regeneration. *Inf. Syst. Res.* **18,** 13–24 (2016).
43. Keshtkar, S., Azarpira, N. & Ghahremani, M. H. Mesenchymal stem cell-derived extracellular vesicles: Novel frontiers in regenerative medicine. *Stem Cell Res. Ther.* **9,** 1–9 (2018).
44. Mushahary, D., Spittler, A., Kasper, C., Weber, V. & Charwat, V. Isolation, cultivation, and characterization of human mesenchymal stem cells. *Cytom. Part A* **93,** 19–31 (2018).
45. Gimona, M., Pachler, K., Laner-Plamberger, S., Schallmoser, K. & Rohde, E. Manufacturing of human extracellular vesicle-based therapeutics for clinical use. *Int. J. Mol. Sci.* **18,** (2017).
46. Ferreira, A. da F. & Gomes, D. A. Stem cell extracellular vesicles in skin repair. *Bioengineering* **6,** 1–18 (2019).
47. Kotmakçı, M. & Akbaba, G. E. Exossome Isolation: Is There an Optimal Method with Regard to Diagnosis or Treatment? in *Novel Implications of Exosomes in Diagnosis and Treatment of Cancer and Infectious Diseases* (ed. InTech) **3,** 163–181 (2017).
48. Phan, J. *et al.* Engineering mesenchymal stem cells to improve their exosome efficacy and yield for cell-free therapy. *J. Extracell. Vesicles* **7,** (2018).

49. Caruso, S. & Poon, I. K. H. Apoptotic cell-derived extracellular vesicles: More than just debris. *Front. Immunol.* **9,** (2018).
50. Hartjes, T. A., Mytnyk, S., Jenster, G. W., van Steijn, V. & van Royen, M. E. Extracellular vesicle quantification and characterization: Common methods and emerging approaches. *Bioengineering* **6,** (2019).
51. Doyle, L. M. & Wang, M. Z. Overview of Extracellular Vesicles, Their Origin, Composition, Purpose, and Methods for Exosome Isolation and Analysis. *Cells* **8,** 727 (2019).
52. Shah, R., Patel, T. & Freedman, J. E. Circulating extracellular vesicles in human disease. *N. Engl. J. Med.* **379,** 958–966 (2018).
53. El Andaloussi, S., Mäger, I., Breakefield, X. O. & Wood, M. J. A. Extracellular vesicles: Biology and emerging therapeutic opportunities. *Nat. Rev. Drug Discov.* **12,** 347–357 (2013).
54. Théry, C. *et al.* Minimal information for studies of extracellular vesicles 2018 (MISEV2018): a position statement of the International Society for Extracellular Vesicles and update of the MISEV2014 guidelines. *J. Extracell. Vesicles* **7,** (2018).
55. Lucchetti, D., Fattorossi, A. & Sgambato, A. Extracellular Vesicles in Oncology: Progress and Pitfalls in the Methods of Isolation and Analysis. *Biotechnol. J.* **14,** 1–10 (2019).
56. Sokolova, V. *et al.* Characterisation of exosomes derived from human cells by nanoparticle tracking analysis and scanning electron microscopy. *Colloids Surfaces B Biointerfaces* **87,** 146–150 (2011).
57. Szatanek, R., Baran, J., Siedlar, M. & Baj-Krzyworzeka, M. Isolation of extracellular vesicles: Determining the correct approach (review). *Int. J. Mol. Med.* **36,** 11–17 (2015).
58. Jeyaram, A. & Jay, S. M. Preservation and Storage Stability of Extracellular Vesicles for Therapeutic Applications. *AAPS J.* **20,** (2018).
59. Konoshenko, M. Y., Lekchnov, E. A., Vlassov, A. V. & Laktionov, P. P. Isolation of Extracellular Vesicles: General Methodologies and Latest Trends. *Biomed Res. Int.* **2018,** (2018).
60. Momen-Heravi, F. *et al.* Current methods for the isolation of extracellular vesicles. *Biol. Chem.* **394,** 1253–1262 (2013).
61. Serrano-Pertierra, E. *et al.* Characterization of plasma-derived extracellular vesicles isolated by different methods: A comparison study. *Bioengineering* **6,** 1–13 (2019).
62. Patel, G. K. *et al.* Comparative analysis of exosome isolation methods using culture supernatant for optimum yield, purity and downstream applications. *Sci. Rep.* **9,** 1–10 (2019).
63. Rosa-Fernandes, L., Rocha, V. B., Carregari, V. C., Urbani, A. & Palmisano, G. A perspective on extracellular vesicles proteomics. *Front. Chem.* **5,** 1–19 (2017).
64. Zarovni, N. *et al.* Integrated isolation and quantitative analysis of exosome shuttled proteins and nucleic acids using immunocapture approaches. *Methods* **87,** 46–58 (2015).
65. Tofiño-Vian, M., Guillén, M. I. & Alcaraz, M. J. Extracellular vesicles: A new therapeutic strategy for joint conditions. *Biochem. Pharmacol.* **153,** 134–146 (2018).
66. Bandu, R., Oh, J. W. & Kim, K. P. Mass spectrometry-based proteome profiling of extracellular vesicles and their roles in cancer biology. *Exp. Mol. Med.* **51,** (2019).
67. Gézsi, A., Kovács, Á., Visnovitz, T. & Buzás, E. I. Systems biology approaches to investigating the roles of extracellular vesicles in human diseases. *Exp. Mol. Med.* **51,** (2019).
68. Leal, L. B., Nogueira, M. S., Canevari, R. A. & Carvalho, L. F. C. S. Vibration spectroscopy and body biofluids: Literature review for clinical applications. *Photodiagnosis Photodyn. Ther.* **24,** 237–244 (2018).
69. Yaghoubi, Y. *et al.* Human umbilical cord mesenchymal stem cells derived-exosomes in diseases treatment. *Life Sci.* **233,** 116733 (2019).
70. Hong, P., Yang, H., Wu, Y., Li, K. & Tang, Z. The functions and clinical application potential of exosomes derived from adipose mesenchymal stem cells: a comprehensive review. *Stem Cell Res. Ther.* **10,** 242 (2019).
71. Rani, S., Ryan, A. E., Griffin, M. D. & Ritter, T. Mesenchymal stem cell-derived extracellular vesicles: Toward cell-free therapeutic applications. *Mol. Ther.* **23,** 812–823 (2015).
72. Najar, M. *et al.* Mesenchymal Stromal Cell-Based Therapy: New Perspectives and Challenges. *J. Clin. Med.* **8,** 626 (2019).
73. Fujita, Y., Kadota, T., Araya, J., Ochiya, T. & Kuwano, K. Clinical Application of Mesenchymal Stem Cell-Derived Extracellular Vesicle-Based Therapeutics for Inflammatory

Lung Diseases. *J. Clin. Med.* **7,** 355 (2018).
74. Cominal, J. G. *et al.* Emerging Role of Mesenchymal Stromal Cell-Derived Extracellular Vesicles in Pathogenesis of Haematological Malignancies. *Stem Cells Int.* **2019,** 1–12 (2019).
75. Qiu, G. *et al.* Mesenchymal stem cell-derived extracellular vesicles affect disease outcomes via transfer of microRNAs. *Stem Cell Res. Ther.* **9,** 1–9 (2018).
76. Chen, Y., Tang, Y., Fan, G. C. & Duan, D. D. Extracellular vesicles as novel biomarkers and pharmaceutic targets of diseases. *Acta Pharmacol. Sin.* **39,** 499–500 (2018).
77. Sadovska, L., Eglitis, J. & Line, A. Extracellular vesicles as biomarkers and therapeutic targets in breast cancer. *Anticancer Res.* **35,** 6379–6390 (2015).
78. Mihály, J. *et al.* Characterization of extracellular vesicles by IR spectroscopy: Fast and simple classification based on amide and C[sbnd]H stretching vibrations. *Biochim. Biophys. Acta - Biomembr.* **1859,** 459–466 (2017).
79. Smith, B. *Fundamentals of Fourier Transform Infrared Spectroscopy*. (2011). doi:10.1088/0953-8984/10/15/011
80. Stuart, B. *Infrared Spectroscopy: Fundamentals and Aplications*. (2004).
81. De Bruyne, S., Speeckaert, M. M. & Delanghe, J. R. Applications of mid-infrared spectroscopy in the clinical laboratory setting. *Crit. Rev. Clin. Lab. Sci.* **55,** 1–20 (2018).
82. Türker-Kaya, S. & Huck, C. W. A review of mid-infrared and near-infrared imaging: Principles, concepts and applications in plant tissue analysis. *Molecules* **22,** (2017).
83. Allison, R. R. The electromagnetic spectrum: current and future applications in oncology. *Futur. Sience Gr.* **9,** 657–667 (2013).
84. Higdon, T. FT-IR Spectroscopy Technology , Market Evolution and Future Strategies of Bruker Optics Inc . by FT-IR Spectroscopy Technology , Market Evolution and Future Strategies of Bruker Optics Inc . by. *Matrix* (2010).
85. Duygu, D., Baykal, T., Açikgöz, I. & Yildiz, K. Fourier transform infrared (FT-IR) spectroscopy for biological studies. *Gazi Univ. J. Sci.* **22,** 117–121 (2009).
86. Berthomieu, C., Ae, C. B. & Hienerwadel, R. Fourier transform infrared (FTIR) spectroscopy Molecular mechanisms of uranium tolerance View project Radionuclide-protein interactions View project Fourier transform infrared (FTIR) spectroscopy. 157–170 (2009). doi:10.1007/s11120-009-9439-x
87. Moraes, L. G. P. *et al.* Infrared spectroscopy: A tool for determination of the degree of conversion in dental composites. *J. Appl. Oral Sci.* **16,** 145–149 (2008).
88. Novais, Â., Freitas, A. R., Rodrigues, C. & Peixe, L. Fourier transform infrared spectroscopy: unlocking fundamentals and prospects for bacterial strain typing. *Eur. J. Clin. Microbiol. Infect. Dis.* **38,** 427–448 (2019).
89. Bellisola, G. & Sorio, C. Infrared spectroscopy and microscopy in cancer research and diagnosis. *Am. J. Cancer Res.* **2,** 1–21 (2012).
90. Barth, A. Infrared spectroscopy of proteins. *Biochim. Biophys. Acta - Bioenerg.* **1767,** 1073–1101 (2007).
91. Movasaghi, Z., Rehman, S. & ur Rehman, D. I. Fourier Transform Infrared (FTIR) Spectroscopy of Biological Tissues. *Appl. Spectrosc. Rev.* **43,** 134–179 (2008).
92. Jesús, O. & Dittrich, M. Fourier Transform Infrared Spectroscopy for Molecular Analysis of Microbial Cells. in *Microbial Systems Biology: Methods and Protocols - Methods in Molecular Biology* (ed. Springer Science+Business Media, L. 2012) **881,** 187–211 (2012).
93. Blum, M. M. & John, H. Historical perspective and modern applications of Attenuated Total Reflectance - Fourier Transform Infrared Spectroscopy (ATR-FTIR). *Drug Test. Anal.* **4,** 298–302 (2012).
94. López-Lorente, Á. I. & Mizaikoff, B. Mid-infrared spectroscopy for protein analysis: Potential and challenges. *Anal. Bioanal. Chem.* **408,** 2875–2889 (2016).
95. Usoltsev, D., Sitnikova, V., Kajava, A. & Uspenskaya, M. Systematic FTIR Spectroscopy Study of the Secondary Structure Changes in Human Serum Albumin under Various Denaturation Conditions. 1–17 (2019).
96. Wang, M., Karlsson, J. O. M. & Aksan, A. FTIR Analysis of Molecular Changes Associated with Warming Injury in Cryopreserved Leukocytes. *Langmuir* **35,** 7552–7559 (2019).
97. Han, Y. *et al.* Insight into rapid DNA-specific identification of animal origin based on FTIR analysis: A case study. *Molecules* **23,** (2018).

98. Al-Jorani, K. *et al.* The application of ATR-FTIR spectroscopy and the reversible DNA conformation as a sensor to test the effectiveness of platinum(II) anticancer drugs. *Sensors (Switzerland)* **18,** (2018).
99. Zucchiatti, P. *et al.* Contribution of Ribonucleic Acid (RNA) to the fourier transform infrared (FTIR) Spectrum of eukaryotic cells. *Anal. Chem.* **88,** 12090–12098 (2016).
100. El-Azazy, M. Infrared Spectroscopy - A Synopsis of the Fundamentals and Applications. in *Infrared Spectroscopy - Principles, Advances, and Applications* (ed. IntechOpen) 1–10 (2018). doi:http://dx.doi.org/10.5772/intechopen.82210
101. Aksoy, C. & Severcan, F. Role of vibrational spectroscopy in stem cell research. *Spectrosc. (New York)* **27,** 167–184 (2012).
102. Sulé-Suso, J., Forsyth, N. R., Untereiner, V. & Sockalingum, G. D. Vibrational spectroscopy in stem cell characterisation: Is there a niche? *Trends Biotechnol.* **32,** 254–262 (2014).
103. Birkner, N. & Wang, Q. Chemistry LibreTexts. *How an FTIR Stectrometer Operates* 1–7 (2019). Available at: https://chem.libretexts.org/link?1844. (Accessed: 6th September 2019)
104. Lau, K. Vibrational Spectroscopy on Stem Cells in Wound Healing. (Faculty of Ohysical Chemistry of the Friedrich Schiller, 2011).
105. Thermo Fisher Scientific. Introduction to Fourier Transform Infrared Spectroscopy. (2013).
106. Chandra, A., Talari, S. & Martinez, M. A. G. Advances in Fourier Transform Infrared (FTIR) Spectroscopy of Biological Tissues. **4928,** (2016).
107. Wenning, M. & Scherer, S. Identification of microorganisms by FTIR spectroscopy: Perspectives and limitations of the method. *Appl. Microbiol. Biotechnol.* **97,** 7111–7120 (2013).
108. Perez-Guaita, D., Garrigues, S. & de la, M. Infrared-based quantification of clinical parameters. *TrAC - Trends Anal. Chem.* **62,** 93–105 (2014).
109. Hughes, C. *et al.* Assessing the challenges of Fourier transform infrared spectroscopic analysis of blood serum. *J. Biophotonics* **7,** 180–188 (2014).
110. Miller, L. M., Bourassa, M. W. & Smith, R. J. FTIR spectroscopic imaging of protein aggregation in living cells. *Biochim. Biophys. Acta - Biomembr.* **1828,** 2339–2346 (2013).
111. Bellisola, G. *et al.* Rapid recognition of drug-resistance/sensitivity in leukemic cells by fourier transform infrared microspectroscopy and unsupervised hierarchical cluster analysis. *Analyst* **138,** 3934–3945 (2013).
112. Landgrebe, D. *et al.* On-line infrared spectroscopy for bioprocess monitoring. *Appl. Microbiol. Biotechnol.* **88,** 11–22 (2010).
113. Liu, K. Z., Xu, M. & Scott, D. A. Biomolecular characterisation of leucocytes by infrared spectroscopy. *Br. J. Haematol.* **136,** 713–722 (2007).
114. Heneczkowski, M. & Kuzniar, A. Infrared Spectrum Analysis of Some Flavonoids. *Acta Plonise Pharm. - Drug Res.* **58,** 415–420 (2001).
115. Sevinc, A., Yonar, D. & Severcan, F. Investigation of neurodegenerative diseases from body fluid samples using Fourier transform infrared spectroscopy. *Biomed. Spectrosc. Imaging* **4,** 341–357 (2015).
116. Hughes, C. *et al.* SR-FTIR spectroscopy of renal epithelial carcinoma side population cells displaying stem cell-like characteristics. *Analyst* **135,** 3133–3141 (2010).
117. Pijanka, J. K. *et al.* Vibrational spectroscopy differentiates between multipotent and pluripotent stem cells. *Analyst* **135,** 3126–3132 (2010).
118. Tanthanuch, W., Thumanu, K., Lorthongpanich, C., Parnpai, R. & Heraud, P. Neural differentiation of mouse embryonic stem cells studied by FTIR spectroscopy. *J. Mol. Struct.* **967,** 189–195 (2010).
119. Ami, D. *et al.* Embryonic stem cell differentiation studied by FT-IR spectroscopy. *Biochim. Biophys. Acta - Mol. Cell Res.* **1783,** 98–106 (2008).
120. Aksoy, C., Guliyev, A., Kilic, E., Uckan, D. & Severcan, F. Bone marrow mesenchymal stem cells in patients with beta thalassemia major: Molecular analysis with attenuated total reflection-fourier transform infrared spectroscopy study as a novel method. *Stem Cells Dev.* **21,** 2000–2011 (2012).
121. Grasso, L., Wyss, R. & Vogel, H. Use of Fourier Transform Infrared Spectroscopy Analysis of Extracellular Vesicles isolated from body fluis for diagnosing, prognosing and monitoring pathophysiological states and method therfor. 1–14 (2016).

122. Zlotogorski-Hurvitz, A., Dekel, B. Z., Malonek, D., Yahalom, R. & Vered, M. FTIR-based spectrum of salivary exosomes coupled with computational-aided discriminating analysis in the diagnosis of oral cancer. *J. Cancer Res. Clin. Oncol.* **145,** 685–694 (2019).
123. Lee, J. *et al.* Infrared spectroscopic characterization of monocytic microvesicles (microparticles) released upon lipopolysaccharide stimulation. *FASEB J.* **31,** 2817–2827 (2017).
124. Han, C. *et al.* Human umbilical cord mesenchymal stem cell derived exosomes encapsulated in functional peptide hydrogels promote cardiac repair. *Biomater. Sci.* **7,** 2920–2933 (2019).
125. Gautam, R., Vanga, S., Ariese, F. & Umapathy, S. Review of multidimensional data processing approaches for Raman and infrared spectroscopy. *EPJ Tech. Instrum.* **2,** (2015).
126. Morais, C. L. M. *et al. Standardization of complex biologically derived spectrochemical datasets*. *Nature Protocols* **14,** (Springer US, 2019).
127. Perez-Guaita, D., Kuligowski, J., Quintás, G., Garrigues, S. & De La Guardia, M. Atmospheric compensation in fourier transform infrared (FT-IR) spectra of clinical samples. *Appl. Spectrosc.* **67,** 1339–1342 (2013).
128. Lasch, P. Spectral pre-processing for biomedical vibrational spectroscopy and microspectroscopic imaging. *Chemom. Intell. Lab. Syst.* **117,** 100–114 (2012).
129. Bruker Optik GmbH. Manipulate - Baseline Correction. in *OPUS Spectroscopy Software - Quick Reference Guide* 105–106 (2004).
130. Camo Software AS. *The Unscrambler X v10.3 User Manual*. (2014).
131. Vivó-Truyols, G. & Schoenmakers, P. J. Automatic selection of optimal Savitzky-Golay smoothing. *Anal. Chem.* **78,** 4598–4608 (2006).
132. Tafintsev, D. Multivariate Classification Methods for Spectroscopic Data with Multiple Class Structure. (Norges miljo-og biovitenskapelige universitet, 2016).
133. Guo, J. Diagnosing Changes in Cells Using FTIR Microspectroscopy. (Georgia State University, 2011).
134. Pereira, M. J. Evaluating the Impact of Culture Conditions on Human Mesenchymal Stem / Stromal Cell-derived Exosomes through FTIR Spectroscopy. (Instituto Superior Técnico, Universidade de Lisboa, 2018).
135. invitrogen by life technologies. Total Exosome Isolation (from cell culture media). *MAN0006949* (2012).
136. Antibody Design Labs. Small-Scale Preparation of Filamentous Bacteriophage by PEG Precipitation. (2015). Available at: http://www.abdesignlabs.com/technical-resources/bacteriophage-preparation/. (Accessed: 16th September 2019)
137. Lee, C. *et al.* 3D plasmonic nanobowl platform for the study of exosomes in solution. *Nanoscale* **7,** 9290–9297 (2015).
138. Marques, V. *et al.* Characterization of gastric cells infection by diverse Helicobacter pylori strains through Fourier-transform infrared spectroscopy. *Spectrochim. Acta - Part A Mol. Biomol. Spectrosc.* **210,** 193–202 (2019).